Interpretation of Laboratory Tests on Mactaquac Cores

Report submitted to GEMTEC

by

Prof. Victor E. Saouma

With Contribution from

Dr. Tetsuya Katayama

May 4, 2021

x-elastica

Contents

List of Figures

List of Tables

1 Introduction

1.1 Objective

Safety assessment of a dam with an ongoing alkali aggregate reaction (AAR) can be a complex and daunting task. Fig. 1.1 illustrates an all-inclusive approach for such an undertaking, and the tasks addressed in this report is within the dotted line.

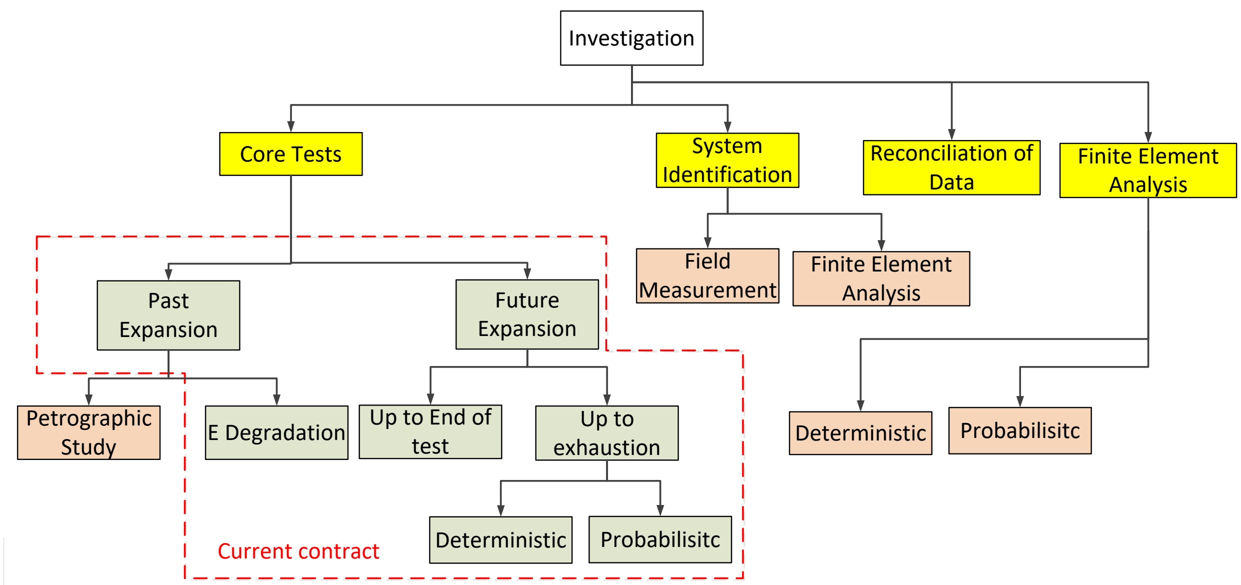

Figure 1.1: Schematic of complete tasks for a structural assessment

We were provided with two data sets. The first is a record of accelerated expansion tests in cores extracted at three different locations of Mactacuaq (MQ) dam. The second are results of mechanical tests on cores extracted from the dam, and then tested over nearly two years for elastic modulu E, compressive and tensile strengths (F_c and $_t$).

Those two data sets were found to be very well organized, tests systematically performed according to well established protocols, yet only approximate qualitative observations could be made by mere inspection of the spreadsheets and some of the accomnying plots.

The objective of this report is to systematically analyse those data sets, and seek a rational way to "make them talk" in order to assist with future decision making process in the context of Fig. 1.1.

1.2 Data Analysis

It is important to note that when experimental data is analysed, and a mathematical model desired, then we have two options:

First-Principle based model: This is a model rooted in the underlying physics of the problem, resulting in what some have referred to as a semi-analytical model. That is a (mechanics in this case) based model is first derived, and then coefficients are determined through fitting with the experimental data. However, frequently, those models are principled but imperfect representations of reality due to incomplete physical description of the underlying phenomenon. In this report, we will use such a model for the expansion based on (Ulm, Coussy, Kefei, and Larive, 2000).

Data-Driven model: In this case, no model is *a priori* given, and whatever mathematical curve best fits the data is adopted. This would lead to an emperical (heuristic) model, and one should be particularly careful not to apply it outside the range of available data (i.e. extrapolation). Such a model will be used for concrete degradation.

The former will be used for the expansion data(§1.3) and the acticvation energies, the second for the degradation of mechanical properties.

1.3 Mathematical Model of ASR Kinetics

Expansion data analysis in this report is based on the mathemaitical model of the reaction kinetics. Hence, it is critical that this simple model be first understood.

A model, nearly universally accepted was first developed by Ulm, Coussy, Kefei, and Larive (2000) and later validated by Larive (1998). Larive conducted one of the most extensive and rigorous alkali silica reaction (ASR) investigation in which more than 600 specimens, Figure 1.2(a), with various mixes, ambient and mechanical conditions were tested. The model came to be commonly referred as "Larive's model".

The thermodynamically-based, semi-analytical model of (Ulm, Coussy, Kefei, and Larive, 2000) was calibrated using laboratory results in order to determine two key parameters: the latency, τ_l, and characteristic, τ_c, times shown in Figure 1.2(a)for the normalized expansion.

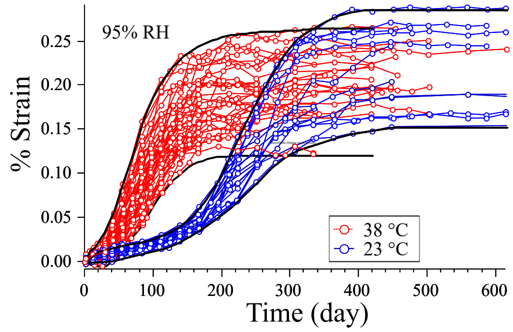

(a) Bracket of experimentally measured expansion at two different temperatures (Larive, 1998)

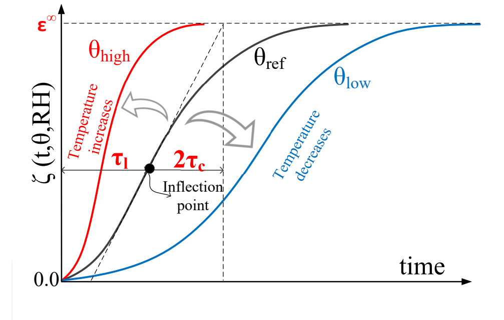

(b) Expansion Curve ($\xi(t,T,RH) = \varepsilon^{ASR}/\varepsilon^{\infty}$)

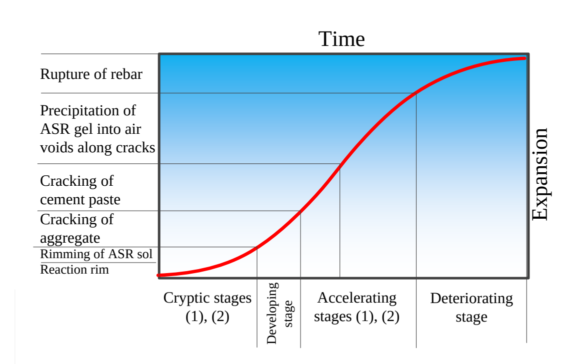

(c) Physical deterioration associated with AAR (Saouma, Martin, Hariri-Ardebili, and Katayama, 2015)

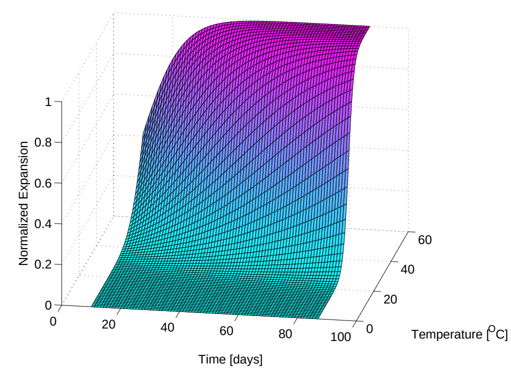

(d) Role of Temperature

Figure 1.2: ASR expansion curve

The model is really a sigmoid curve capturing the slow initiation process, followed by an acceleration, and then further slowing as either the silica or the alkali are exhausted (Saouma, Martin, Hariri-Ardebili, and Katayama, 2015):

$$\varepsilon^{ASR}(t,T,RH) = \underbrace{\frac{1-e^{-\frac{t}{\tau_c(T)}}}{1+e^{-\frac{(t-\tau_l(T))}{\tau_c(T)}}}}_{\text{Normalized expansion } \xi(t,T)} \varepsilon^{\infty}_{RH} \tag{1.1}$$

where T is the temperature, $\varepsilon^{\infty}(RH)$ the asymptotic expansion depends on the relative humidity Capra and Bournazel (1998)

$$\varepsilon^{\infty}_{RH} = \varepsilon^{\infty}_{RH=1} RH^m \tag{1.2}$$

however inside a dam the RH is very likely to be above 85% a threshold below which there is no expansion, hence the impact of RH can be safely ignored (except for a few inches of exposed surfaces).

τ_l and τ_c are the latency and characteristic times, calibrated at T_0. The first corresponds to the inflection point while the second is defined relative to the intersection of the tangent at τ_c with the asymptotic unit value of ξ, Fig. 1.2(b) .

It should be noted that the curve has sufficient "flexibility" to accomodate sigmoidal expansion, as well as linear ones (within the time frame of interest), however it can not accomodate decreasing expansion.

Latency and characteristic times are temperature dependent, Figure 1.2(d):

$$\begin{aligned} \tau_l(T) &= \tau_l(T_0) \exp\left[U_l \left(\frac{1}{T} - \frac{1}{T_0}\right)\right] \\ \tau_c(T) &= \tau_c(T_0) \exp\left[U_c \left(\frac{1}{T} - \frac{1}{T_0}\right)\right] \end{aligned} \tag{1.3}$$

where U_l and U_c are the activation energies required to trigger the reaction for latency and characteristic times, respectively.

Takeaway: Model

Expansion can be mathematically captured in terms of three parameters: τ_c, τ_l and ε^∞

1.4 Report Organization

This report is broken in the four chapters

1. This introduction.
2. Describes the laboratory testing program undertaken by the University of New Brunswick for cores recovered from Mactacuaq.
3. Will provide some visualization of measured laboratory values, along with some preliminary qualitative observation.
4. Data analsysi of recorded values.
5. Summarizes this study findings.

Throughout this investigation, we use Matlab for plotting and data analysis. Furthermore, Chapters 4 and 5 separately address expansion from mechanical property degradation.

To facilitate reading of the report, many of the preliminary plots are placed in the appendix.

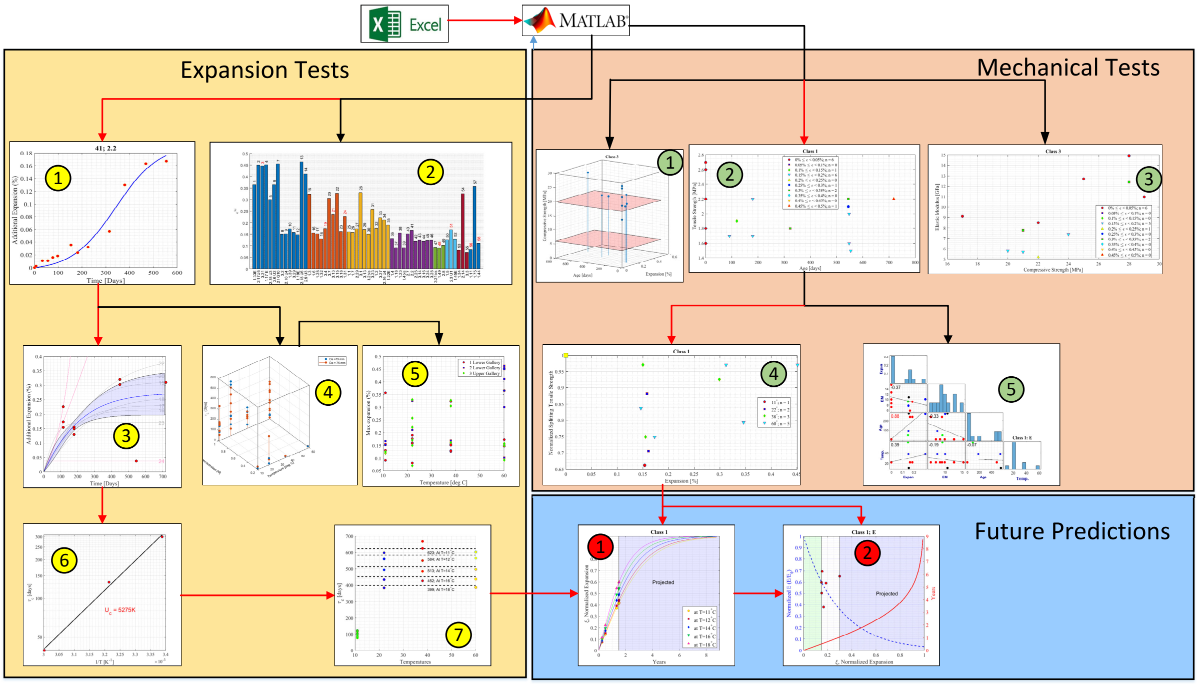

Figure 1.3: Report Organization

Expansion

The expansion test data interpretation, that stradles two chapters, is organized as follows, Fig. 1.3:

1. For each test, fit the data into a sigmoid, determine the parameters, and plot
2. For each test, summarize the expansion curve parameters
3. † For each test series, compute the mean and standard deviation.
4. 3D plots of expansions parameters in terms of storage conditions and aggregate sizes
5. 2D plots of expansion parameters in terms of storage conditions and aggregate sizes
6. † Compute the activaiton energy from all means
7. † Plot τ_c equivalent for different temepratures

† denotes plots on the crietical path to perform predictions, other are for illustrative/qualititative purposes.

Degradation

1. 3D plots of E, f_c and f_t in ters of age and expansion

2. †2D plots of E, f_c and f_t, in terms of age, expansion (age and temepratture egends), and storage temperature
3. Plots of E, f_c
4. †Normalized plots of degradation
5. Correlation coeffecients plots

Future Predictions

1. †Expansion
2. †Degradation

1.5 Warning

The analyses reported are based on data from cores recovered from a major hydrualic structures. Some of them were stored in the dam itself (at 11°C) and others in the laboratory. Though a very clear protocol was followed for testing, we are nevertheless dealing with a limited data set and with the large variability expected to find in dam cores.

Incidentally, no error bars were plotted in this report, as we had no indication of what were the margin of errors in the various measurements.

On the other hand, though one can easily determine qualitative trends by mere inspection of the spreadsheet, a better approach is to fit the data with mechanics based, or heuristic models.

Hence, the reader should be cautioned not to be excesively concerned about the occasional variability of the results, and remain reassured that the best analytical tools will be used to "make the data talk".

Another point to make is that the cores were unrestrained in the laboratory. In the dam, expansion along the direction of major principal stress will be reduced (i.e. we typicaaly observe lower vertical expansion at the base of the dam, as captured by the reduction in the elastic modulus). however we also know that the expansion will be re-directed in orhogonal ones (as pointed out by Multon and Toutlemonde (2006)).

2 Core Testing Procedure

`Chapter adapted from Moffatt and Thomas (2018)`

2.1 Core description

Cores (nominally 6-inch/152-mm, diameter) have been exposed to one of two exposure conditions Moffatt and Thomas (2018):

- Immersed in a solution of sodium hydroxide
- Placed in a cylindrical container that is only slightly larger than the core with a small annular space surrounding the core being filled with an alkali hydroxide solution representative of the concrete pore solution.

Concrete cores stored in the first storage condition were measured for length change and, after reaching certain predetermined levels of expansion, selected cores were removed to determine mechanical properties (compressive strength, indirect splitting tensile strength and modulus of elasticity). Concrete cores in the second storage condition were measured for length change only.

2.1.1 Core Locations

One hundred and thirty, nominal 6-inch (152-mm) diameter cores were extracted from the upstream face in the lower (100 cores) and upper (30 cores) inspection galleries in the fall of 2015.

The lower inspection gallery is encapsulated in both Class 1 and 2 concrete, and cores were taken along the upstream face (Class 2 concrete) of the gallery as indicated by the black arrow in Figure 2.2. Thirty cores were removed from the upper inspection gallery (Class 4 concrete). Upon removal from the structure, cores were wrapped in wet burlap in order to avoid moisture loss during transport to the University of New Brunswick (UNB).

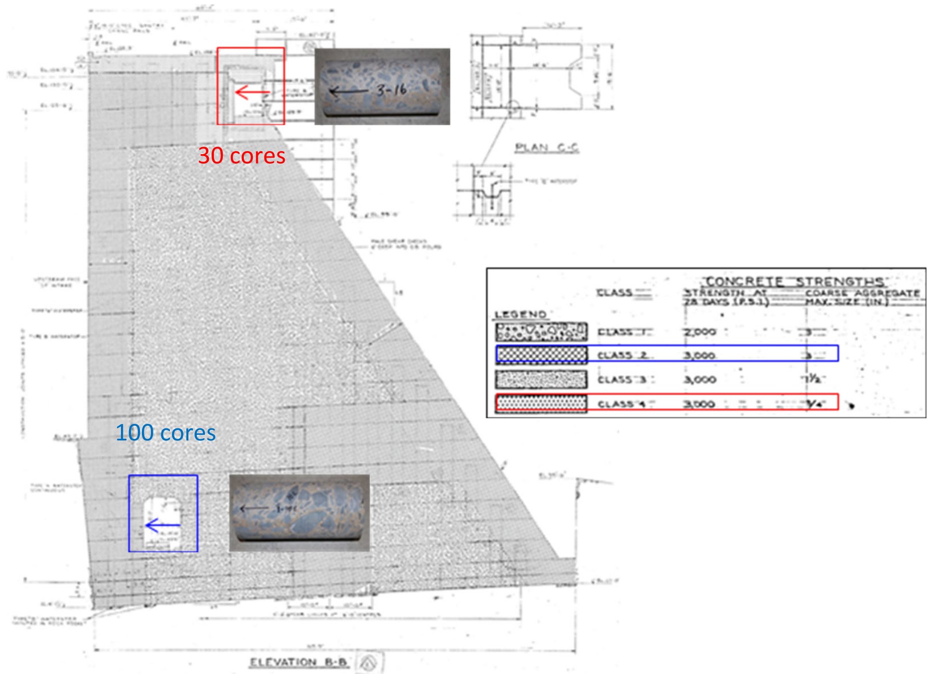

(a) Dam X-Section

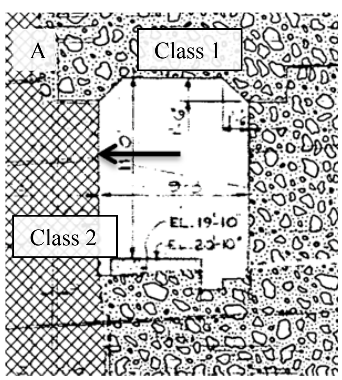

(b) Lower

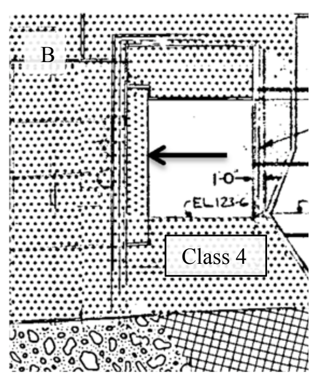

(c) Upper

Figure 2.1: Dam X-section and Inspection galleries

Table 2.1: Concrete properties

Class	# Cores	MSA		$\simeq$ CC		f'_c	
		inch	mm	lb/yd^3	kg/m^3	psi	MPA
			Lower inspection gallery				
1-X	70	3	75	310	185	2,000	13.8
2-X	30	3	75	395	234	3,000	20.7
			Upper inspection gallery				
3-X	30	1.5	38	435	258	3,000	20.7
4-X	30	0.75	19	460	273	3,000	20.7

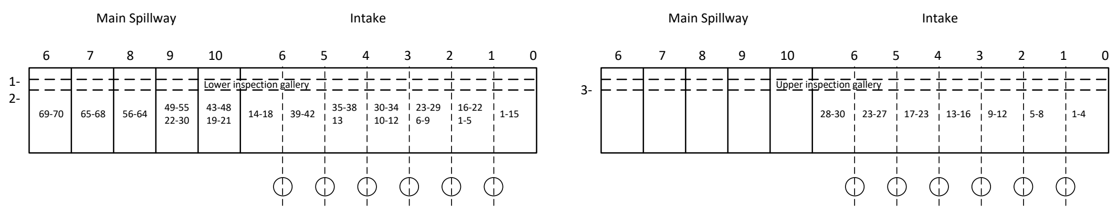

(a) Lower (b) Upper

Figure 2.2: Core location in galleries

Upon removal of the first 70 cores from the lower inspection gallery, it was observed that the final twenty cores (labeled 1.50 to 1.70) had slightly larger aggregates than the first fifty. A second round of coring was then conducted on the lower inspection gallery, where thirty cores were extracted between location 1.1 and 1.50, Figure 2.2(a). Thirty cores were also removed from the upper inspection gallery where the aggregate size was found to be consistent along the length of the gallery, Figure 2.2(b). Table 2.1 indicates the labeling system used to designate cores from various locations. For example, Core 2-12 represents a core taken from the lower inspection gallery, during the second round of coring.

2.1.2 Specimen Preparation

Once received at UNB, the cores were cut and end-ground to a length of approximately 290 mm (11.4 in.). A hole was then drilled in each end to accommodate a 1/4 in, (6-mm) threaded rod, which was epoxied into place. The pins were installed to facilitate length change measurements as shown in Figure 2.3.

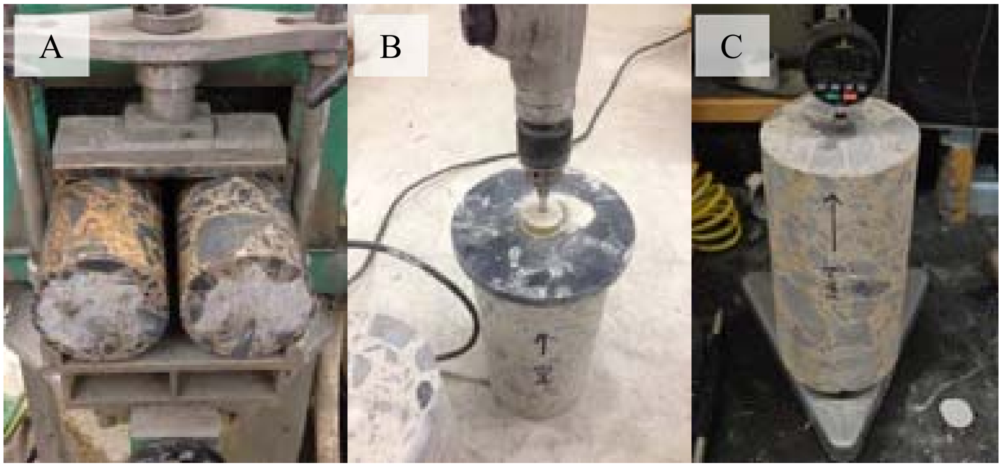

Figure 2.3: A) end-grinding cores, (B) drilling a quarter inch hole in each end using a template to ensure holes are drilled in the center of each end, (C) length measurement

2.1.3 Storage conditions

Cores were then placed in one of two storage solutions in order to simulate alkali availability within the dam (Condition #2) or accelerated the rate of expansion and measure the effect on mechanical properties (Condition #1).

Storage Condition #1: cores were placed in sealed containers containing a 1M NaOH solution. This condition was designed to maximize the rate of expansion and represents the worst-case scenario by exposing cores to an inexhaustible supply of alkali. In order to accelerate the rate of expansion, cores were exposed to various storage temperatures as presented in Table 2.2. The compressive strength, modulus of elasticity (MOE) and splitting tensile strength were then measured, Figure 2.4 once the cores had reached a target expansion in order to generate a relationship similar to that presented in Figure 2.5.

Storage Condition #2: This condition was created in order to expose cores to an annulus of alkaline solution representing the pore solution within concrete at the Mactaquac Dam; see Figure 2.6. This condition was selected in order to maintain alkali equilibrium between the surrounding (host) and pore solutions. These cores are currently being measured for expansion at the same temperatures as Storage Condition #1, however, mechanical properties are not being measured.

Table 2.2: storage condition # 1

Storage	Target expansion %			
Temp (°C)	0.15	0.3	0.45	0.6
60	X	X	X	X
38	X	X		
23	X	X		
MQ	X	X		

X-6 cores tested at each level: 3 for splitting strength and 3 for MOE followed by compressive strength
MQ Cores stoed in lower inspection gallery ($\simeq$ 11°C)

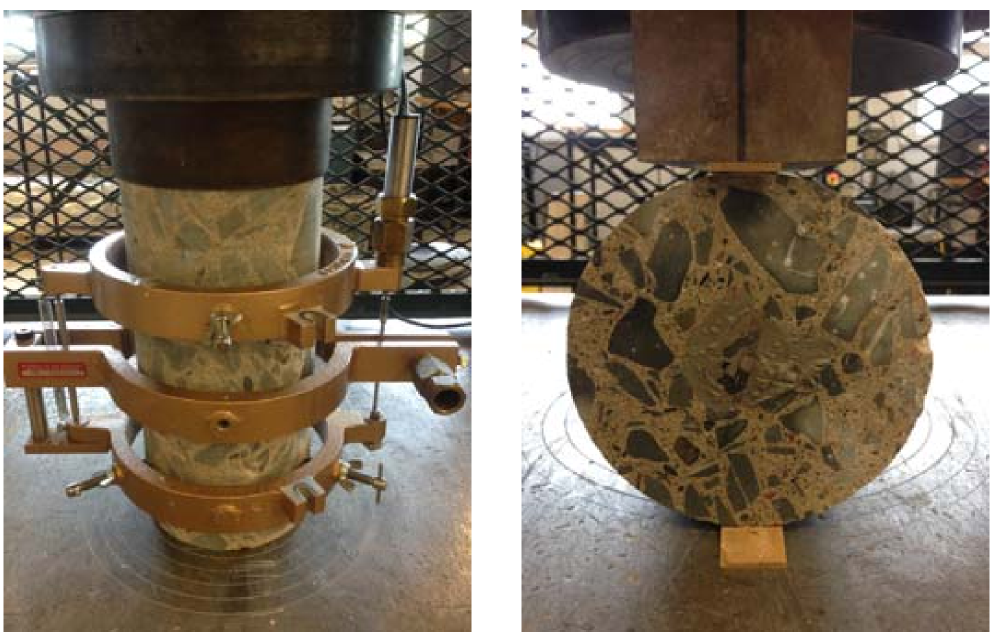

Figure 2.4: Modulus of elasticity, ASTM C469; and splitting tensile strength, ASTM C496

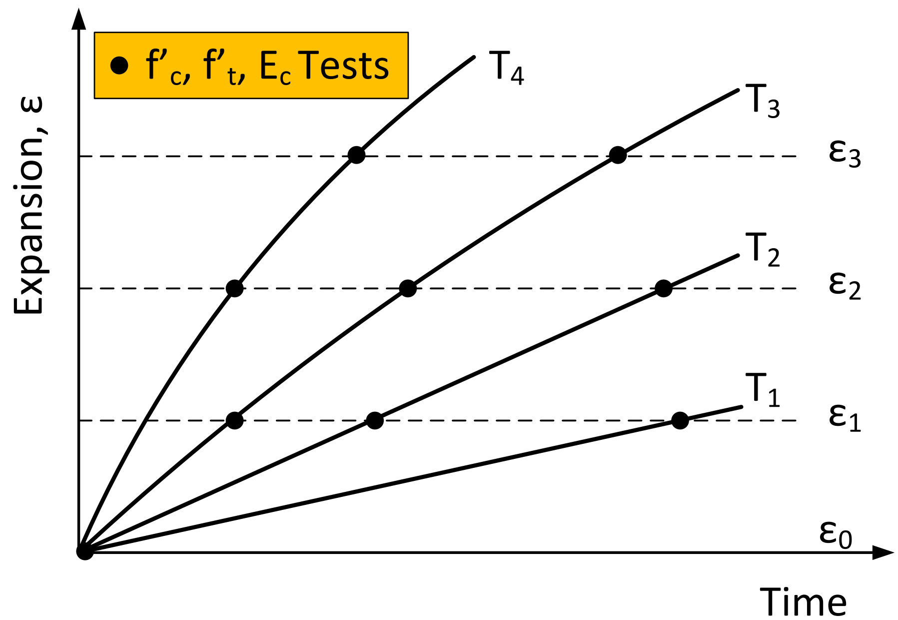

Figure 2.5: Expansion tests conducted at various temperatures $T1 < T2 < T3 < T4$ with mechanical tests (f'_c, f'_t, E_c) being conducted prior to test ($\varepsilon_0 = 0$) and after different levels of additional expansion are achieved

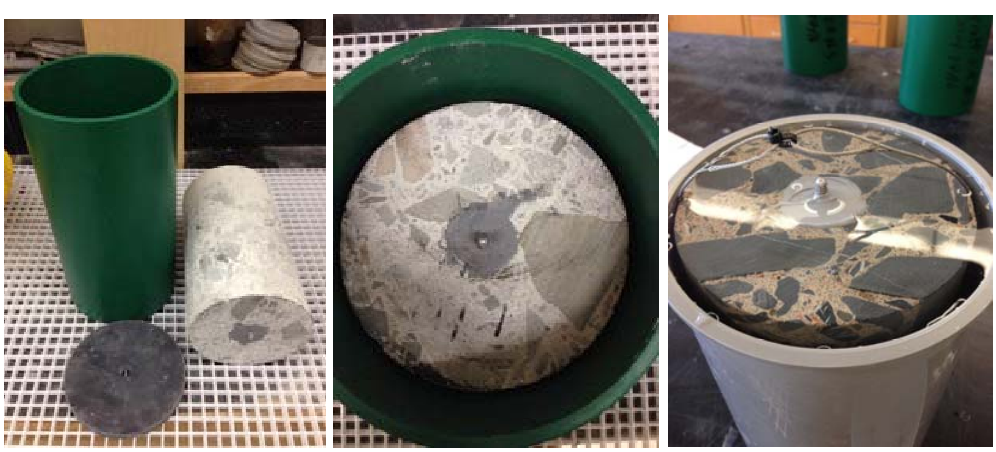

Figure 2.6: Storage condition # 2

3 Expansion

This chapter will first generate multiple plots of the raw data (some of them will be placed in the appendix), and then perform a preliminary qualitative set of observations.

Those will be furher expanded in the next chapter.

3.1 Curve Fitting

Data reported in the spreadshhet file `Mactaquac data.xlsx` has readings spanning up to 1,383 days (just under 4 years). Given that the core were extracted in 2015 (Moffatt and Thomas, 2018), this implies that the last reading may have been taken around 2019.

Each measurement was fitted through Larive's model, Eq. 1.1 and corresponding τ_c, τ_l and ε^{∞} determined.

Results are shown in Appendix A (Figs. A.1-A.8) and tabulated in Table 3.1, where increasing values of are color-coded to faciltate assessment.

Specimen which are deemed "unreliable" (either due to low R^2 or unrelistic ε^{AAR}) are tagged in red, and will be ignored in subsequent data analysis.

Table 3.1: Data analysis summary of all expansion tests

	label	NaOH M	Temp °C	Loc	f'_c MPa	D_a mm	# days days	τ_l days	τ_c days	ε^{∞} %	R^2 -
	Fig. A.1										
1	1.33E	1	60	1	20.7	75	685	0.00	158	0.36	0.98
2	2.17U6	1	60	2	20.7	75	685	0.00	181	0.44	0.97
3	3.21	1	60	3	20.7	38	685	5441.51	905	159.96	0.98
4	1.17 E	1	60	1	20.7	75	1347	0.00	262	0.38	0.94
5	2.28 U3	1	60	2	20.7	75	415	0.00	82	0.29	0.98
6	2.6 U2	1	60	2	20.7	75	415	0.00	101	0.31	0.94
7	2.21 G10	1	60	2	20.7	75	685	0.00	277	0.49	0.95
8	3.2	1	60	3	20.7	38	113	0.00	36	0.17	0.97

Continued on next page

	label	NaOH M	Temp °C	Loc	f'_c MPa	D_a mm	# days days	τ_l days	τ_c days	ε^∞ %	R^2 -
9	2.10 U4	1	60	2	20.7	75	82	0.00	35	0.18	0.94
10	1.39	1	60	1	20.7	75	82	0.00	11	0.15	0.95
11	3.29	1	60	3	20.7	38	82	0.00	42	0.21	0.98
12	1.19E	1	60	1	20.7	75	82	0.00	32	0.17	0.97
13	2.18 U6	1	60	2	20.7	75	1265	0.00	358	0.46	0.96
14	2.9 U3	1	60	2	20.7	75	1265	0.00	336	0.40	0.93
					Fig. A.2						
15	1.3	1	38	1	20.7	75	718	31.20	131	0.31	0.99
16	1.6	1	38	1	20.7	75	179	0.00	98	0.22	0.97
17	1.28	1	38	1	20.7	75	179	0.00	115	0.23	0.96
18	1.32	1	38	1	20.7	75	179	0.00	163	0.26	0.97
19	3.4	1	38	3	20.7	38	115	1687.74	1254	8.90	0.97
20	3.7	1	38	3	20.7	38	448	0.00	158	0.34	0.99
21	3.13	1	38	3	20.7	38	115	781.34	98	303.52	0.86
22	3.15	1	38	3	20.7	38	448	0.00	203	0.40	0.97
23	3.18	1	38	3	20.7	38	115	0.00	39	0.17	0.97
24	1.31	1	38	1	20.7	75	545	0.11	0	0.04	0.01
					Fig. A.3						
25	1.1	1	22	1	20.7	75	548	0.00	227	0.16	0.95
26	1.7	1	22	1	20.7	75	548	0.00	311	0.21	0.94
27	2.29	1	22	2	20.7	75	1383	0.00	464	0.18	0.95
28	3.1	1	22	3	20.7	38	666	0.00	186	0.35	0.97
29	3.13	1	22	3	20.7	38	1383	1008.28	491	0.27	0.96
30	3.2bis	1	22	3	20.7	38	721	427.69	108	0.14	0.91
31	3.23	1	22	3	20.7	38	1383	0.00	522	0.30	0.99
32	1.2	1	22	1	20.7	75	1383	273.64	160	0.16	0.97
33	3.27	1	22	3	20.7	38	387	0.00	192	0.25	0.91
34	2.26 U4	1	22	2	20.7	75	1319	0.00	394	0.23	0.97
35	1.22E	1	22	1	20.7	75	548	0.00	65	0.17	0.88
					Fig. A.4						
36	1.4	1	11	1	20.7	75	554	0.00	175	0.12	0.93
37	1.18	1	11	1	20.7	75	1238	0.00	163	0.08	0.96
38	1.23	1	11	1	20.7	75	554	184.22	146	0.18	0.98
39	1.4bis	1	11	1	20.7	75	1238	0.00	150	0.07	0.89
40	2.7	1	11	2	20.7	75	554	0.00	331	0.21	0.94
41	2.2	1	11	2	20.7	75	554	341.35	91	0.19	0.96
42	2.25	1	11	2	20.7	75	1238	76.76	54	0.09	0.81
43	3.14	1	11	3	20.7	38	1238	133.77	83	0.09	0.83
44	3.16	1	11	3	20.7	38	1238	81.06	135	0.08	0.76
45	3.24	1	11	3	20.7	38	1238	210.10	136	0.08	0.78

Continued on next page

	label	NaOH M	Temp °C	Loc	f'_c MPa	D_a mm	# days days	τ_l days	τ_c days	ε^∞ %	R^2 -
46	3.28	1	11	3	20.7	38	1238	161.20	138	0.12	0.98
				Fig. A.5							
47	3.21bis	0.225	60	3	20.7	38	1340	4.24	5	0.08	0.48
48	1.49	0.225	60	1	20.7	75	1340	1.22	1	0.05	0.16
49	2.8	0.225	60	2	20.7	75	1340	3.60	4	0.08	0.59
				Fig. A.6							
50	1.5	0.225	38	1	20.7	75	1340	3.30	4	0.07	0.38
51	2.3 U1	0.225	38	2	20.7	75	1340	4.93	6	0.10	0.16
52	1.45E	0.225	38	1	20.7	75	1340	2.96	3	0.08	0.34
				Fig. A.7							
53	1.34	0.225	22	1	20.7	75	1340	103.75	38	0.08	0.93
54	2.14	0.225	22	2	20.7	75	1340	0.00	263	0.28	0.94
55	3.3	0.225	22	3	20.7	38	1340	0.00	47	0.07	0.98
				Fig. A.8							
56	1.11	0.225	11	1	20.7	75	1192	29.04	3	0.03	0.05
57	1.75	0.225	11	1	20.7	75	1192	501.26	17	0.35	0.99
58	1.44	0.225	11	1	20.7	75	1192	53.19	99	0.05	0.11

3.2 Observations

We start by plotting results of all 58 individual expansion data fitting (In the appendix, Fig. A.1-A.8), with summary in Fig. 3.1 . From these figures, we note that:

1. There is a great disparity in recorded times in the cores kept at 1M, whereas those stored with 0.225M are continuously monitored, Fig. 3.1(a). This could impact ultimately on the reliability of the results.
2. R^2 shows poor fit with Eq. 1.1 for those specimens stored in 0.225M except those at 22°C, Fig. 3.1(b),.
3. The maximum expansion, Fig. 3.1(c), is for the most part around 0.2, with notable exception for those specimens stored at 60°C in 1M solution. This is to be expected, as higher temperatures accelerate the expansion.
4. The latency times, Fig. 3.1(e) are mostly zero (as expected because by the time the cores where extracted, expansion intitated) with a few notable exceptions that may be associated with poor fitting with Eq. 3.1(c).
5. The characteristic times, Fig. 3.1(d), are mostly identical and will be examined in further detail later.

Note that those expansion tests which were deemed to be unreliable (per Table 3.1) are marked in red.

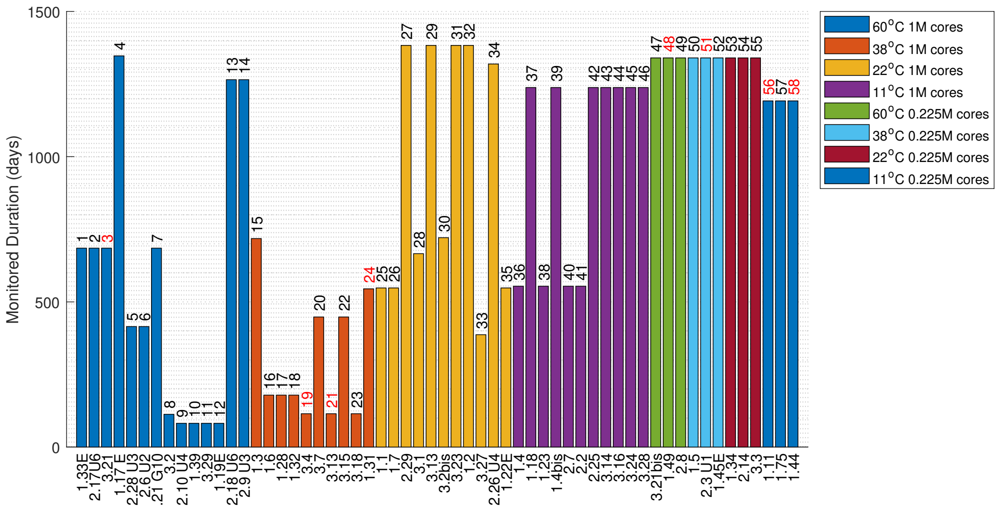

(a) Maximum recorded time

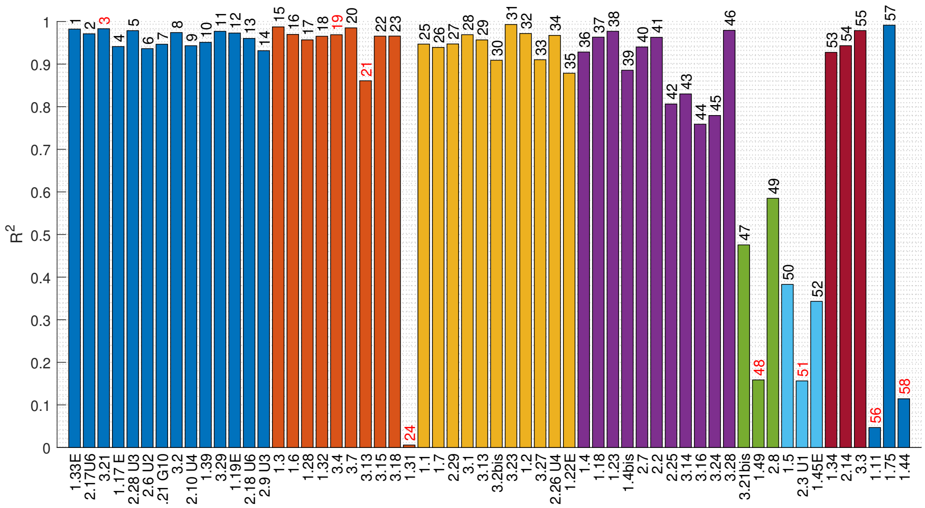

(b) R^2

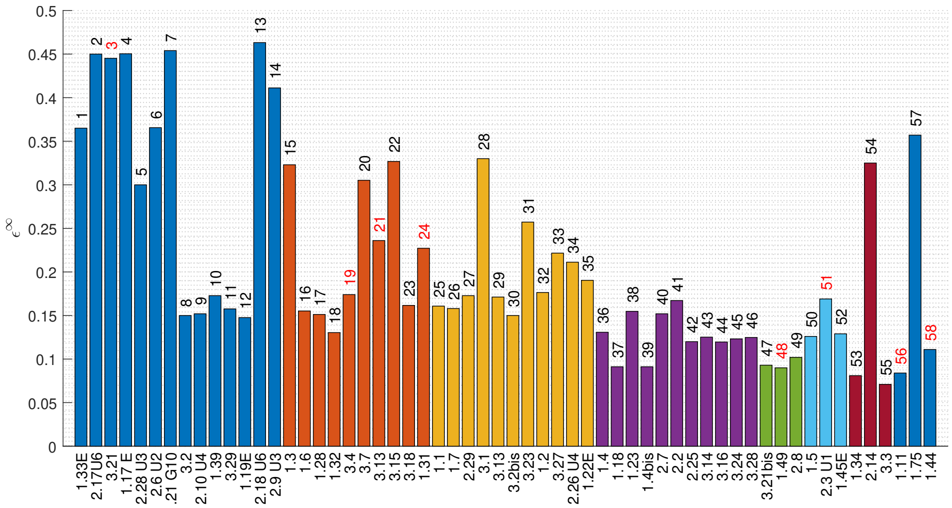

(c) Maximum expansionε^∞

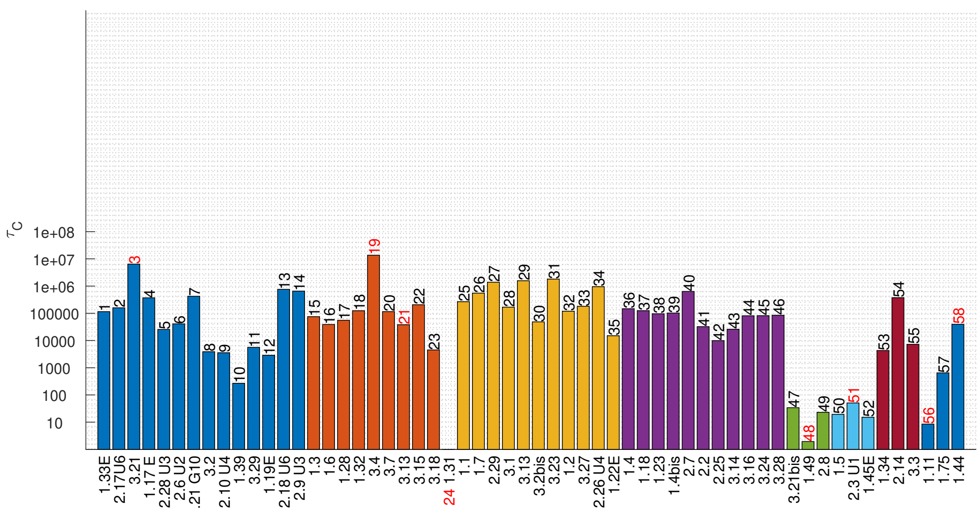

(d) Characterisitc times

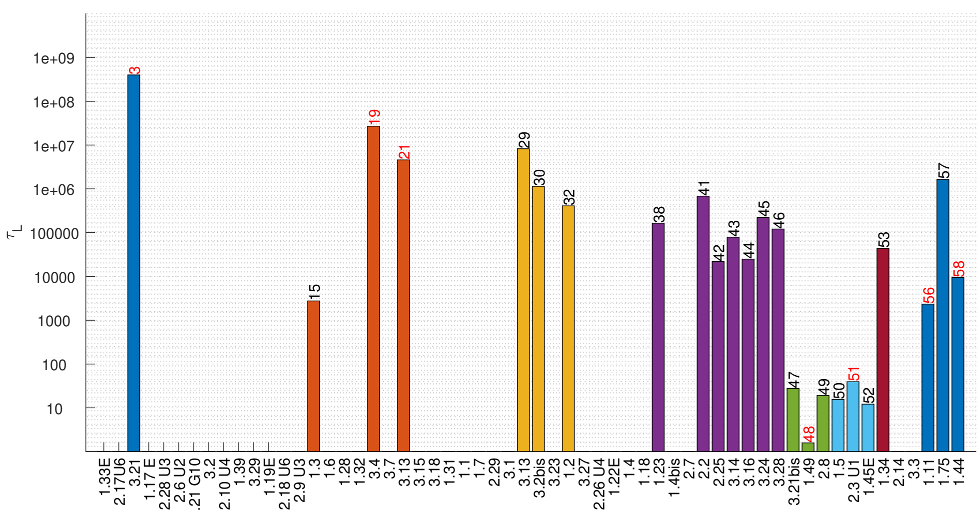

(e) Latency times

Figure 3.1: Summary Expansion Results; Larive

We note that some data are clearly unreliable (those with a R^2 smaller than $\simeq 0.7$), and other show continued expansion increase.

Takeaway: Expansion

58 measurements were fitted through Larive's curve. Some measurements are clearly unreliable, others are indicative of continuous increase in expansion with no sign of slowing.

3.3 Data Analysis

A hierarchical data analysis of the result will be performed:

1. Each of the 58 individual test results (maximum expansion, R^2 of the fitted Larive model, ε^∞, τ_l and τ_c). Though shown in Figs. A.1-A.8 they are tabulated in Table 3.1, where increasing values of are color-coded to faciltate assessment.
2. Each of the eight groups will be analyzed next.
3. Integrated analysis of all tests.

3.3.1 Mean Expansion Curves

Next, we shall plot the expansion of tests grouped in 8 categories (1 M *vs.* 0.225 M, and same storage temperature). They are shown in Fig. 3.2 with tabulation in Table 3.2.

Note that the curves in Fig. 3.2 corresponding to the fitted data, that is thery are not the experimetal values, but the mathematical model based on Larive's equation (Eq. 1.1). The last point of the experimental measurements is marked by filled red circle. Finally, the red curves correspond to those deemed unreliable.

Then the mean curve is determined based on the fitted ones (excluding thoses considered unreliable), including the extrapolaiton beyond the red points. Once the blue mean curve is obtained, than in turn the corresponding Larive coefficient are determined, and are shown in Table 3.2.

Back to the plots, the mean is clearly shown in blue and the opaque region corresponds to $\pm$ one standard deviation. This corresponds to a total of 68.2% of the data (34.1% on either side). This may be slightly misleading, as the blue "bracket" encompasses both actual fited data, and extrapolated ones (beyond the red circle).

These plots call for the following observations

1. Though expansion recording took plase over 1,200 days, specimens stored 0.225M, for the most part, yield unreliable results.
2. lowest expansions occur at 38°C and 60°C (0.08%), 60°C. on the other hand, as the temperature drops, then the mean expansion increases (which is in violation of thermodynamics).
3. Data doe specimens stored in 1M NaOh appear to be more consistent.
4. Maximum expnasion increases with time.
5. Expansion are defintely lower than their counterparts stored at 0.225M.

6. In all cases τ_L is zero as expansion had already started when specimens were collected from Mactacuaq.

Table 3.2: Expansion characterisitcs for each group

Set	Temp [°C]	Concentration [Moles]	τ_L [days]	τ_c [days]	ε^{∞} -	R^2
1	60	1	0	152.0	0.29	0.97
2	38	1	0	131.3	0.27	1.00
3	22	1	0	282.6	0.20	1.00
4	11	1	115	166.7	0.12	1.00
5	60	0.225	4	4.3	0.08	1.00
6	38	0.225	3	4.6	0.08	1.00
7	22	0.225	0	166.1	0.14	0.99
8	11	0.225	501	16.6	0.35	1.00

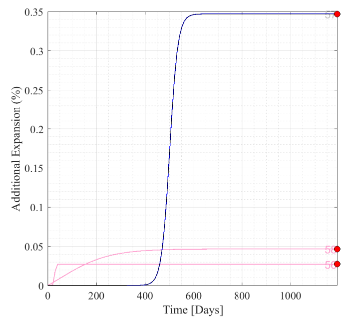

(a) 0.225M @ 11°: τ_l=501 , τ_c=16.6, ε^{∞}=0.35

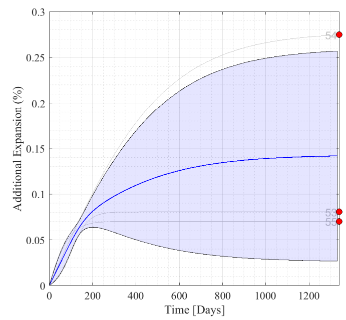

(b) 0.225M @ 22°: τ_l = 0.0 , τ_c=166.1, ε^{∞}=0.14

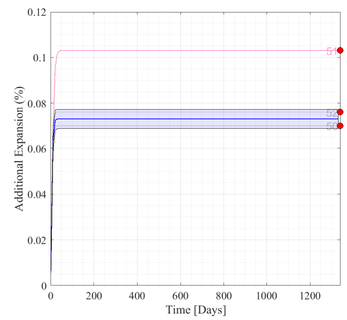

(c) 0.225M @ 38°: τ_l =3.0 , τ_c=4.6, ε^{∞}=0.08

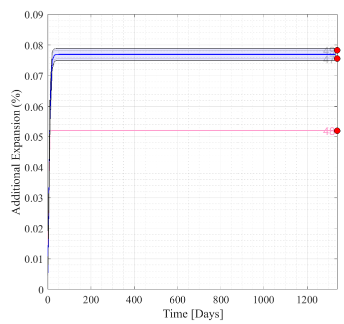

(d) 0.225M @ 60°: τ_l =4 , τ_c=4.3, ε^{∞}=0.08

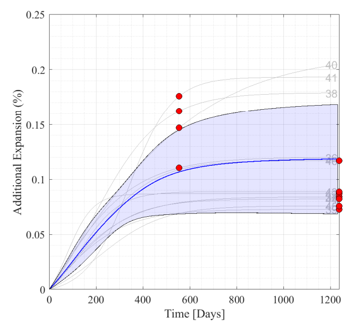

(e) 1M @ 11°: τ_l =0.0 , τ_c=282.6, ε^{∞}=0.20

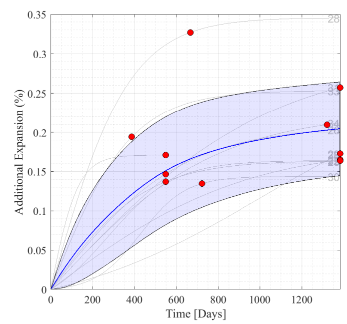

(f) 1M @ 22°: τ_l =0.0 , τ_c=282.6, ε^{∞}=0.20

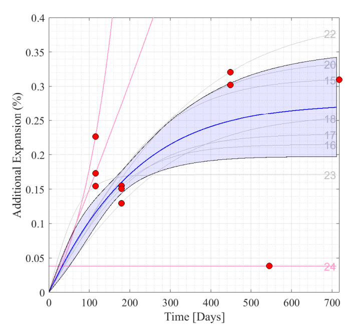

(g) 1M @38°: τ_l =0.0 , τ_c=131.3, ε^{∞}=0.27

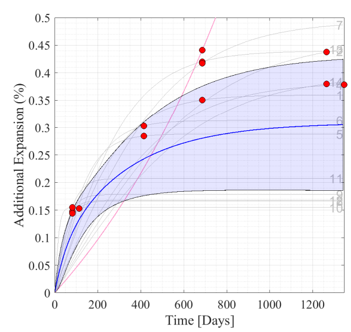

(h) 1M @ 60°: τ_l =0.0 , τ_c=152.0, ε^{∞}=0.29

Figure 3.2: Test means of specimens stored at 1M

3.3.2 Observations

Finally, we attempt to perform a coarse/integrative assessment of the results through Fig. 3.3 and 3.4. Note that in those plots the unreliable data (marked in red in Table 3.1 or corresponding to red curves in Fig. 3.2) have been ommitted. This leads to the following observations

1. Both aggregate sizes are equally associated with ASR expansion. However at low

temperature (specimens stored on site) the large aggregates are far more reactive, Fig. 3.3(a)

2. At high temperatures, cores from the lower gallery are most expansive than those the upper gallery. Otherwise, we can draw any tangible conclusion on the impact of location, Fig. 3.3(b)
3. Maximum expansion increase with temperature for 1M (and decrease at 0.225M), Fig. 3.3(c)
4. Aggregate sizes do not appear to play a role on the characteritic time, Fig. 3.3(d)
5. Location of core extraction does not appear to play a role on the characteritic time, Fig. 3.3(e)
6. Cores stored at 1M yield longer characteritic time, Fig. 3.3(f). τ_c at 0.225 are substantially smaller.

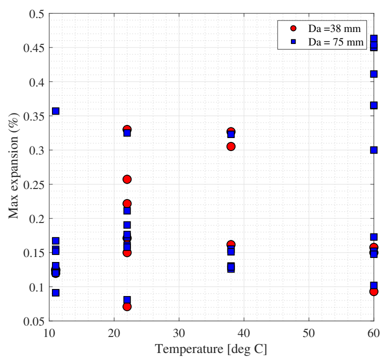

(a) Aggregate sizes on maximum expansion

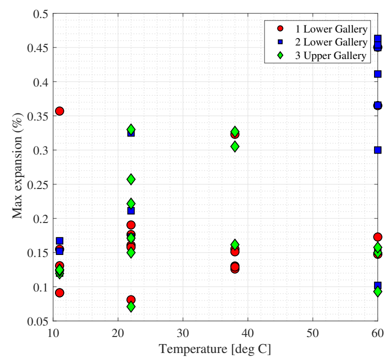

(b) Core location on maximum expansion

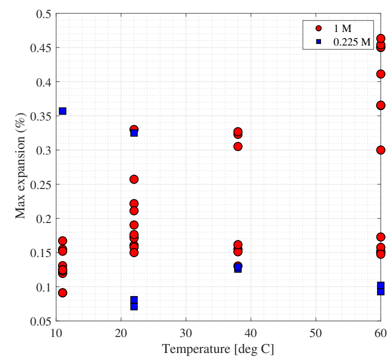

(c) Impact of NaOH concentration on maximum expansion

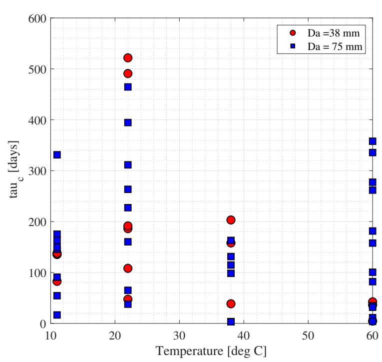

(d) Aggregate sizes on τ_c

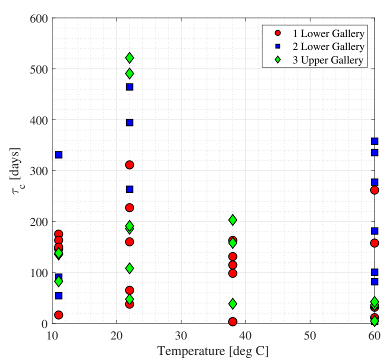

(e) Core location on τ_c

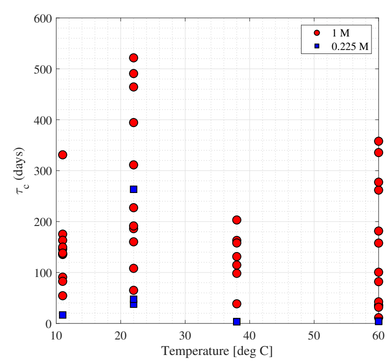

(f) NaOH concentration on τ_c

Figure 3.3: Impact of individual factors and temperature

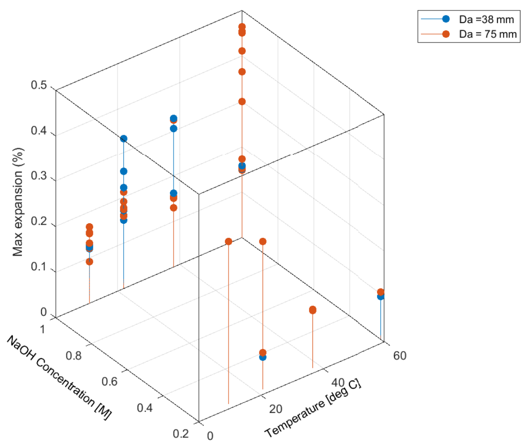

(a) Agggregate size on maximum expansion

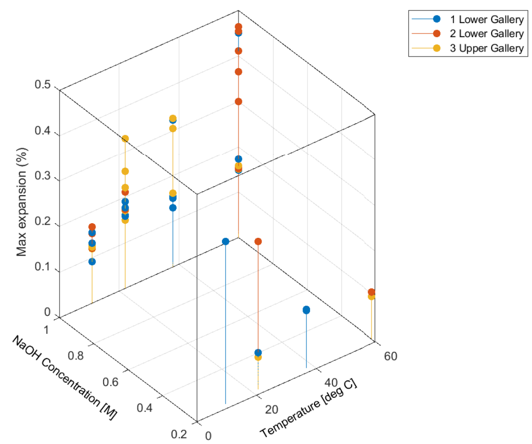

(b) Core location on maximum expansion

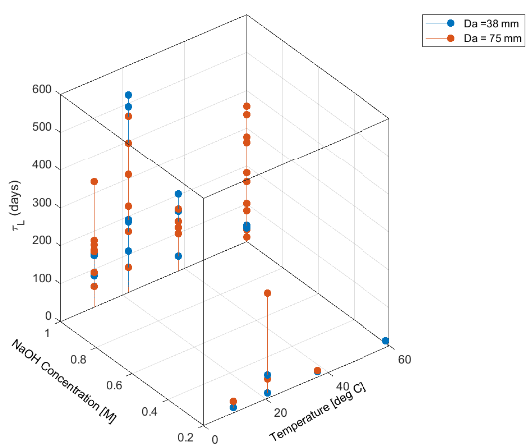

(c) Agggregate size on τ_c

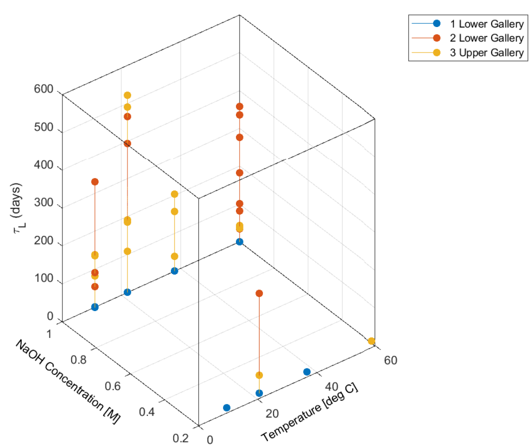

(d) Location on τ_c expansion

Figure 3.4: Combined effects of temperature and NaOh concentration

3.4 Activation Energy

3.4.1 Procedure

Eq. 1.3 is essentially Arrhenius Law (Arrhenius, 1889), which relates the dependence of the reaction rate to temperature.

The second equation can be rewritten as

$$\tau_c(T) = \tau_c(T_0)\exp\left[U_c\left(\frac{1}{T}-\frac{1}{T_0}\right)\right] \tag{3.1}$$

$$\log(\tau_c) = \log\left(\tau_c(T_0)\right) + U_c\left(\frac{1}{T}-\frac{1}{T_0}\right) \tag{3.2}$$

which is the equation of a straight line in the semi-log plot, with slope U_c, Figure 3.5.

We can thus determine the activation energy from different τ observed at different temperatures by simply plotting $\log\tau$ as a function of $1/T$.

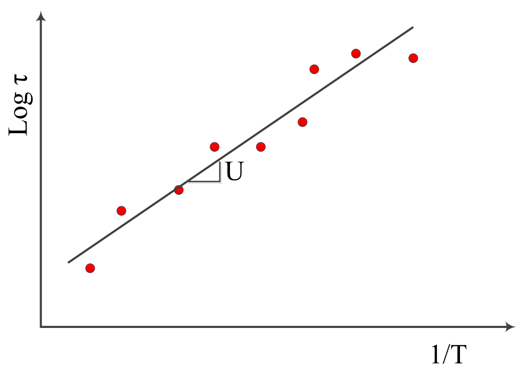

Figure 3.5: Determination of Activation Energies

3.4.2 Calculation

As previously noted, τ_L is zero in all cores (sonce the reactions had started by the time cores were extracted).

First, averages of τ_c at each of the four temperatures are computed, and the activation energy U_c determined, Fig. 3.6(a). We note that the data point corresponding to measurement taken on site (11°C) is an outlier. The erratic nature[1] of this point is confirmed from From Fig. 3.3(e).

Indeed, From Fig. 3.3, it is evident that only cores at 1M with d_a=38mm and T=[22-60], meet that condition. Incidentally, those correspond to cores extracted from the upper gallery. Thus, the τ_c computed (for all cores) in Table 3.2, are re-evaluated for cores at 1M with d_a=38mm and T=[22-60], and are shown in Table 3.3

[1]With refernce to Fig. 1.2(d), one would expect τ_c to decrease as the temperature increases.

Table 3.3: τ_C values, 1M

Set	Temp [°C]	τ_c All (Tab. 3.2) [days]	τ_c d$_a$=38 mm [days]
1	60	152.0	39.3
2	38	131.3	133.3
3	22	282.6	299.7
4	11	166.7	123.1

Hence, calculations are repeated by discarting measurements taken at 11°C, Fig. 3.6(b) and the activation energy U_c determine form those points. Linear regression yields 5,275 K.

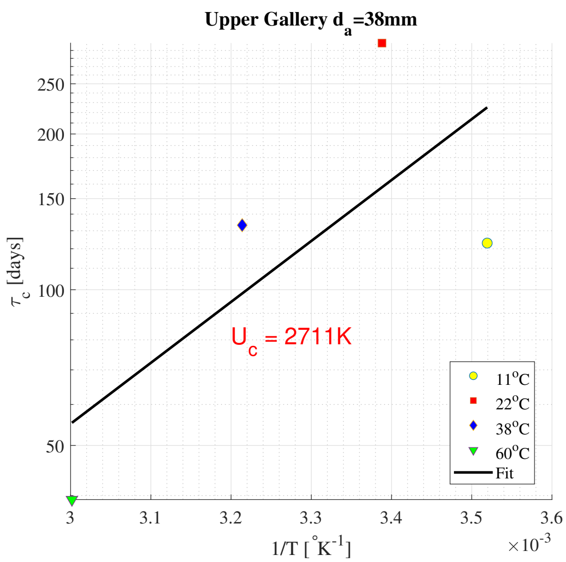

(a) Temp: 11, 22, 38, 60

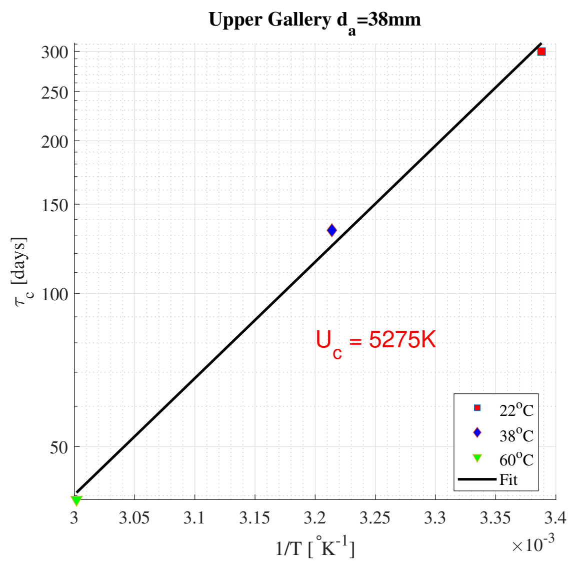

(b) Temp: 22, 38, 60

Figure 3.6: Activation energy U_C for d$_a$=38 mm in 1M solution

This is to be compared with the reported value of 5,400 (± 500) by Ulm, Coussy, Kefei, and Larive (2000). This 2.3% difference (from the mean), and barely outside the reported range, is to be expected as we are comparing actual concrete from a dam, with laboratory prepared cores.

3.4.3 τ_c Verifications

Using Eq. 1.3, we compute the equivalent τ_c at the dam 5 temperatures to be the likely dam temperaturs (11, 12, 14, 16 and 18°C), Fig. 4.2. ideally, we should get the same equivalent values. Indeed, the τ_c are in a narow banld for the three reference temperatures, except the one at 11°C (which will be ignored). The average of the three values is retained. As expected,

τ_c increases with a decrease in temperature (i.e. slower reaction). Tose temperatures (and corresponding τ_c will be used in §5.1).

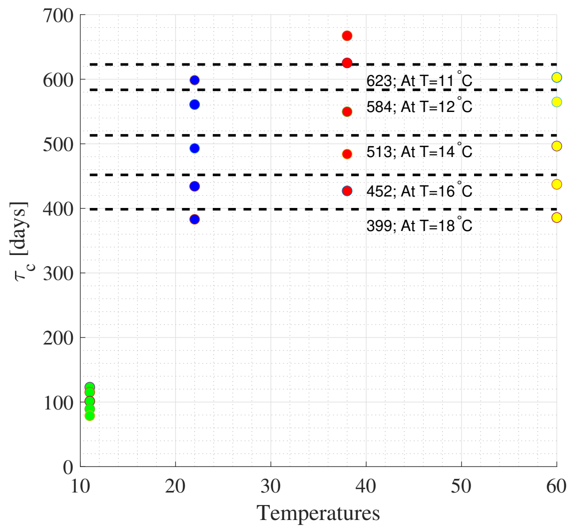

Figure 3.7: τ_C adjusted at 11°C

3.5 Brunetaud's Model

3.5.1 Equation

Brunetaud, Divet, and Damidot (2004) extended the original Larive model for a continuously growing expansion over a long period while investigating delayed etringite formation (EDF). The original three parameters model (τ_L, τ_c, and ε^∞, Φ, δ) is now enriched with two correction terms (Φ and δ; $\Phi < \delta$))

$$\varepsilon(t) = \varepsilon^\infty \frac{1 - e^{-\frac{t}{\tau_c(T)}}}{1 + e^{-\frac{(t-\tau_l(T))}{\tau_c(T)}}} \left(1 + \frac{\tau_c}{\tau_l}\alpha_{W/C}\frac{\beta\tau_l}{\beta\tau_l + t - t_0}\right) \quad \text{From his Thesis} \tag{3.3}$$

where $\alpha_{w/c}$ impacts only the sigmoid curve, $\alpha_{0.48} = 0.0065$ and $\alpha_{0.35} = 0.0160$, and β dampens the linear portion of the expansion. It was determined that $\beta = 0.3$ would yield good results.

(Kawabata, Yamada, Ogawa, Martin, Y., J.F., and Toutlemonde, 2016) have revisited this equation and adapted it to ASR as found it to provide a better model

$$\varepsilon(t) = \varepsilon^\infty \frac{1 - e^{-\frac{t}{\tau_c(T)}}}{1 + e^{-\frac{(t-\tau_l(T))}{\tau_c(T)}}} \left(1 - \frac{\Phi}{t + \delta}\right) \quad \text{Katayama} \tag{3.4}$$

The two parameters (Φ and δ) are only empirical and must satisfy $0 < \Phi < \delta$.

This formula, including a negative sign in the correction term, was used by Martin, Renaud, and Toutlemonde (2010) to describe long-term expanding behavior of delayed ettringite formation, and later by Kawabata, Yamada, Ogawa, Martin, Y., J.F., and Toutlemonde

(2016) for ASR expansion of alkali-wrapping concrete prisms that did not converge expansion in a short term.

3.5.2 Results

From the 58 individual expansion data fitting (In the appendix, Fig. A.9-A.16) and their summary in Fig. 3.7 (to be compared with FIg. 3.1 for Larive's model) . From these figures, we note that many projected values of ε^{∞} are unrealistically high, and as such this model will be discarded.

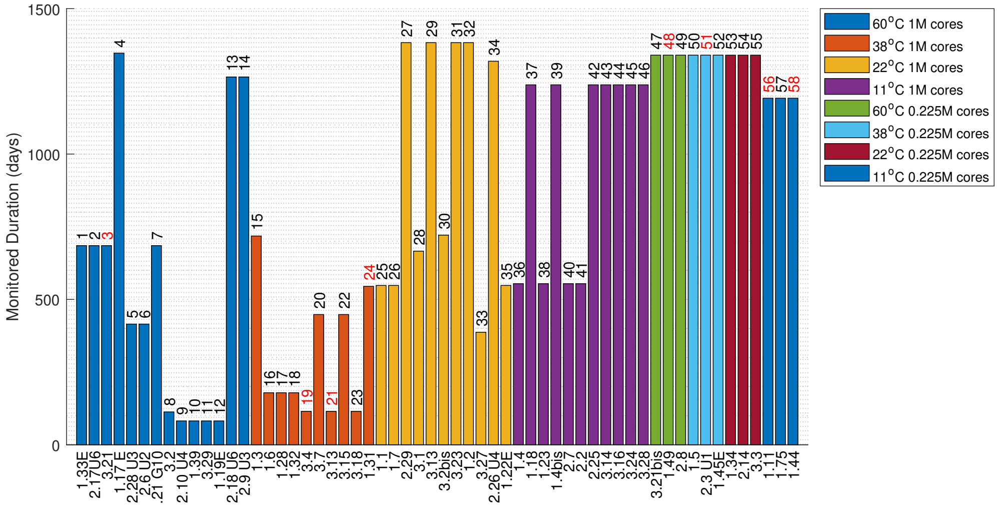

(a) Maximum recorded time

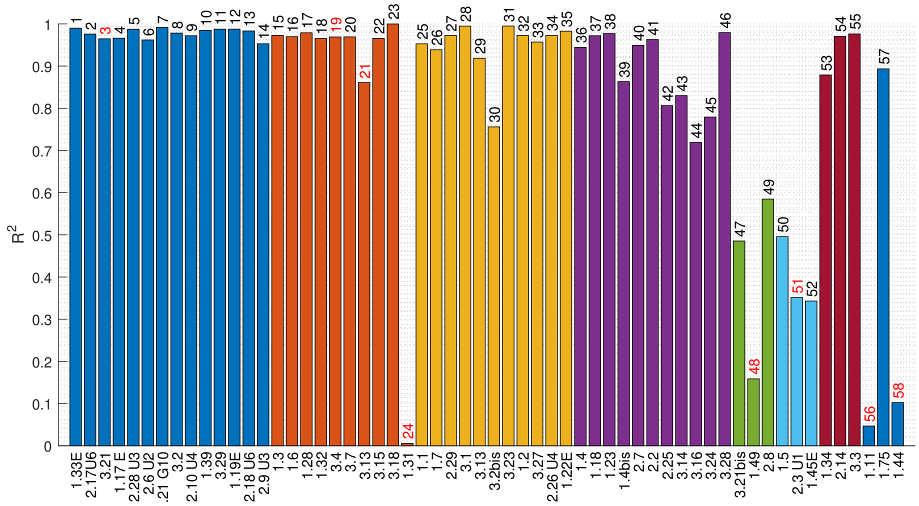

(b) R^2

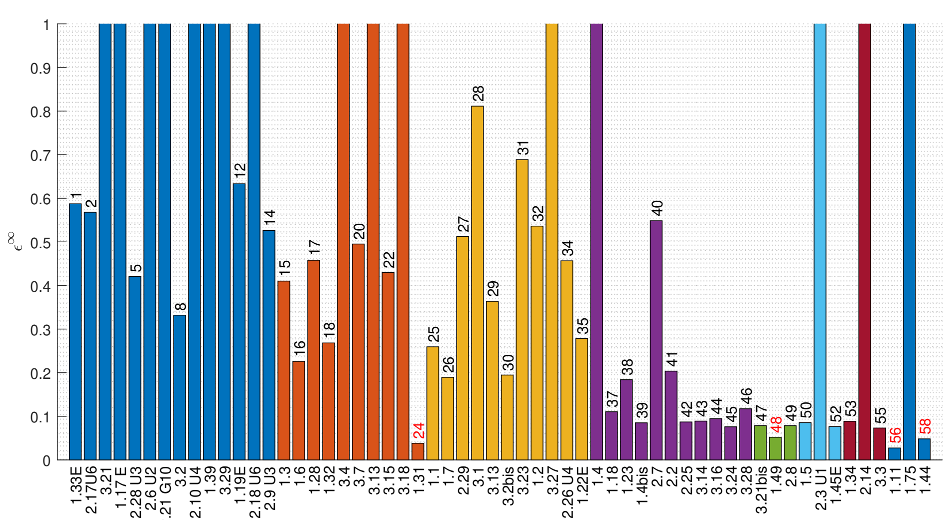

(c) Maximum expansionε^{∞}

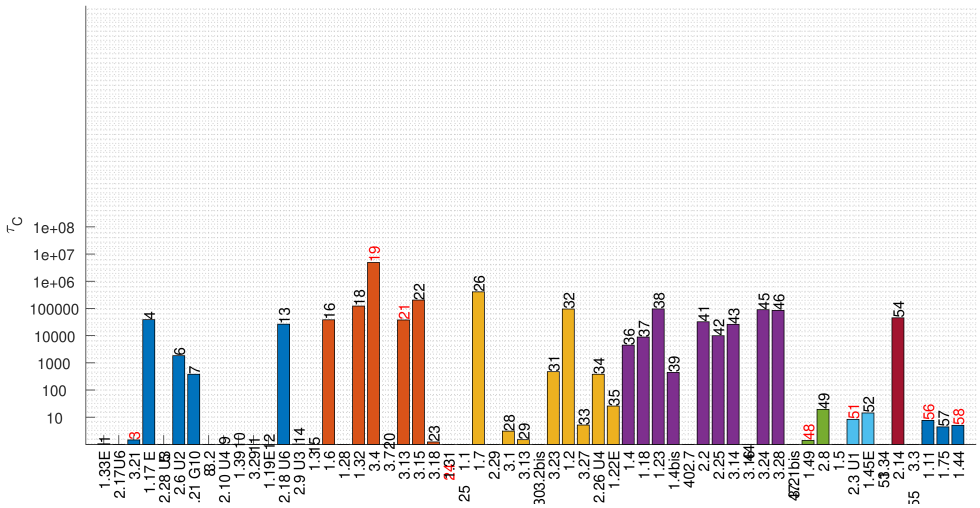

(d) Characterisitc times

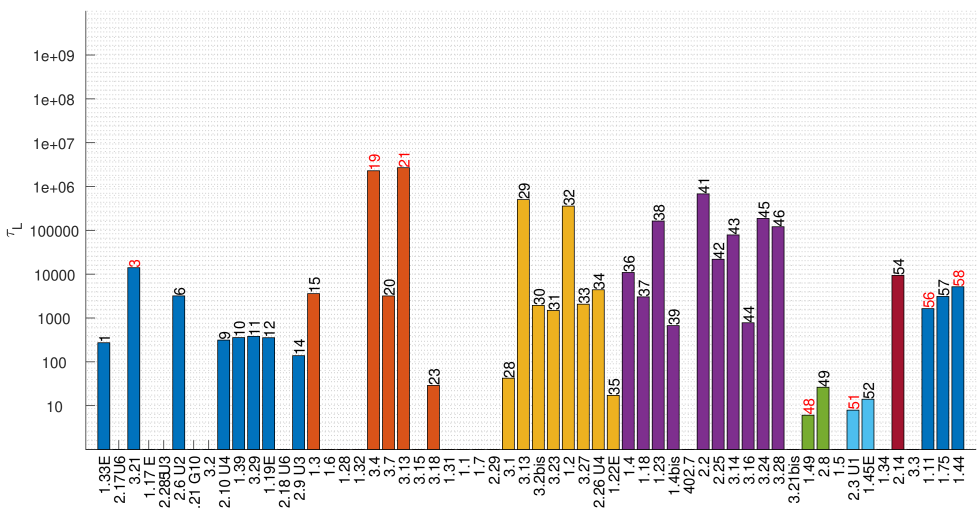

(e) Latency times

Figure 3.7: Brunetaud's Summary Expansion Results

Activation Energy

Activation energy for τ_c was determined for d_a=38mm cored stored in 1M NaOH solution. This will allow adjustment of AAR expansion properties for field conditions.

Data Reliability

That the determined value is very close to what is reported in the litterature "legitemizes" the reliability of a large segment of the recorded expansion measurements, and ensuing data analysis.

4 Degradation

Elastic modulus, compressive and splitting tensile strengths were recorded over a two years period according to the protocol shown in Fig. 2.5. Specimens were stored in 1M solution and at temperatures varying between 11 and 68°.

Measurements are shown in Table 4.1.

Some assumptions (based on context) had been made to address core id identification not starting with 1, 2 or 3.

ID	Original	Replaced by
33	2.20 G10	2.2
55	UG U2 INT. 4	3.91
56	UG U2 INT. 6	3.92
57	UG U2 INT. 8	3.93
58	UG U2 INT. 11	3.94
59	UG U2 INT. 3	3.95
60	UG U2 INT. 5	3.96
61	UG U2 INT. 7	3.97
62	UG U2 INT. 9	3.98

Based on this table, multiple plots were generated. Those are shown in Appendix B (Figs. B.1-B.7), and will be interpretated below.

4.1 Qualitative Observations

Raw data from the mechanical property degradation are reported in Appendix B (Figs. B.1-B.7), and they call for the following *qualitative* observations (which of course are corraborated by the previously determined correlation coefficients).

4.1.1 Class 1

1. Elastic modulus will decrease with time, Fig. B.1(a)
2. Expansion will cause decrese of the elastic modulus, B.1(b)
3. There is no clear correlation between core stroage temperature and elastic modulus, B.1(c)
4. Storage temperature impact on elastic modulus and expansion is not clear, B.1(d)

Table 4.1: Mechanical properties *vs.* time

	T °C	Core	Age days	ε^{AAR} %	E Gpa	f_c Mpa	f_s Mpa
1	22	1.1	548	0.1608			1.6
2	22	1.14	0	0	12.6	23	
3	60	1.15	119	0.1464			1.9
4	22	1.17	0	0			2.2
5	60	1.19	91	0.1476	9.2	23	
6	22	1.22	485	0.1864	9.1	23	
7	11	1.23	554	0.1548	10.7	21	
8	38	1.28	180	0.1512	7.7	22	
9	22	1.29	0	0	8.5	19	
10	22	1.3	0	0			2.6
11	38	1.3	545	0.299			2.1
12	38	1.30	663	0.3			
13	60	1.3	718	0.451			2.2
14	38	1.31	545	0.3	10	21	
15	22	1.32	485	0.1654	5.8	22	
16	38	1.32	180	0.1504			2.2
17	60	1.33	545	0.312			2.2
18	22	1.36	0	0			1.8
19	22	1.38	0	0	9.9	16	
20	60	1.39	91	0.1728			1.7
21	11	1.4	554	0.1534			1.5
22	60	1.51	323	0.346			1.8
23	22	1.55	0	0	15.4	26	
24	22	1.57	0	0	12.7	21	
25	22	1.58	0	0			2.7
26	38	1.6	180	0.1552			1.7
27	22	1.7	0	0	7.3	15	
28	22	1.70	548	0.158			2
29	22	1.74	0	0			2.7
30	22	1.8	0	0			1.6
31	60	2.10	91	0.152	8.8	23	

	T °C	Core	Age days	ε^{AAR} %	E Gpa	f_c Mpa	f_s Mpa
32	60	2.17	356	0.325	7.4	28	
33	11	2.20	468	0.1632	9.9	25	
34	60	2.21	685	0.455	9.7	25	
35	60	2.21	545	0.345			2.1
36	60	2.28	256	0.299	9.7	20	
37	60	2.6	415	0.366	8.3	22	
38	11	2.7	554	0.15			2
39	22	3.10	451	0.223	5.2	22	
40	38	3.13	112	0.236			1.9
41	38	3.15	448	0.327			2
42	38	3.18	112	0.1616	5.8	20	
43	38	3.19	545	0.323			2.5
44	22	3.20	721	0.334	12.4	28	
45	60	3.2	91	0.1436			2.1
46	60	3.21	718	0.454			1.9
47	22	3.25	0	0			1.9
48	22	3.26	0	0			2.5
49	22	3.27	387	0.2216			1.8
50	60	3.29	91	0.1576	5.7	21	
51	38	3.4	112	0.174	7.4	24	
52	22	3.5	0	0	14.9	28	
53	22	3.6	0	0	9.1	17	
54	38	3.7	448	0.305	7.8	21	
55	22	3.91	0	0	12.7	25	
56	22	3.92	0	0	8.5	22	
57	22	3.93	0	0	11	29	
58	22	3.94	0	0	13.6	29	
59	22	3.95	0	0			2.4
60	22	3.96	0	0			2.6
61	22	3.97	0	0			2.3
62	22	3.98	0	0			2

5. There is only a mild correlation between age and compressive strength, B.1(e)
6. Weak correlation between expansion and compressive strength, B.1(f)
7. Increase of storage temperature shows an effect to increase compressive strength, B.1(g)
8. Tensile strength reduces with time, B.1(h)
9. Expansion reduces the tensile strength, B.1(i)
10. Storage temperature does not have a significant impact on tensile strength, B.1(j)
11. Both age and Max. expansion reduce elastic modulus, B.2(a)
12. Neither age or Max. expansion have a significant impact on compressive strength, B.2(b)
13. Age will reduce the tensile strength, however, the impact of maximum expansion is difficult to ascertain B.2(c)

4.1.2 Class 2

1. Impact of time on elastic modulus is minimal, B.3(a)
2. Impact of maximum expansion on elastic modulus is minimal B.3(b)
3. High storage temperature (60°C) induce more expansion than lower ones (11°C), B.3(c)
4. High storage temperature (60°C) cause more reduction of elastic modulus than at lower ones (11°C), B.3(d)
5. There is an increase of compressive strength with time, B.3(e)
6. Increase of maximum xpansion does not significantly impact the compressive strength, B.3(f)
7. Storage temperature does not significantly impact the compressive strength, B.3(g)
8. Time causes a decrease of the tensile strength, B.3(h)
9. Increase of maximum expansion increases tensile strength (note we only have two data points), B.3(i)
10. High storage temperature (60°C) causes higher tensile strength (note we only have two data points), B.3(j)
11. Neither age nor maximum expansion do not significantly impact the elastic modulus, B.4(a)
12. Neither age nor maximum expansion impact significantly the tensile strength, B.4(b)

4.1.3 Class 3

1. Age does not significantly impact elastic modulus, B.5(a)
2. Maximum expansion does not significantly impact elastic modulus, B.5(b)
3. Higher storage temperature causes larger Max. expansion, B.5(c)
4. Higher storage temperature causes a decrease of the elastic modulus, B.5(d)
5. Age causes higher maximum expansion, but does not show significantly impact the compressive strength, B.5(e)
6. Maximum expansion does not significantly impact the compressive strength, B.5(f)
7. Higher storage temperature shows will reduce the compressive strength, B.5(g)
8. Agereduces the tensile strength, B.5(h)

9. Maximum expansion reduces the tensile strength, B.5(i)
10. Higher storage temperature has only a mild effect on the reduction of the tensile strength, B.5(j)
11. Both age and maximum expansion reduce elastic modulus, B.6(a)
12. Age increases the compressive strength, B.6(b)
13. Impact of age and maximum expansion on tensile strength is not clear, B.6(c)

4.1.4 E *vs.* f_c

1. For all three classes, there is a direct correlation between between elastic modulus and compressive strength, B.7(a), B.7(b), and B.7(c)
2. Increase of Max. expansion causes lower E/f_c, B.7(a), B.7(b), and B.7(c)
3. Since Class 2 does not have test results at 0% expansion, its range of elastic modulus is significantly lower than the other two classes, B.7(b)

4.2 Modeling

To each of the three mechanical properties (E, f_c and f_t), for each of the three concrete classes, are assosicated three characteristics: (strorage temperature, age of measurement, and correpsonding expansion). Hence, an initial assessment of the laboratory results can be performed by examining the correlation coefficients between those quantities.

4.2.1 Correlation Coefficients

A correlation coefficient r_{xy} between two vectors $\mathbf{x}$ and $\mathbf{y}$ (of equal length) is defined as the the covariance of the variables divided by the product of their standard deviations and is thus an indicator to the strength of relationship between them.

$$r_{xy} = \frac{\sum_{i=1}^{n}(x_i - \bar{x})(y_i - \bar{y})}{\sqrt{\sum_{i=1}^{n}(x_i - \bar{x})^2}\sqrt{\sum_{i=1}^{n}(y_i - \bar{y})^2}} \tag{4.1}$$

where n is the sample size, x_i, y_i the individual sampled values indexed with i, and $\bar{x}$, $\bar{y}$ are the mean values of the sample.

It is commonly assumesd that $0 < r_{xy} < \pm 0.3$ is indicative of a weak positive (negative) linear relationship; $0.3 < r_{xy} < \pm 0.7$ moderate relationship; $0.7 < r_{xy} < \pm 1.0$ strong relationship; whereas r_{xy} indicates that there is no linear relationship.

Plots of the correlation coefficients of the three concrete classes are given in Fig. B.8-B.10 and are reported in Table 4.2

The trends are consistent with what was qualitatively observed in the previous section, and now a *quantitative* assessment is reported.

However, a word of caution is imperative, not much should be read from the table as we have only limited number of data points, and some of those coefficients are driven by

Hwever, given the small sample size we should use caution in interpreting the correlations as several of them are spurious (e.g. 0.88) and are due to two values at the extremes.

Nevertheles,, they provide a reassuring indicator.

Table 4.2: Summary of concrete degradation observations

	E			fc			ft		
	1	2	3	1	2	3	1	2	3
Age	B.1(a)	B.3(a)	B.5(a)	B.1(e)	B.3(e)	B.5(e)	B.1(h)	B.3(h)	B.5(h)
	-0.33	0.22	-0.18	0.22	0.09	0.02	-0.27	-0.34	-0.31
Temperature	B.1(d)	B.3(d)	B.5(d)	B.1(g)	B.3(g)	B.5(g)	B.1(j)	B.3(j)	B.5(j)
	-0.19	-0.11	-0.60	0.21	0.17	-0.40	-0.08	-0.09	-0.04
Expansion	B.1(b)	B.3(b)	B.5(b)	B.1(f)	B.3(f)	B.5(f)	B.1(i)	B.3(i)	B.5(i)
	-0.37	0.1	-0.44	0.28	00.24	-0.16	-0.22	-0.28	-0.29

4.2.2 Means and Standard Deviations

Mean and Coefficient of Variation (standard deviation divided by mean) at time $t = 0$, $T = 22°\text{C}$) were first computed, Table 4.3

Table 4.3: Mean and CV of mechanical properties at $t = 0$ and $T = 22°$

	E		f_c		f_t	
Class	μ GPA	CV %	μ MPA	CV %	μ MPA	CV %
1	11.1	27.4	20.0	21.0	2.27	21.19
2	11.6		25.0	-	2.28	-
3	11.6	21.8	25.0	19.1	2.28	12.2

It should be noted that no reference tests were conducted for Class 2. From Table 2.1 Class 2 has the same compressive strength as class 3, and nearly the same cement content, Hence, Class2 means were assumed to be the same as those of class 3.

4.2.3 Normalized Values

Normalized values are plotted in Fig. 4.1-4.2. They provide an indicator of the degradation of mechanical properties with time in terms of expansion (only quantity thransferable from laboratory to field).

Data associated with Location 2 are not plotted as they found to be unreliable.

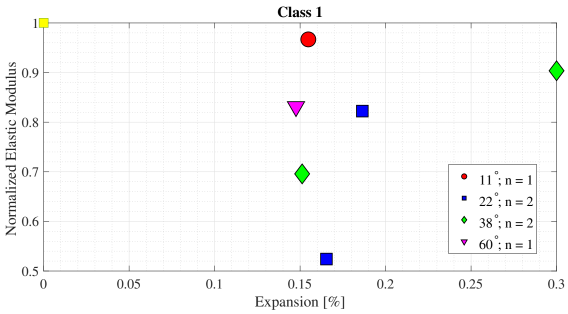

(a) E

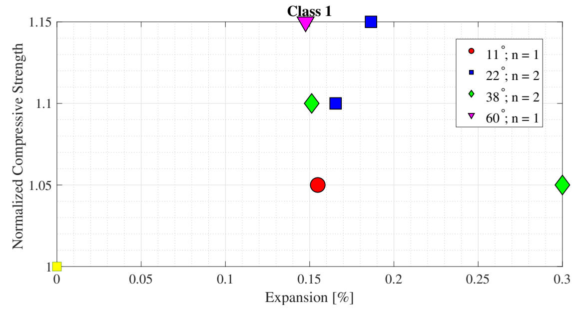

(b) f_c

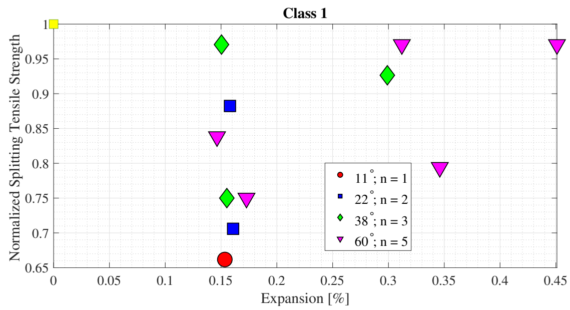

(c) f_t

Figure 4.1: Class 1: Normalized values

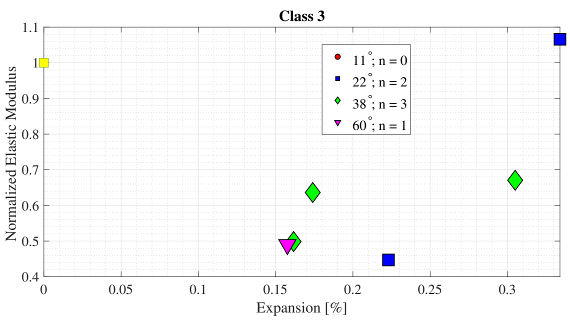

(a) E

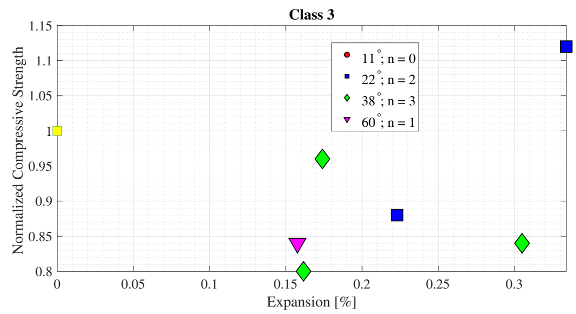

(b) f_c

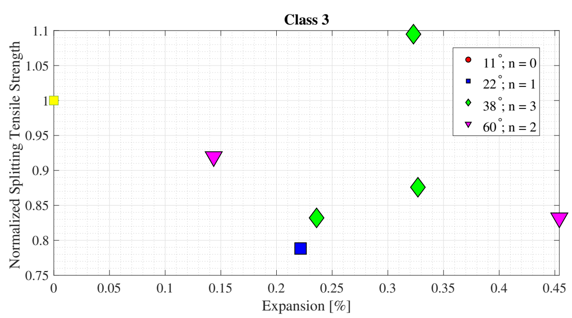

(c) f_t

Figure 4.2: Class 3: Normalized values

Mechanical Degradation

ELastic modulus, compressive and tensile strength were plotted, normalized and analyzed. All data exhibit large coefficient of variation.

5 Predictions

Whereas it is important to fully understand and interpret labroatory data, more consequential would be our ability to reasonably predict future expansion and degradation of the concrete.

Whereas such prediction is to be carefully interpretated given the various uncertainties, this i a critical step to a ubsequent predictive finite element simulation (addresed in §C).

5.1 Future Expansions

Having determined

- Mean expansion curves §3.3.1.
- Activation energy §3.4.

we can now project the *normalized expansion* (Eq. 1.1) beyond the last data point of E for dam temperatures equal to 11, 12, 14, 16, 18 degC for each of the three classes. Curves are shown in Fig. 5.1. We note that the anticipated peak expansion is likely to occur about 9 years after the the begining of testing (∼2024 if testing started in 2015).

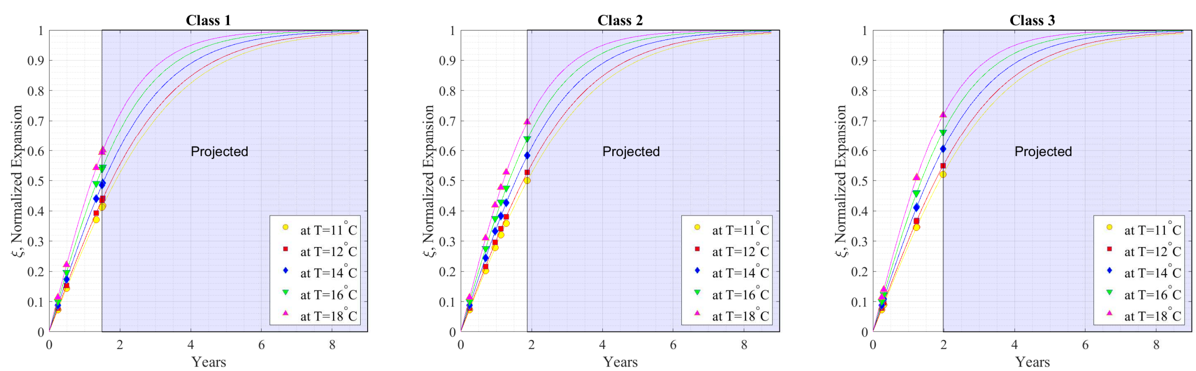

(a) Class 1 (b) Class 2 (c) Class 3

Figure 5.1: Projected expansions

5.2 Future Degradation

As there is no "First Principle" based model to quanitfy the deterioration in terms of either time (t) or normalized expansion $\xi(t,T)$, a "data-driven" one will be examined.

In this context, what we seek is the reduction in where $(.) = \left[\frac{E}{E_0}|\frac{fc}{fc_0}|\frac{ft}{ft_0}\right]$. Indeed, data is available for (.) in terms of both time (t) or expansion $()\xi$). As in the end, it is expansion, and not time, that induces deterioration, we opt to seek a model that capture ((.) in terms of ξ. The following simple exponential model is proposed:

$$(.) = \exp(\beta\xi) \tag{5.1}$$

As multiple measurements for a given test were made for a given class, data were normalized with respect to the largest one of them, (§4.2.3).

As to the expansion-time relationship it was obtained from the expansion tests addressed in §3, and more specifically table 3.2. Using the activation energy (§3.4)

The resulting models are shown in Fig. 5.2 and 5.3 for Class 1 and 3 concrete[1]. In those plots:

- The filled red circles correspond to the actual measurements.
- The blue line corresponds to Eq. 5.1.
- The fitted curve is expanded all the way to a fully degraded concrete with ξ=1.
- The red curve corresonds to the time-normalized expansion shown in Fig. 5.1.

Hence, to estimate how long would it take for say E/E_0 to drop from 1 (corresponding to a $\xi = 0$) to 0.3, one would first determine the corresponding $\xi = 0.35$ on the dashed blue line, then drop vertically to the red curve, and then horizontally to read the number of years (since testing).

A word of caution, the experimental data are not as consistent as they should be. The β means and as importantly the respective coefficients of variations (CV) are shon in Table 5.1. The CV are indeed significant.

Table 5.1: β coeffecients for degradation model

Class	Variable	Mean	CV
1	E	-3.40	46%
	f_c	-0.95	28%
	f_t	-1.96	58%
3	E	-3.89	55%
	f_c	-1.31	60%
	f_t	-1.01	57%

[1]No analysis was undertaken for Class 2 concrete as there was no sufficient data.

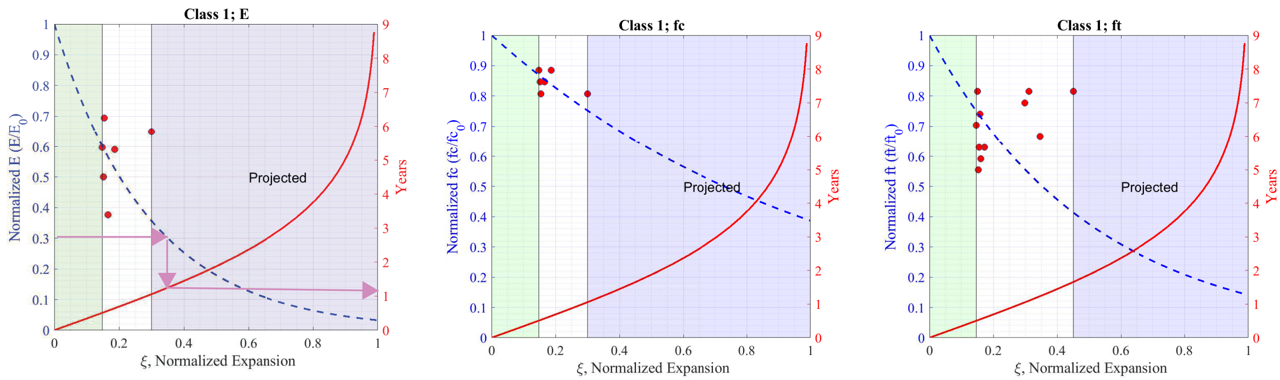

(a) E (b) f_c (c) ft

Figure 5.2: Projected deterioration for Class 1 concrete

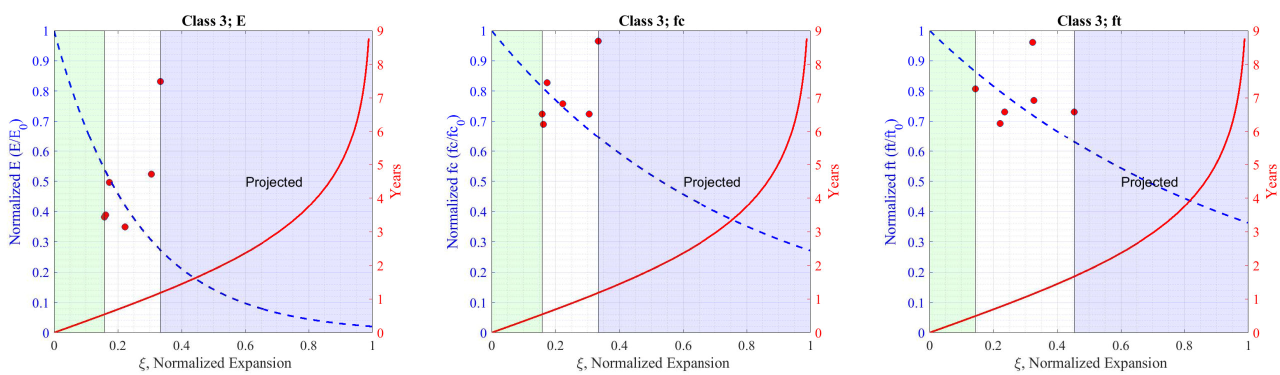

(a) E (b) f_c (c) ft

Figure 5.3: Projected deterioration for Class 3 concrete

Bibliography

Arrhenius, S. (1889). “On the Reaction Velocity of the Inversion of Cane Sugar by Acids”. In: *Zeitschrift für physikalische Chemie* 4, p. 226.

Brunetaud, X., L. Divet, and D. Damidot (2004). “Delayed ettringite formation: suggestion of a global mechanism in order to link previous hypotheses”. In: *Proc. 7th CANMET/ACI International Conference on recent Advances in Concrete technology*, pp. 63–76.

Capra, B. and J.P. Bournazel (1998). “Modeling of induced mechanical effects of alkali-aggregate reactions”. In: *Cement and Concrete Research* 28(2), pp. 251–260.

Comi, C., R. Fedele, and U. Perego (2009). “A chemo-thermo-damage model for the analysis of concrete dams affected by alkali-silica reaction”. In: *Mechanics of Materials* 41(3), pp. 210 –230.

Huang, H. and B. Spencer (2016). “Grizzly model for fully coupled heat transfer, moisture, diffusion, alkali-silica reaction and fractureing process in concrete”. In: *9th International Conference on Fracture Mechanics of Concrete and Concrete Structures; FraMCoS-9*. Ed. by V.E. Saouma, J. Bolander, and E. Landis. Berkeley, CA.

Joshi, Nirmal R, Thanadet Sriprasong, Shingo Asamoto, and Pakawat Sancharoen (2021). “Time-Dependent Deformation of a Concrete Arch Dam in Thailand-Numerical Study on Effect of Alkali Silica Reaction on Deflection of Arch”. In: *Journal of Advanced Concrete Technology* 19(3), pp. 181–195.

Kawabata, Y., K. Yamada, S. Ogawa, R.P. Martin, Sagawa Y., Seignol J.F., and F. Toutlemonde (2016). “Correlation between laboratory expansion and field expansion of concrete: prediction based on modified concrete expansion test”. In: *Proc. 15th International Conference on Alkali-Aggregate Reaction (ICAAR)*. Sao Paolo, Brasil.

Larive, C. (1998). *Apports Combinés de l’Experimentation et de la Modélisation à la Comprehension del’Alcali-Réaction et de ses Effets Mécaniques*. Tech. rep. *In French*. Paris: *Ecole Normale des Ponts et Chaussées*.

Malla, S. and M. Wieland (1999). “Analysis of an arch-gravity dam with a horizontal crack”. In: *Computers & Structures* 72(1), pp. 267–278.

Martin, R.P., J.C. Renaud, and F. Toutlemonde (June 2010). “Experimental investigations concerning combined delayed ettringite formation and alkali aggregate reaction”. In: *6th International conference on concrete under severe conditions CONSEC10*. Mexico, 8p.

Moffatt, T. and M Thomas (2018). *Predicting Residual Expansion and Changes in Mechanical Properties of the Concrete at Mactaquac Generating Station*. Tech. rep. Department of Civil Engineering, University of New Brunswick.

Multon, S. and F. Toutlemonde (2006). “Effect of Applied Stresses on Alkali-Silica Reaction Induced Expansions”. In: *Cement and Concrete Research* 36(5), pp. 912–920.

NOAA (2013). *Satellite and Information Servis (NESDIS)*.

Saouma, V.E., ed. (2020). *Diagnosis & Prognosis of AAR Affected Structures; State-of-the-Art Report of the RILEM Technical Committee 259-ISR*. Springer Nature.

Saouma, V.E. and M.Z. Hariri-Ardebili (2021). *Aging, Shaking and Cracking of Infrastructures; From Mechanics to Concrete Dams and Nuclear Structures*. Ed. by Springer. Springer-Nature.

Saouma, V.E., R. Martin, M.A. Hariri-Ardebili, and T. Katayama (2015). "A Mathematical Model for the Kinetics of the Alkali-Silica Chemical Reaction". In: *Cement and Concrete Research* 68, pp. 184–195.

Saouma, V.E., L. Perotti, and T. Shimpo (2007). "Stress Analysis of Concrete Structures Subjected to Alkali-Aggregate Reactions". In: *ACI Materials Journal* 104(5), pp. 532–541.

Saouma, V.E., J. Červenka, and R.W. Reich (2010). *Merlin Finite Element User's Manual*.

Saouma, V.E. (2014). *Numerical Modeling of AAR*. 324 pages. CRC Press.

Sellier, A., E. Bourdarot, S. Multon, M. Cyr, and E. Grimal (2009). "Combination of structural monitoring and laboratory tests for assessment of alkali aggregate reaction swelling: application to gate structure dam". In: *ACI Material Journal*, pp. 281–290.

Ulm, F., O. Coussy, L. Kefei, and C. Larive (2000). "Thermo-Chemo-Mechanics of ASR Expansion in Concrete Structures". In: *ASCE J. of Engineering Mechanics* 126(3), pp. 233–242.

A Expansion Figures

This appendix illustrates the expansions of each of the 58 specimens.

A.1 Larive Model

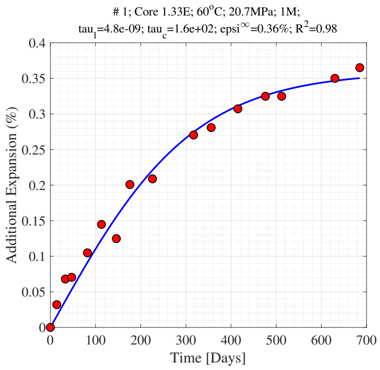

(a) #1; 1.33E; 60°C; 20.7MPa; d$_a$=75mm; 1M; τ_l=0.0; τ_c=158; ε^∞=0.36; R^2= 0.98

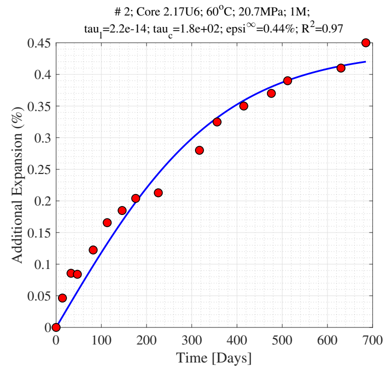

(b) #2; 2.17U6; 60°C; 20.7MPa; d$_a$=75mm; 1M; τ_l=0.0; τ_c=181; ε^∞=0.44; R^2= 0.97

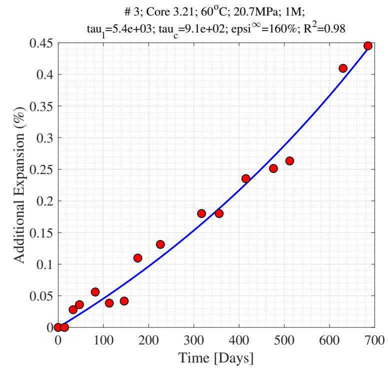

(c) #3; 3.21; 60°C; 20.7MPa; d$_a$=38mm; 1M; τ_l=5441.5; τ_c=905; ε^∞=159.96; R^2= 0.98

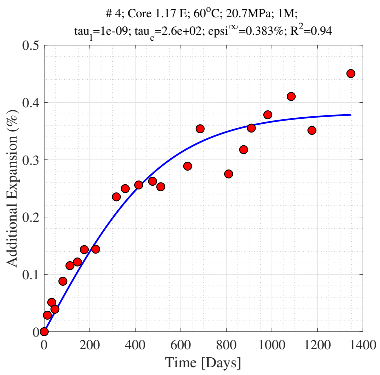

(d) #4; 1.17 E; 60°C; 20.7MPa; d$_a$=75mm; 1M; τ_l=0.0; τ_c=262; ε^∞=0.38; R^2= 0.94

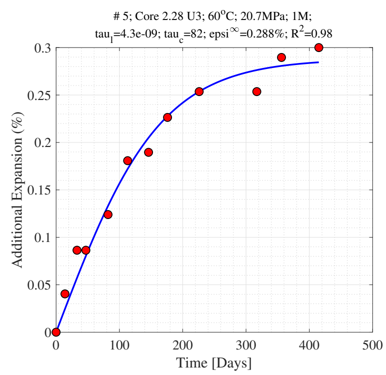

(e) #5; 2.28 U3; 60°C; 20.7MPa; d$_a$=75mm; 1M; τ_l=0.0; τ_c=82; ε^∞=0.29; R^2= 0.98

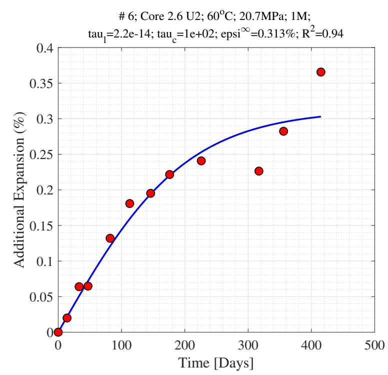

(f) #6; 2.6 U2; 60°C; 20.7MPa; d$_a$=75mm; 1M; τ_l=0.0; τ_c=101; ε^∞=0.31; R^2= 0.94

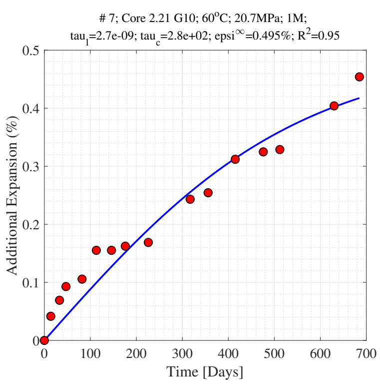

(g) #7; 2.21 G10; 60°C; 20.7MPa; d$_a$=75mm; 1M; τ_l=0.0; τ_c=277; ε^∞=0.49; R^2= 0.95

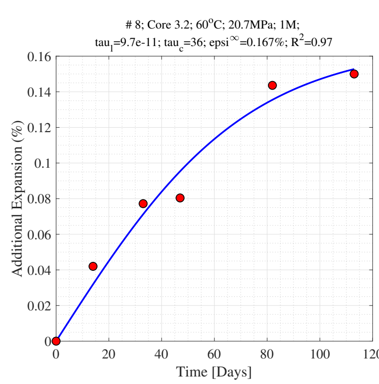

(h) #8; 3.2; 60°C; 20.7MPa; d$_a$=38mm; 1M; τ_l=0.0; τ_c=36; ε^∞=0.17; R^2= 0.97

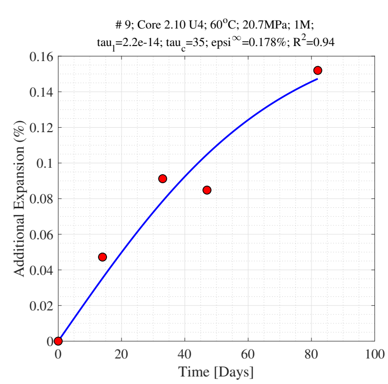

(i) #9; 2.10 U4; 60°C; 20.7MPa; d$_a$=75mm; 1M; τ_l=0.0; τ_c=35; ε^∞=0.18; R^2= 0.94

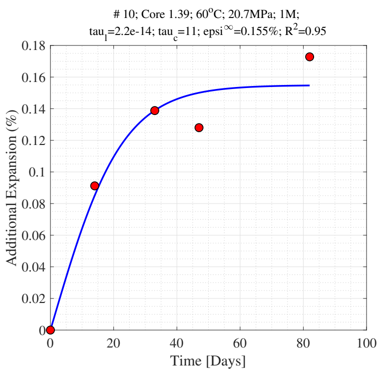

(j) #10; 1.39; 60°C; 20.7MPa; d$_a$=75mm; 1M; τ_l=0.0; τ_c=11; ε^∞=0.15; R^2= 0.95

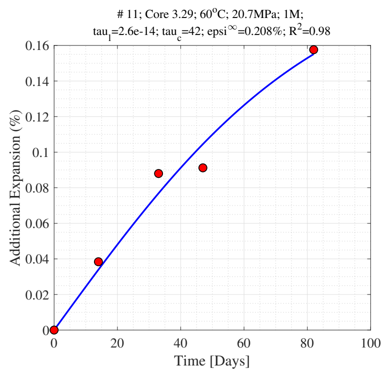

(k) #11; 3.29; 60°C; 20.7MPa; d$_a$=38mm; 1M; τ_l=0.0; τ_c=42; ε^∞=0.21; R^2= 0.98

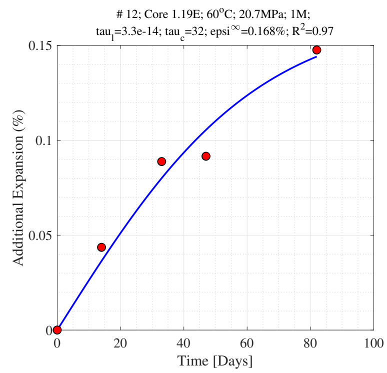

(l) #12; 1.19E; 60°C; 20.7MPa; d$_a$=75mm; 1M; τ_l=0.0; τ_c=32; ε^∞=0.17; R^2= 0.97

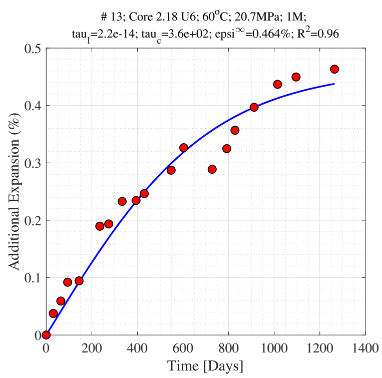

(m) #13; 2.18 U6; 60°C; 20.7MPa; d$_a$=75mm; 1M; τ_l=0.0; τ_c=358; ε^∞=0.46; R^2= 0.96

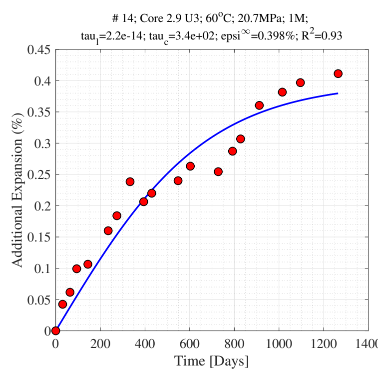

(n) #14; 2.9 U3; 60°C; 20.7MPa; d$_a$=75mm; 1M; τ_l=0.0; τ_c=336; ε^∞=0.40; R^2= 0.93

Figure A.1: Expansion curve for 60° 1M cores

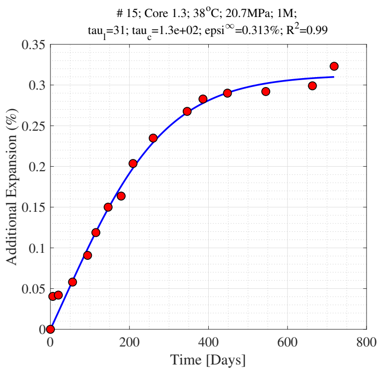

(a) #15; 1.3; 38°C; 20.7MPa; d$_a$=75mm; 1M; τ_l=31.2; τ_c=131; ε^∞=0.31; R^2= 0.99

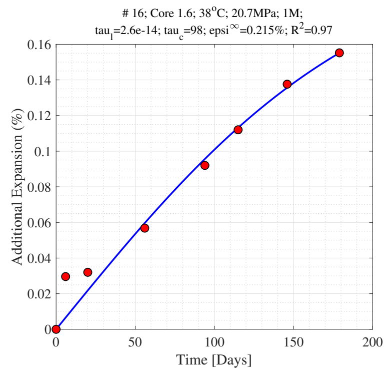

(b) #16; 1.6; 38°C; 20.7MPa; d$_a$=75mm; 1M; τ_l=0.0; τ_c=98; ε^∞=0.22; R^2= 0.97

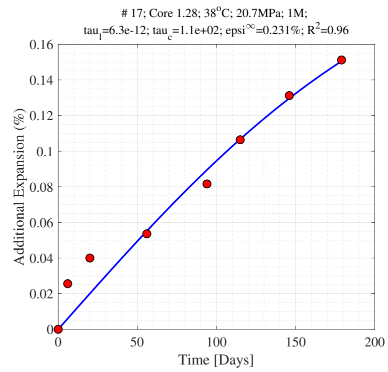

(c) #17; 1.28; 38°C; 20.7MPa; d$_a$=75mm; 1M; τ_l=0.0; τ_c=115; ε^∞=0.23; R^2= 0.96

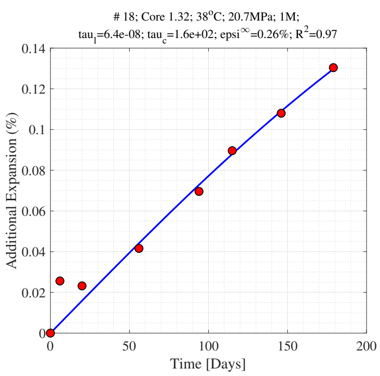

(d) #18; 1.32; 38°C; 20.7MPa; d$_a$=75mm; 1M; τ_l=0.0; τ_c=163; ε^∞=0.26; R^2= 0.97

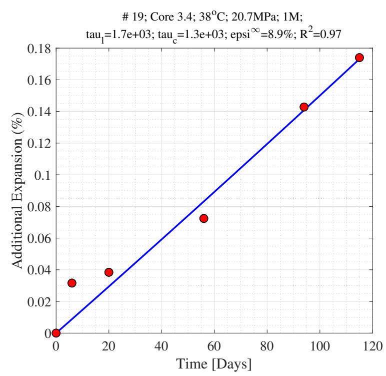

(e) #19; 3.4; 38°C; 20.7MPa; d$_a$=38mm; 1M; τ_l=1687.7; τ_c=1254; ε^∞=8.90; R^2= 0.97

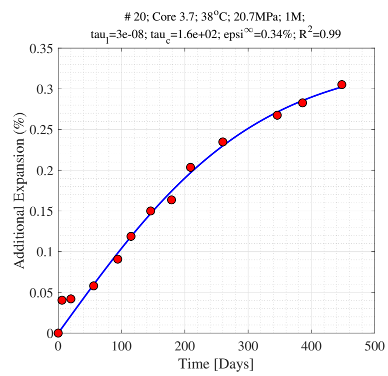

(f) #20; 3.7; 38°C; 20.7MPa; d$_a$=38mm; 1M; τ_l=0.0; τ_c=158; ε^∞=0.34; R^2= 0.99

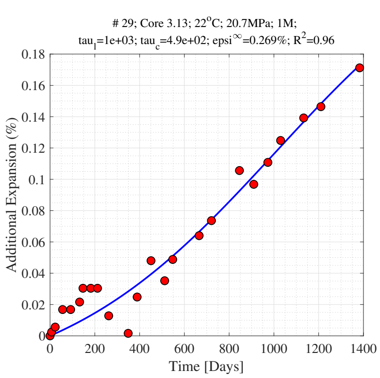

(g) #21; 3.13; 38°C; 20.7MPa; d$_a$=38mm; 1M; τ_l=781.3; τ_c=98; ε^∞=303.52; R^2= 0.86

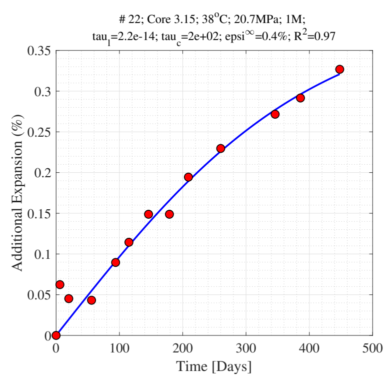

(h) #22; 3.15; 38°C; 20.7MPa; d$_a$=38mm; 1M; τ_l=0.0; τ_c=203; ε^∞=0.40; R^2= 0.97

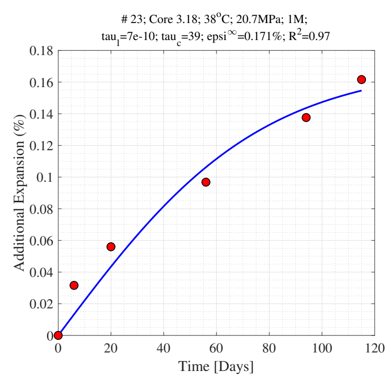

(i) #23; 3.18; 38°C; 20.7MPa; d$_a$=38mm; 1M; τ_l=0.0; τ_c=39; ε^∞=0.17; R^2= 0.97

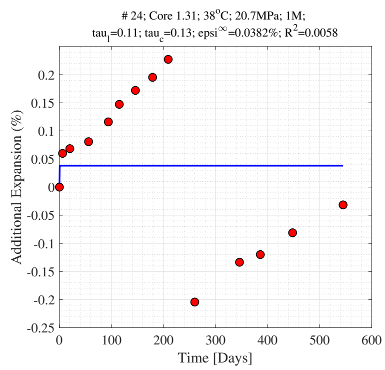

(j) #24; 1.31; 38°C; 20.7MPa; d_a=75mm; 1M; τ_l=0.1; τ_c=0; ε^{∞}=0.04; R^2= 0.01

Figure A.2: Expansion curve for 38° 1M cores

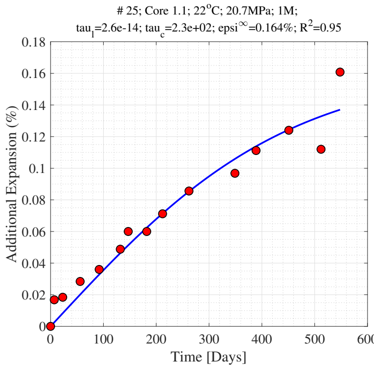

(a) #25; 1.1; 22°C; 20.7MPa; d$_a$=75mm; 1M; τ_l=0.0; τ_c=227; ε^∞=0.16; R^2= 0.95

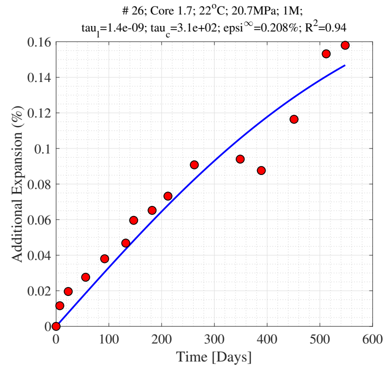

(b) #26; 1.7; 22°C; 20.7MPa; d$_a$=75mm; 1M; τ_l=0.0; τ_c=311; ε^∞=0.21; R^2= 0.94

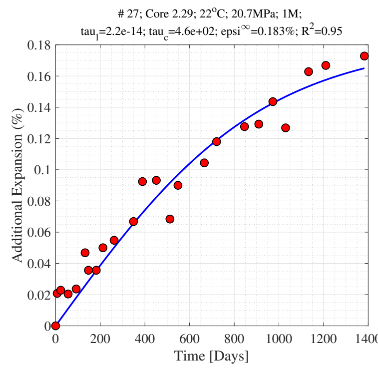

(c) #27; 2.29; 22°C; 20.7MPa; d$_a$=75mm; 1M; τ_l=0.0; τ_c=464; ε^∞=0.18; R^2= 0.95

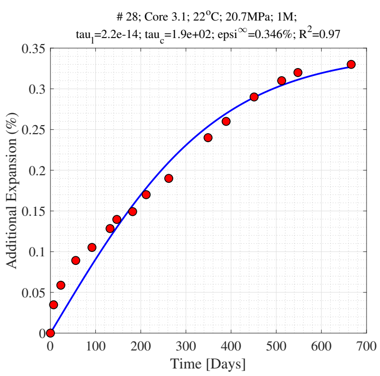

(d) #28; 3.1; 22°C; 20.7MPa; d$_a$=38mm; 1M; τ_l=0.0; τ_c=186; ε^∞=0.35; R^2= 0.97

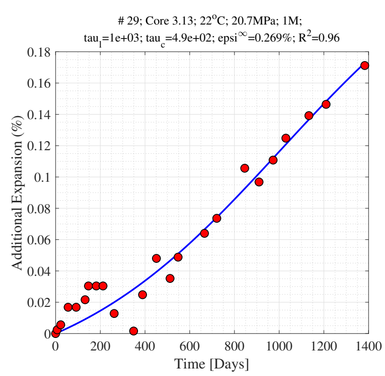

(e) #29; 3.13; 22°C; 20.7MPa; d$_a$=38mm; 1M; τ_l=1008.3; τ_c=491; ε^∞=0.27; R^2= 0.96

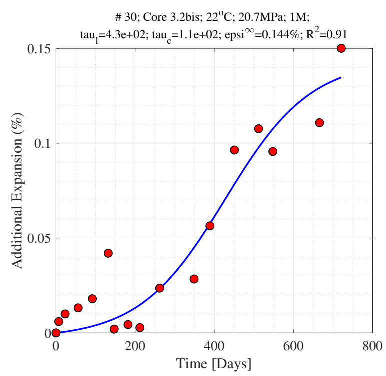

(f) #30; 3.2bis; 22°C; 20.7MPa; d$_a$=38mm; 1M; τ_l=427.7; τ_c=108; ε^∞=0.14; R^2= 0.91

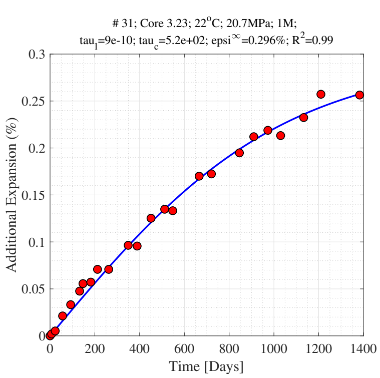

(g) #31; 3.23; 22°C; 20.7MPa; d$_a$=38mm; 1M; τ_l=0.0; τ_c=522; ε^∞=0.30; R^2= 0.99

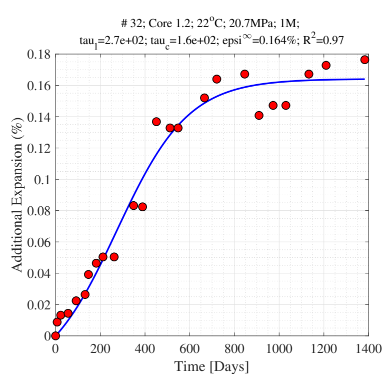

(h) #32; 1.2; 22°C; 20.7MPa; d$_a$=75mm; 1M; τ_l=273.6; τ_c=160; ε^∞=0.16; R^2= 0.97

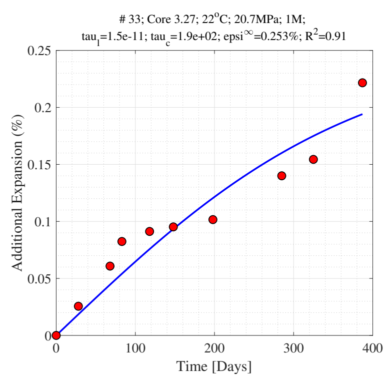

(i) #33; 3.27; 22°C; 20.7MPa; d$_a$=38mm; 1M; τ_l=0.0; τ_c=192; ε^∞=0.25; R^2= 0.91

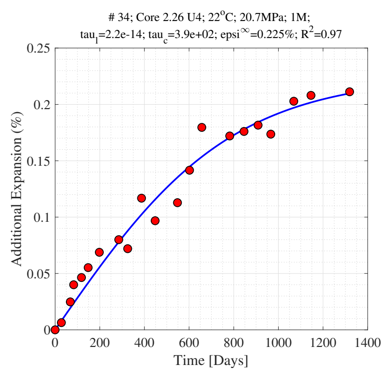

(j) #34; 2.26 U4; 22°C; 20.7MPa; d_a=75mm; 1M; τ_l=0.0; τ_c=394; ε^{∞}=0.23; R^2= 0.97

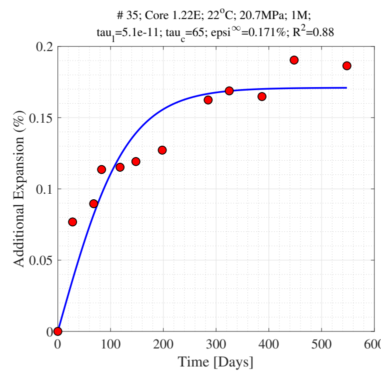

(k) #35; 1.22E; 22°C; 20.7MPa; d_a=75mm; 1M; τ_l=0.0; τ_c=65; ε^{∞}=0.17; R^2= 0.88

Figure A.3: Expansion curve for 22° 1M cores

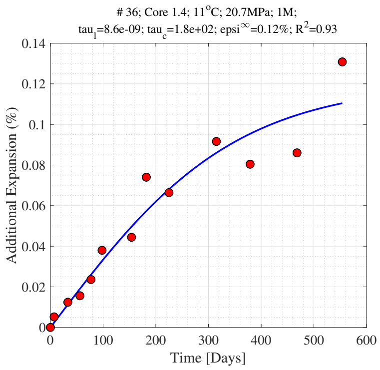

(a) #36; 1.4; 11°C; 20.7MPa; d$_a$=75mm; 1M; τ_l=0.0; τ_c=175; ε^∞=0.12; R^2= 0.93

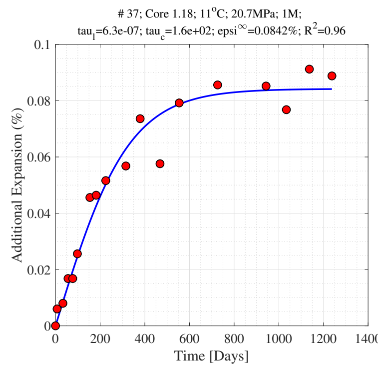

(b) #37; 1.18; 11°C; 20.7MPa; d$_a$=75mm; 1M; τ_l=0.0; τ_c=163; ε^∞=0.08; R^2= 0.96

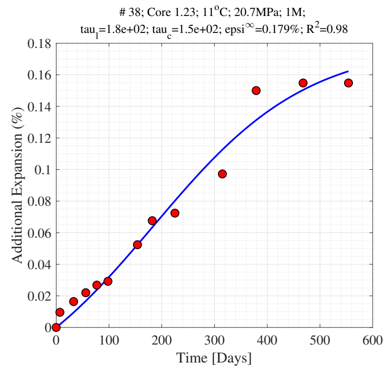

(c) #38; 1.23; 11°C; 20.7MPa; d$_a$=75mm; 1M; τ_l=184.2; τ_c=146; ε^∞=0.18; R^2= 0.98

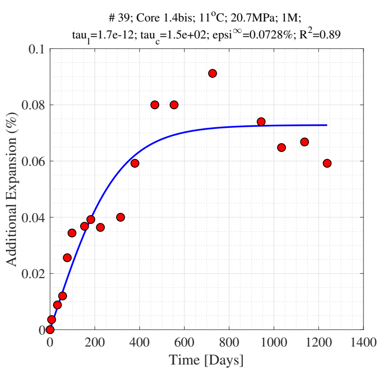

(d) #39; 1.4bis; 11°C; 20.7MPa; d$_a$=75mm; 1M; τ_l=0.0; τ_c=150; ε^∞=0.07; R^2= 0.89

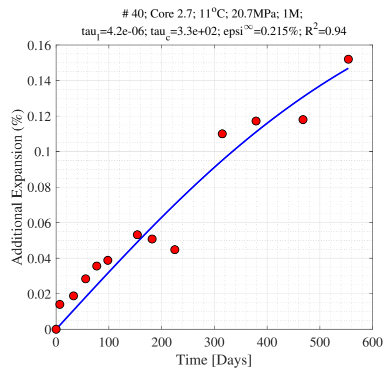

(e) #40; 2.7; 11°C; 20.7MPa; d$_a$=75mm; 1M; τ_l=0.0; τ_c=331; ε^∞=0.21; R^2= 0.94

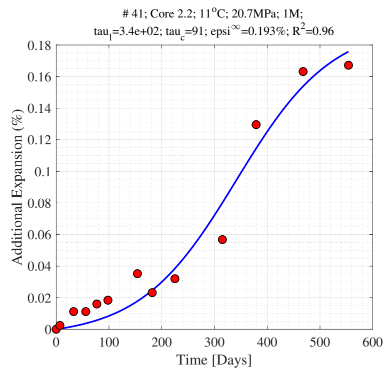

(f) #41; 2.2; 11°C; 20.7MPa; d$_a$=75mm; 1M; τ_l=341.3; τ_c=91; ε^∞=0.19; R^2= 0.96

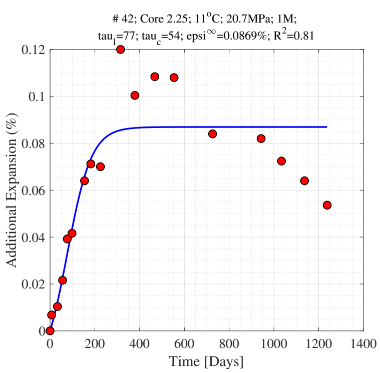

(g) #42; 2.25; 11°C; 20.7MPa; d$_a$=75mm; 1M; τ_l=76.8; τ_c=54; ε^∞=0.09; R^2= 0.81

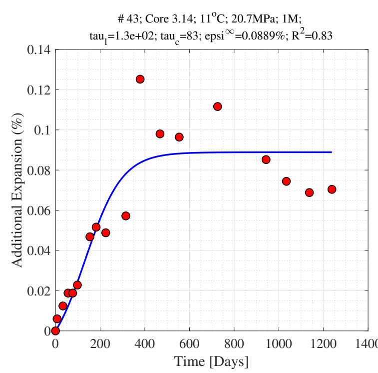

(h) #43; 3.14; 11°C; 20.7MPa; d$_a$=38mm; 1M; τ_l=133.8; τ_c=83; ε^∞=0.09; R^2= 0.83

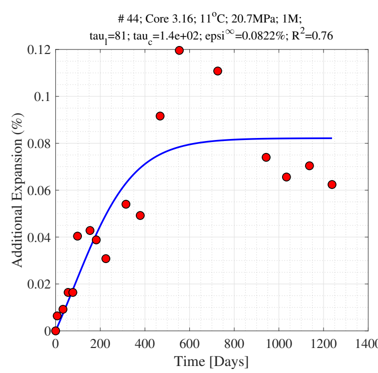

(i) #44; 3.16; 11°C; 20.7MPa; d$_a$=38mm; 1M; τ_l=81.1; τ_c=135; ε^∞=0.08; R^2= 0.76

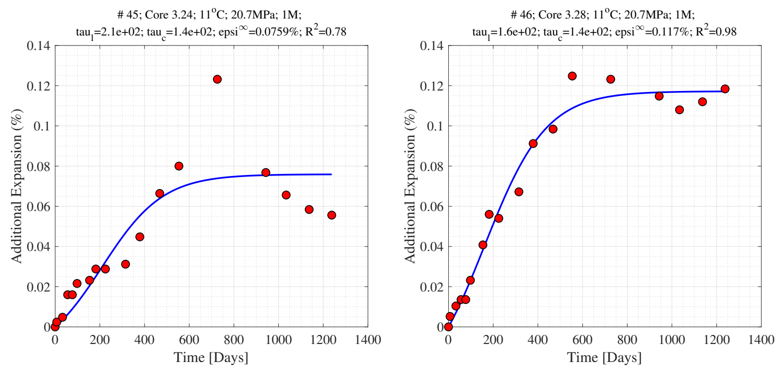

(j) #45; 3.24; 11°C; 20.7MPa; d_a=38mm; 1M; τ_l=210.1; τ_c=136; ε^{∞}=0.08; R^2= 0.78

(k) #46; 3.28; 11°C; 20.7MPa; d_a=38mm; 1M; τ_l=161.2; τ_c=138; ε^{∞}=0.12; R^2= 0.98

Figure A.4: Expansion curve for 11° 1M cores

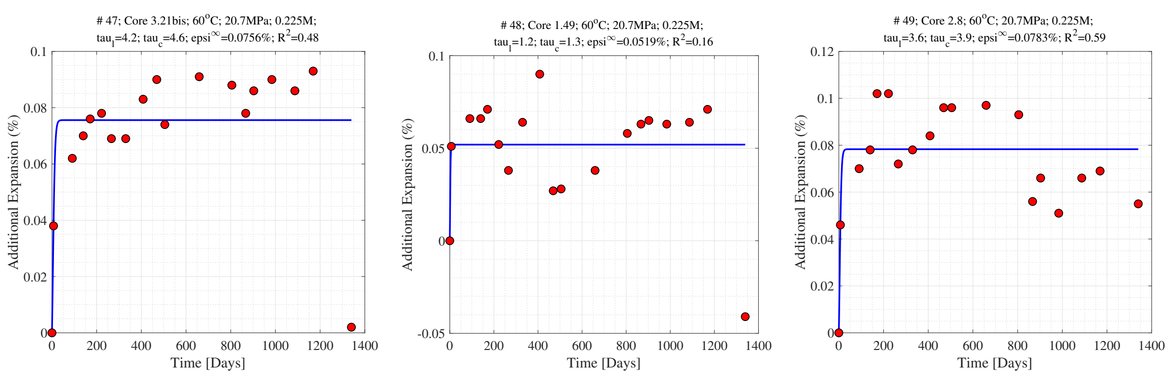

(a) #47; 3.21bis; 60°C; 20.7MPa; d_a=38mm; 0.225M; τ_l=4.2; τ_c=5; ε^{∞}=0.08; R^2= 0.48

(b) #48; 1.49; 60°C; 20.7MPa; d_a=75mm; 0.225M; τ_l=1.2; τ_c=1; ε^{∞}=0.05; R^2= 0.16

(c) #49; 2.8; 60°C; 20.7MPa; d_a=75mm; 0.225M; τ_l=3.6; τ_c=4; ε^{∞}=0.08; R^2= 0.59

Figure A.5: Expansion curve for 60° 0.225M cores

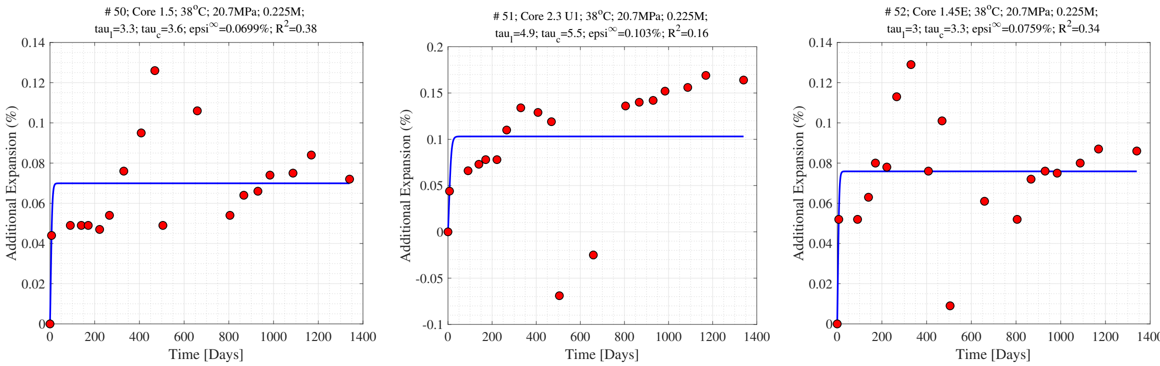

(a) #50; 1.5; 38°C; 20.7MPa; d$_a$=75mm; 0.225M; τ_l=3.3; τ_c=4; ε^∞=0.07; R^2= 0.38

(b) #51; 2.3 U1; 38°C; 20.7MPa; d$_a$=75mm; 0.225M; τ_l=4.9; τ_c=6; ε^∞=0.10; R^2= 0.16

(c) #52; 1.45E; 38°C; 20.7MPa; d$_a$=75mm; 0.225M; τ_l=3.0; τ_c=3; ε^∞=0.08; R^2= 0.34

Figure A.6: Expansion curve for 38° 0.225M cores

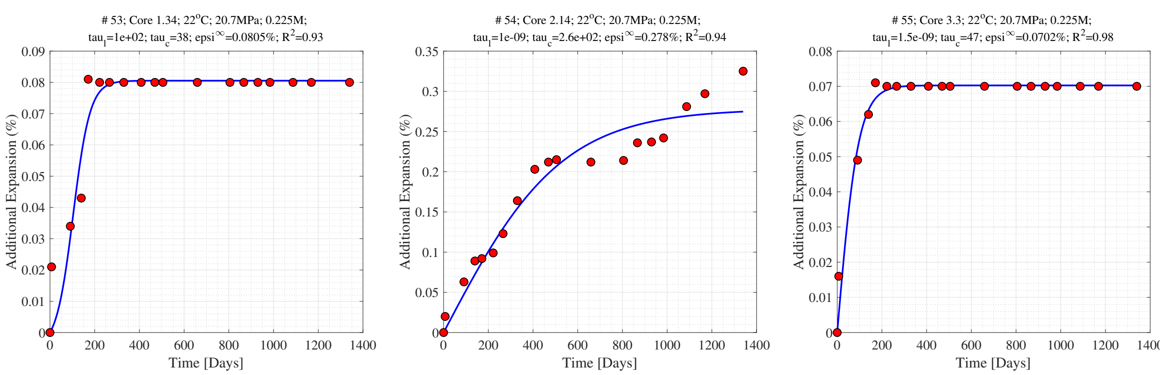

(a) #53; 1.34; 22°C; 20.7MPa; d$_a$=75mm; 0.225M; τ_l=103.8; τ_c=38; ε^∞=0.08; R^2= 0.93

(b) #54; 2.14; 22°C; 20.7MPa; d$_a$=75mm; 0.225M; τ_l=0.0; τ_c=263; ε^∞=0.28; R^2= 0.94

(c) #55; 3.3; 22°C; 20.7MPa; d$_a$=38mm; 0.225M; τ_l=0.0; τ_c=47; ε^∞=0.07; R^2= 0.98

Figure A.7: Expansion curve for 22° 0.225M cores

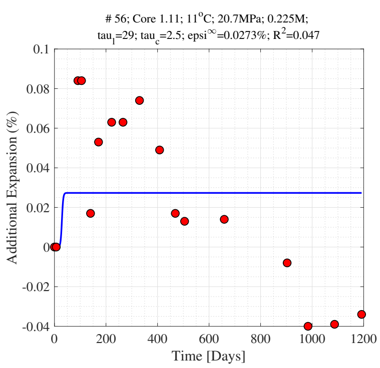

(a) #56; 1.11; 11°C; 20.7MPa; d$_a$=75mm; 0.225M; τ_l=29.0; τ_c=3; ε^∞=0.03; R^2= 0.05

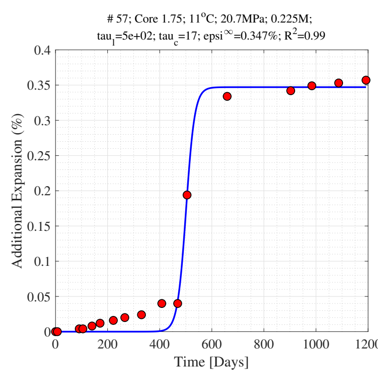

(b) #57; 1.75; 11°C; 20.7MPa; d$_a$=75mm; 0.225M; τ_l=501.3; τ_c=17; ε^∞=0.35; R^2= 0.99

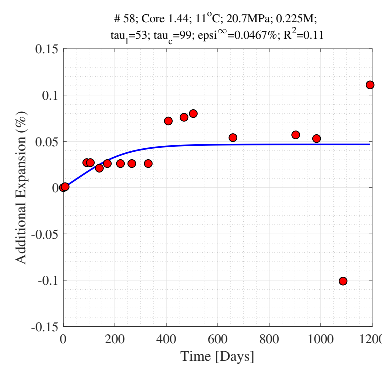

(c) #58; 1.44; 11°C; 20.7MPa; d$_a$=75mm; 0.225M; τ_l=53.2; τ_c=99; ε^∞=0.05; R^2= 0.11

Figure A.8: Expansion curve for 11° 0.225M cores

A.2 Brunetaud Model

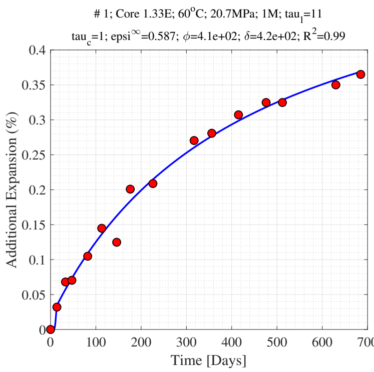

(a) #1; 1.33E; 60°C; 20.7MPa; d$_a$=75mm; 1M; τ_l=11.4; τ_c=1; ε^∞=0.59; R^2= 0.99

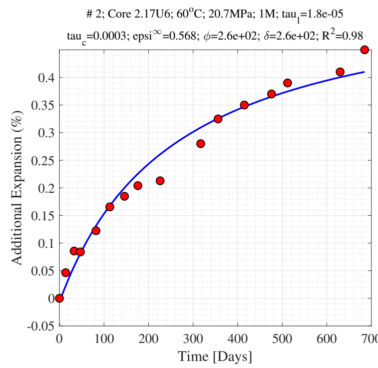

(b) #2; 2.17U6; 60°C; 20.7MPa; d$_a$=75mm; 1M; τ_l=0.0; τ_c=0; ε^∞=0.57; R^2= 0.98

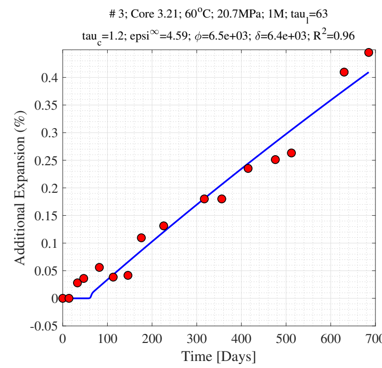

(c) #3; 3.21; 60°C; 20.7MPa; d$_a$=38mm; 1M; τ_l=63.3; τ_c=1; ε^∞=4.59; R^2= 0.96

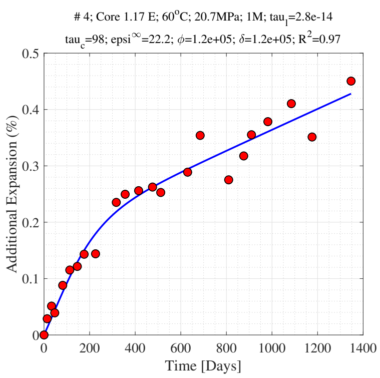

(d) #4; 1.17 E; 60°C; 20.7MPa; d$_a$=75mm; 1M; τ_l=0.0; τ_c=98; ε^∞=22.15; R^2= 0.97

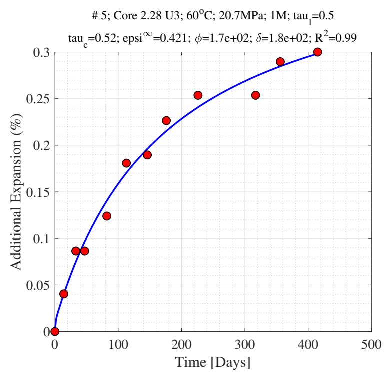

(e) #5; 2.28 U3; 60°C; 20.7MPa; d$_a$=75mm; 1M; τ_l=0.5; τ_c=1; ε^∞=0.42; R^2= 0.99

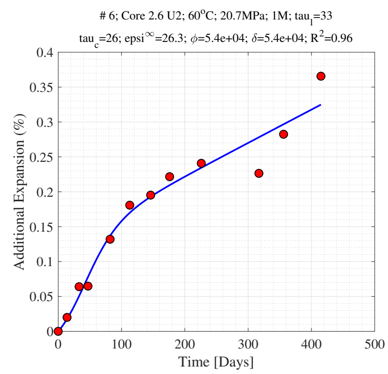

(f) #6; 2.6 U2; 60°C; 20.7MPa; d$_a$=75mm; 1M; τ_l=33.3; τ_c=26; ε^∞=26.33; R^2= 0.96

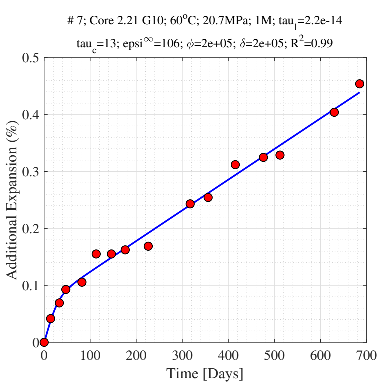

(g) #7; 2.21 G10; 60°C; 20.7MPa; d$_a$=75mm; 1M; τ_l=0.0; τ_c=13; ε^∞=106.20; R^2= 0.99

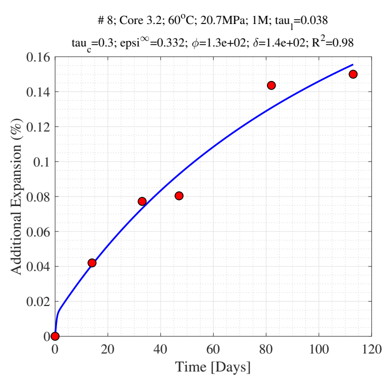

(h) #8; 3.2; 60°C; 20.7MPa; d$_a$=38mm; 1M; τ_l=0.0; τ_c=0; ε^∞=0.33; R^2= 0.98

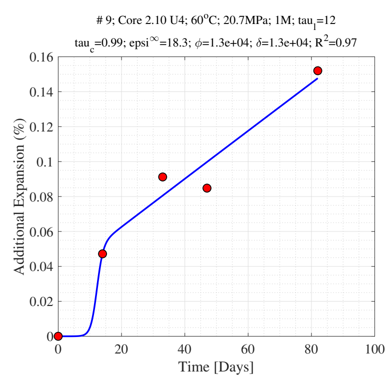

(i) #9; 2.10 U4; 60°C; 20.7MPa; d$_a$=75mm; 1M; τ_l=12.1; τ_c=1; ε^∞=18.28; R^2= 0.97

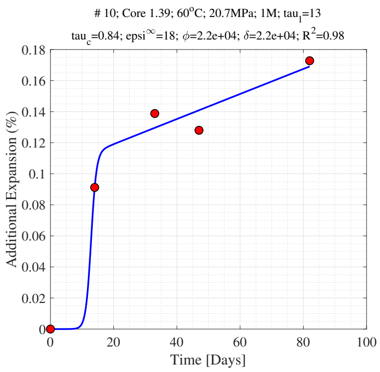

(j) #10; 1.39; 60°C; 20.7MPa; d$_a$=75mm; 1M; τ_l=12.8; τ_c=1; ε^∞=17.98; R^2= 0.98

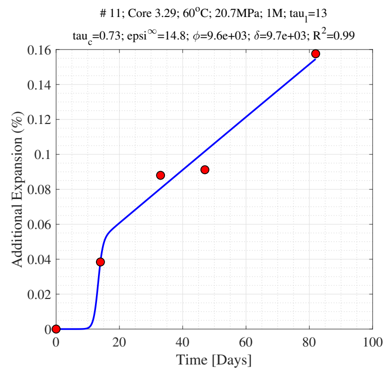

(k) #11; 3.29; 60°C; 20.7MPa; d$_a$=38mm; 1M; τ_l=13.2; τ_c=1; ε^∞=14.80; R^2= 0.99

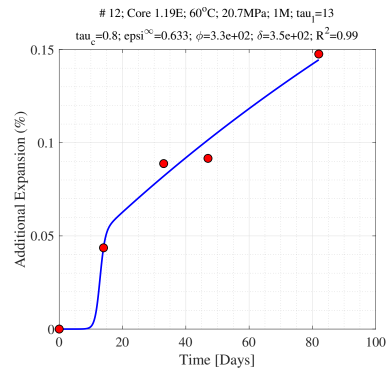

(l) #12; 1.19E; 60°C; 20.7MPa; d$_a$=75mm; 1M; τ_l=12.8; τ_c=1; ε^∞=0.63; R^2= 0.99

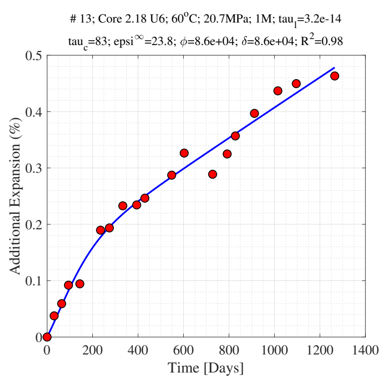

(m) #13; 2.18 U6; 60°C; 20.7MPa; d$_a$=75mm; 1M; τ_l=0.0; τ_c=83; ε^∞=23.82; R^2= 0.98

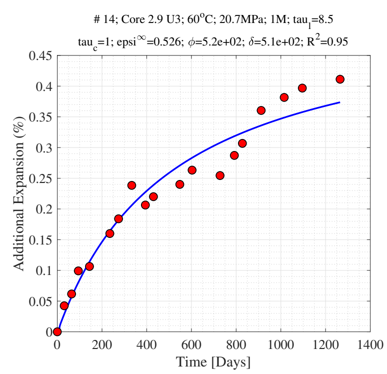

(n) #14; 2.9 U3; 60°C; 20.7MPa; d$_a$=75mm; 1M; τ_l=8.5; τ_c=1; ε^∞=0.53; R^2= 0.95

Figure A.9: Expansion curve for 60° 1M cores

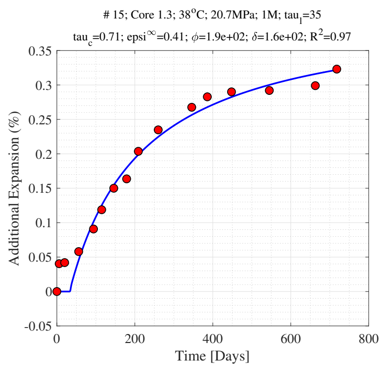

(a) #15; 1.3; 38°C; 20.7MPa; d_a=75mm; 1M; τ_l=35.0; τ_c=1; ε^{∞}=0.41; R^2= 0.97

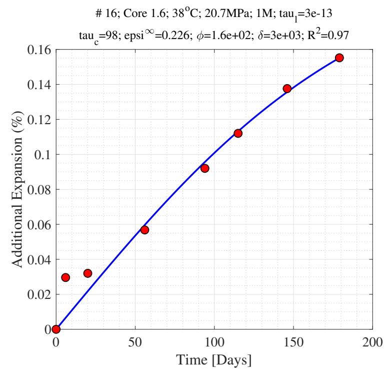

(b) #16; 1.6; 38°C; 20.7MPa; d_a=75mm; 1M; τ_l=0.0; τ_c=98; ε^{∞}=0.23; R^2= 0.97

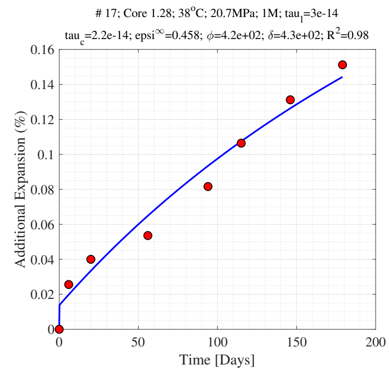

(c) #17; 1.28; 38°C; 20.7MPa; d_a=75mm; 1M; τ_l=0.0; τ_c=0; ε^{∞}=0.46; R^2= 0.98

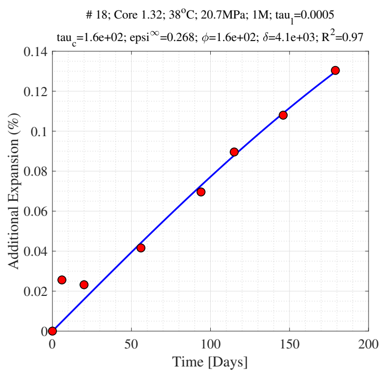

(d) #18; 1.32; 38°C; 20.7MPa; d_a=75mm; 1M; τ_l=0.0; τ_c=162; ε^{∞}=0.27; R^2= 0.97

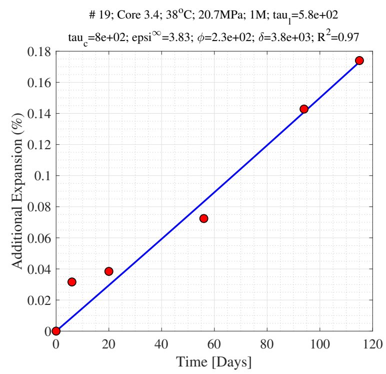

(e) #19; 3.4; 38°C; 20.7MPa; d_a=38mm; 1M; τ_l=577.9; τ_c=805; ε^{∞}=3.83; R^2= 0.97

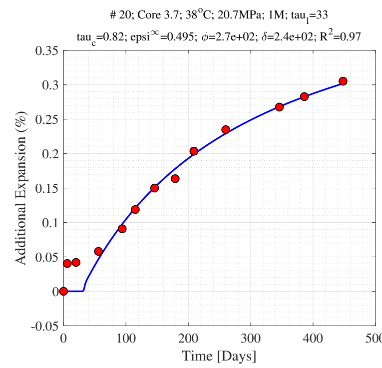

(f) #20; 3.7; 38°C; 20.7MPa; d_a=38mm; 1M; τ_l=33.2; τ_c=1; ε^{∞}=0.50; R^2= 0.97

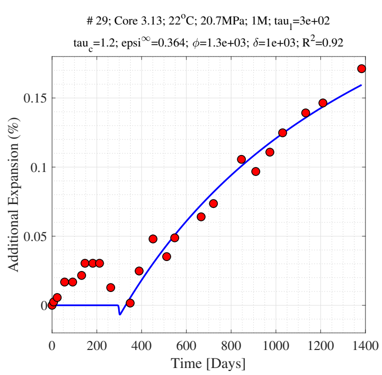

(g) #21; 3.13; 38°C; 20.7MPa; d_a=38mm; 1M; τ_l=619.8; τ_c=97; ε^{∞}=59.59; R^2= 0.86

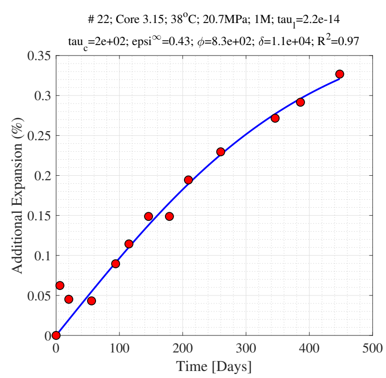

(h) #22; 3.15; 38°C; 20.7MPa; d_a=38mm; 1M; τ_l=0.0; τ_c=202; ε^{∞}=0.43; R^2= 0.97

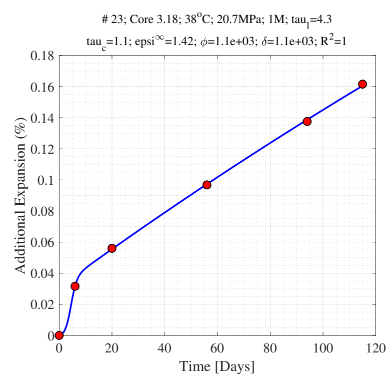

(i) #23; 3.18; 38°C; 20.7MPa; d_a=38mm; 1M; τ_l=4.3; τ_c=1; ε^{∞}=1.42; R^2= 1.00

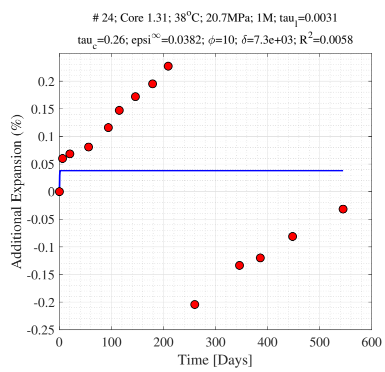

(j) #24; 1.31; 38°C; 20.7MPa; d$_a$=75mm; 1M; τ_l=0.0; τ_c=0; ε^∞=0.04; R^2= 0.01

Figure A.10: Expansion curve for 38° 1M cores

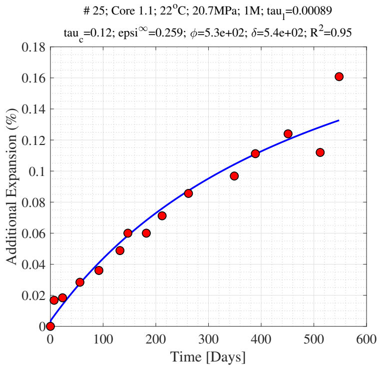

(a) #25; 1.1; 22°C; 20.7MPa; d$_a$=75mm; 1M; τ_l=0.0; τ_c=0; ε^∞=0.26; R^2= 0.95

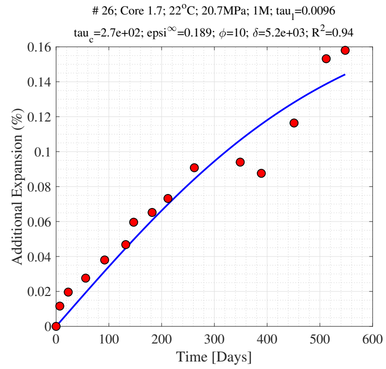

(b) #26; 1.7; 22°C; 20.7MPa; d$_a$=75mm; 1M; τ_l=0.0; τ_c=273; ε^∞=0.19; R^2= 0.94

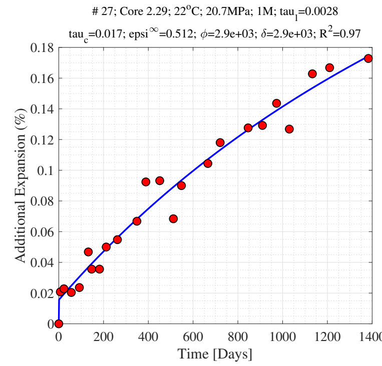

(c) #27; 2.29; 22°C; 20.7MPa; d$_a$=75mm; 1M; τ_l=0.0; τ_c=0; ε^∞=0.51; R^2= 0.97

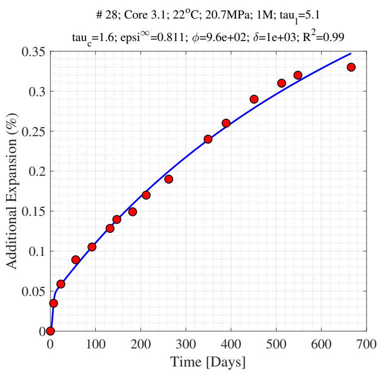

(d) #28; 3.1; 22°C; 20.7MPa; d$_a$=38mm; 1M; τ_l=5.1; τ_c=2; ε^∞=0.81; R^2= 0.99

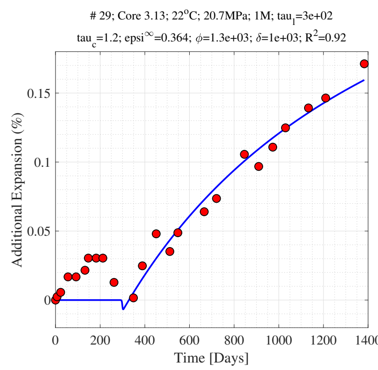

(e) #29; 3.13; 22°C; 20.7MPa; d$_a$=38mm; 1M; τ_l=299.4; τ_c=1; ε^∞=0.36; R^2= 0.92

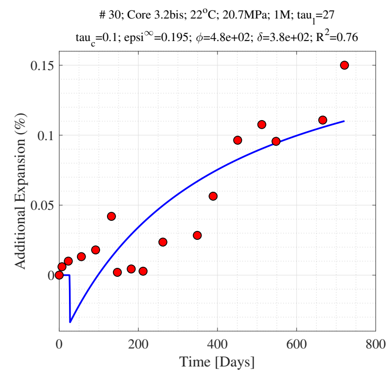

(f) #30; 3.2bis; 22°C; 20.7MPa; d$_a$=38mm; 1M; τ_l=26.8; τ_c=0; ε^∞=0.19; R^2= 0.76

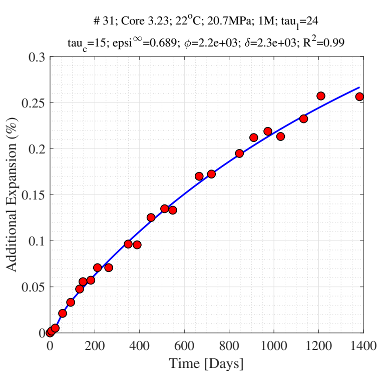

(g) #31; 3.23; 22°C; 20.7MPa; d$_a$=38mm; 1M; τ_l=23.8; τ_c=15; ε^∞=0.69; R^2= 0.99

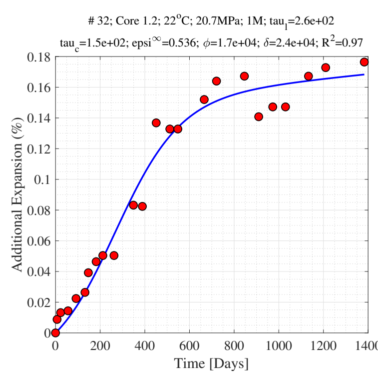

(h) #32; 1.2; 22°C; 20.7MPa; d$_a$=75mm; 1M; τ_l=258.1; τ_c=145; ε^∞=0.54; R^2= 0.97

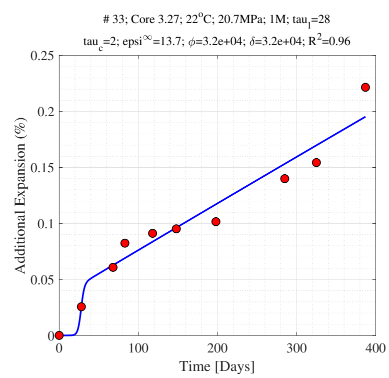

(i) #33; 3.27; 22°C; 20.7MPa; d$_a$=38mm; 1M; τ_l=27.5; τ_c=2; ε^∞=13.66; R^2= 0.96

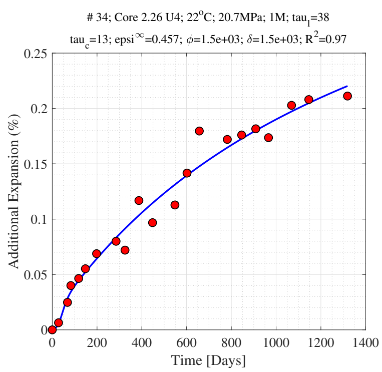

(j) #34; 2.26 U4; 22°C; 20.7MPa; d$_a$=75mm; 1M; τ_l=38.3; τ_c=13; ε^{∞}=0.46; R^2= 0.97

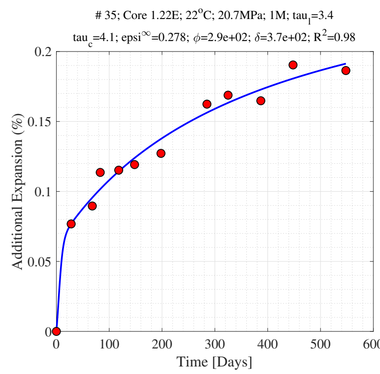

(k) #35; 1.22E; 22°C; 20.7MPa; d$_a$=75mm; 1M; τ_l=3.4; τ_c=4; ε^{∞}=0.28; R^2= 0.98

Figure A.11: Expansion curve for 22° 1M cores

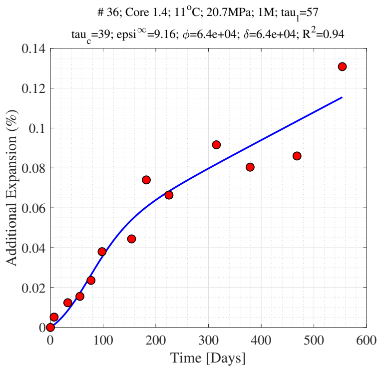

(a) #36; 1.4; 11°C; 20.7MPa; d$_a$=75mm; 1M; τ_l=56.7; τ_c=39; ε^∞=9.16; R^2= 0.94

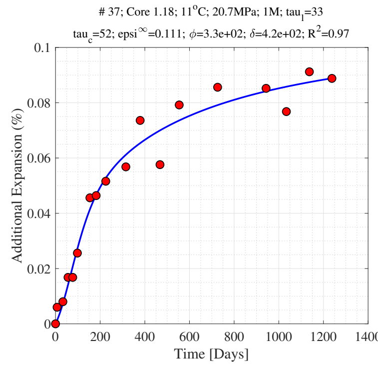

(b) #37; 1.18; 11°C; 20.7MPa; d$_a$=75mm; 1M; τ_l=32.5; τ_c=52; ε^∞=0.11; R^2= 0.97

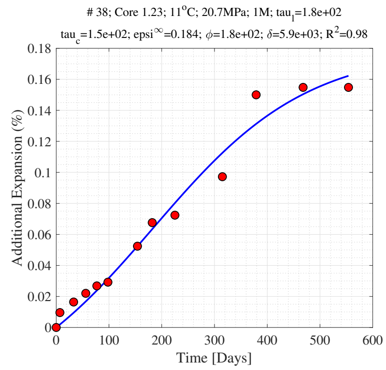

(c) #38; 1.23; 11°C; 20.7MPa; d$_a$=75mm; 1M; τ_l=183.5; τ_c=146; ε^∞=0.18; R^2= 0.98

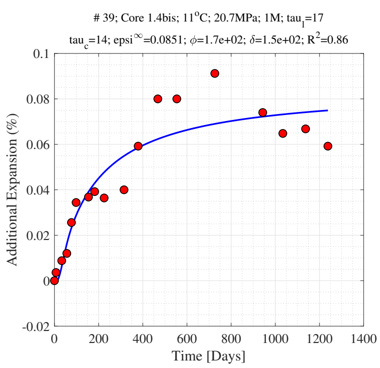

(d) #39; 1.4bis; 11°C; 20.7MPa; d$_a$=75mm; 1M; τ_l=16.9; τ_c=14; ε^∞=0.09; R^2= 0.86

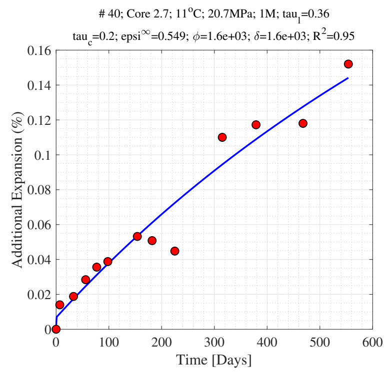

(e) #40; 2.7; 11°C; 20.7MPa; d$_a$=75mm; 1M; τ_l=0.4; τ_c=0; ε^∞=0.55; R^2= 0.95

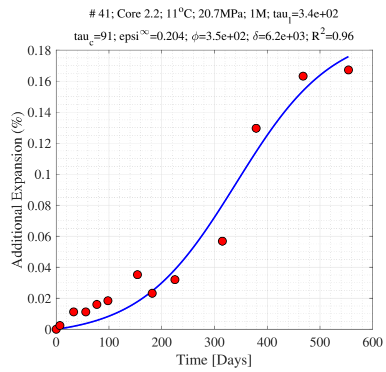

(f) #41; 2.2; 11°C; 20.7MPa; d$_a$=75mm; 1M; τ_l=341.0; τ_c=91; ε^∞=0.20; R^2= 0.96

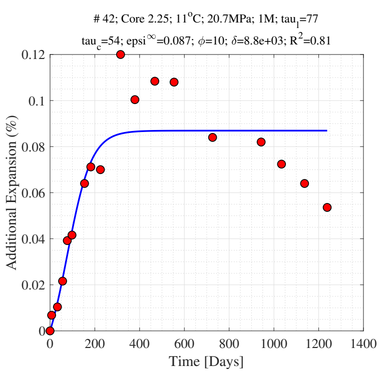

(g) #42; 2.25; 11°C; 20.7MPa; d$_a$=75mm; 1M; τ_l=76.7; τ_c=54; ε^∞=0.09; R^2= 0.81

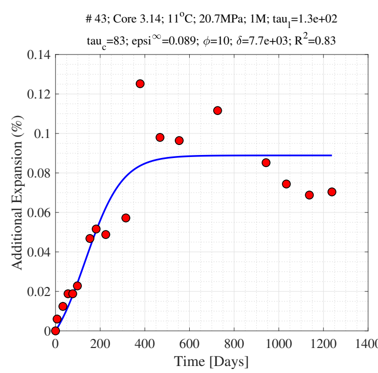

(h) #43; 3.14; 11°C; 20.7MPa; d$_a$=38mm; 1M; τ_l=133.7; τ_c=83; ε^∞=0.09; R^2= 0.83

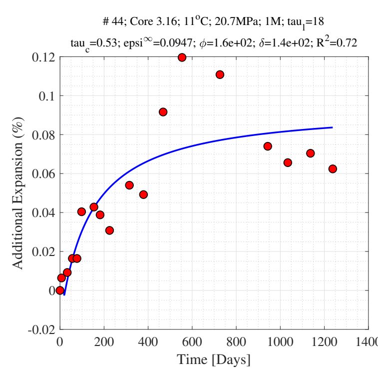

(i) #44; 3.16; 11°C; 20.7MPa; d$_a$=38mm; 1M; τ_l=18.0; τ_c=1; ε^∞=0.09; R^2= 0.72

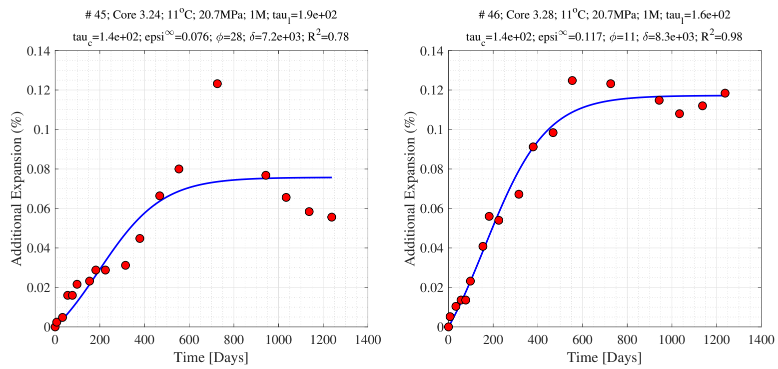

(j) #45; 3.24; 11°C; 20.7MPa; d$_a$=38mm; 1M; τ_l=194.7; τ_c=142; ε^∞=0.08; R^2= 0.78

(k) #46; 3.28; 11°C; 20.7MPa; d$_a$=38mm; 1M; τ_l=161.2; τ_c=138; ε^∞=0.12; R^2= 0.98

Figure A.12: Expansion curve for 11° 1M cores

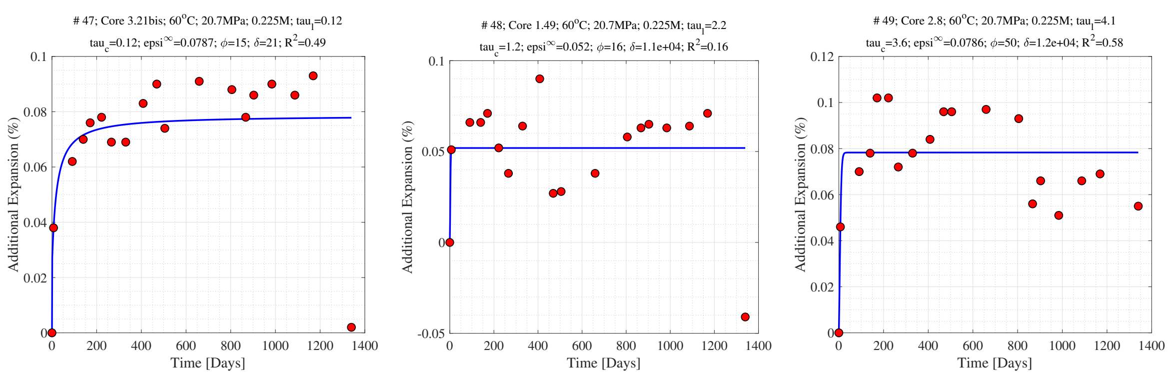

(a) #47; 3.21bis; 60°C; 20.7MPa; d$_a$=38mm; 0.225M; τ_l=0.1; τ_c=0; ε^∞=0.08; R^2= 0.49

(b) #48; 1.49; 60°C; 20.7MPa; d$_a$=75mm; 0.225M; τ_l=2.2; τ_c=1; ε^∞=0.05; R^2= 0.16

(c) #49; 2.8; 60°C; 20.7MPa; d$_a$=75mm; 0.225M; τ_l=4.1; τ_c=4; ε^∞=0.08; R^2= 0.58

Figure A.13: Expansion curve for 60° 0.225M cores

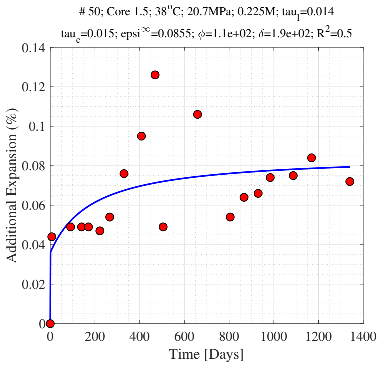

(a) #50; 1.5; 38°C; 20.7MPa; d$_a$=75mm; 0.225M; τ_l=0.0; τ_c=0; ε^{∞}=0.09; R^2= 0.50

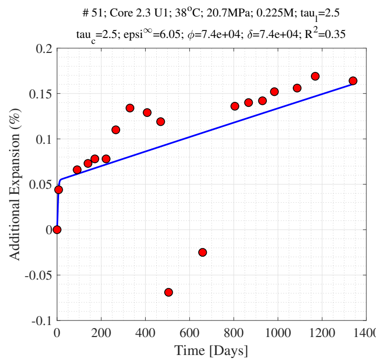

(b) #51; 2.3 U1; 38°C; 20.7MPa; d$_a$=75mm; 0.225M; τ_l=2.5; τ_c=3; ε^{∞}=6.05; R^2= 0.35

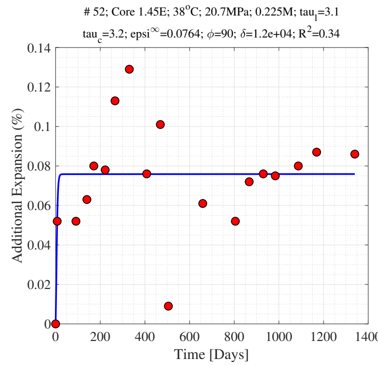

(c) #52; 1.45E; 38°C; 20.7MPa; d$_a$=75mm; 0.225M; τ_l=3.1; τ_c=3; ε^{∞}=0.08; R^2= 0.34

Figure A.14: Expansion curve for 38° 0.225M cores

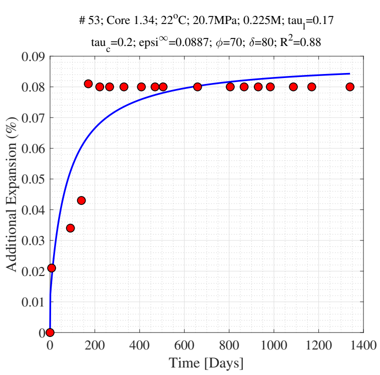

(a) #53; 1.34; 22°C; 20.7MPa; d$_a$=75mm; 0.225M; τ_l=0.2; τ_c=0; ε^{∞}=0.09; R^2= 0.88

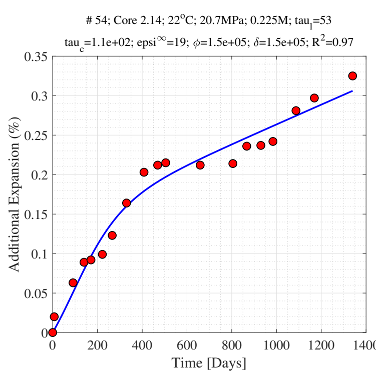

(b) #54; 2.14; 22°C; 20.7MPa; d$_a$=75mm; 0.225M; τ_l=53.1; τ_c=105; ε^{∞}=18.96; R^2= 0.97

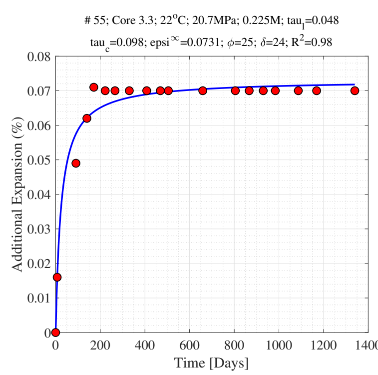

(c) #55; 3.3; 22°C; 20.7MPa; d$_a$=38mm; 0.225M; τ_l=0.0; τ_c=0; ε^{∞}=0.07; R^2= 0.98

Figure A.15: Expansion curve for 22° 0.225M cores

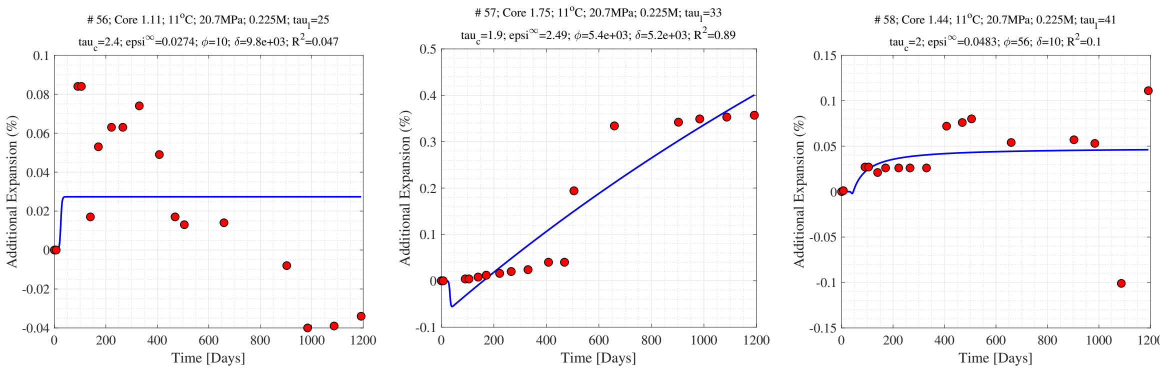

(a) #56; 1.11; 11°C; 20.7MPa; d_a=75mm; 0.225M; τ_l=24.9; τ_c=2; ε^∞=0.03; R^2= 0.05

(b) #57; 1.75; 11°C; 20.7MPa; d_a=75mm; 0.225M; τ_l=32.8; τ_c=2; ε^∞=2.49; R^2= 0.89

(c) #58; 1.44; 11°C; 20.7MPa; d_a=75mm; 0.225M; τ_l=41.0; τ_c=2; ε^∞=0.05; R^2= 0.10

Figure A.16: Expansion curve for 11° 0.225M cores

B Degradation Figures

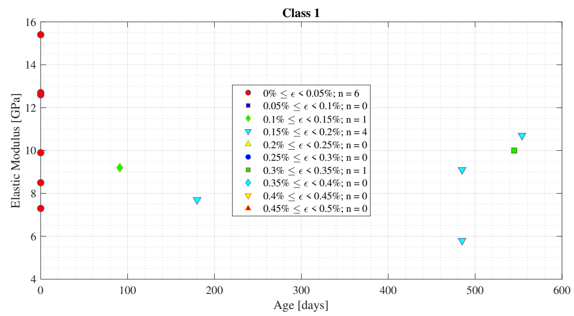

(a) E vs. age

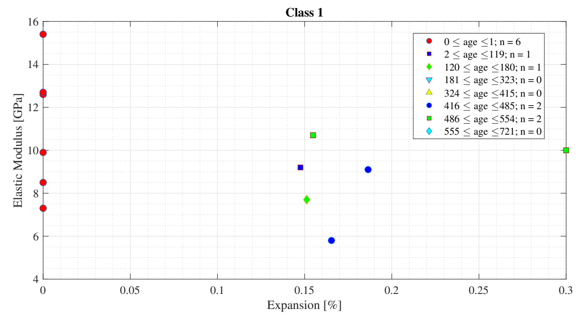

(b) E vs. expansion (age)

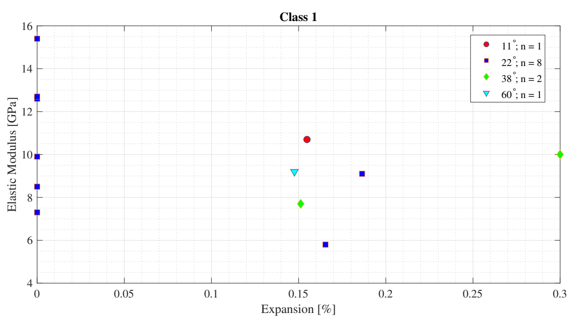

(c) E vs. expansion (Temperature)

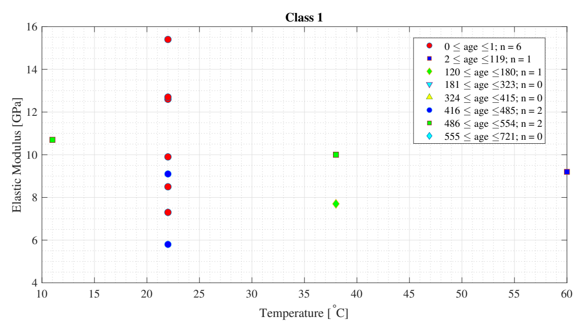

(d) E vs. storage temperature

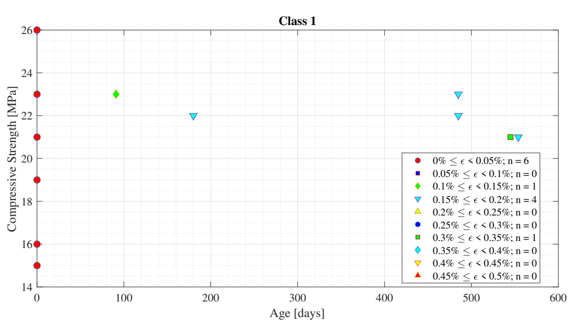

(e) f_c vs. age

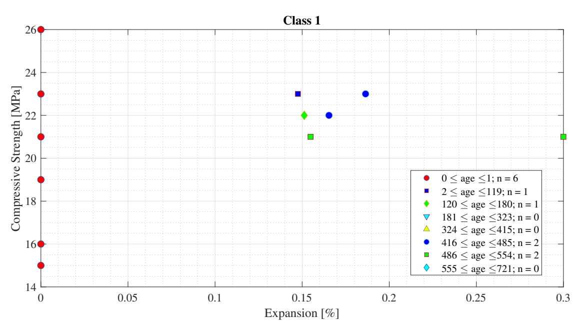

(f) f_c vs. expansion

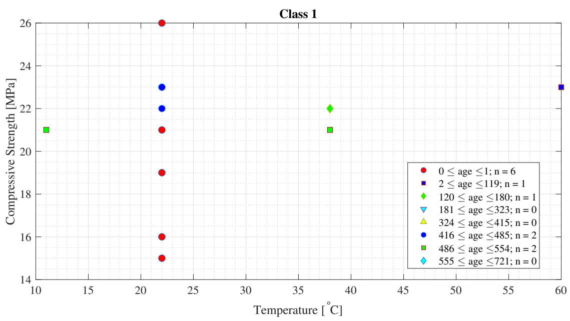

(g) f_c vs. storage temperature

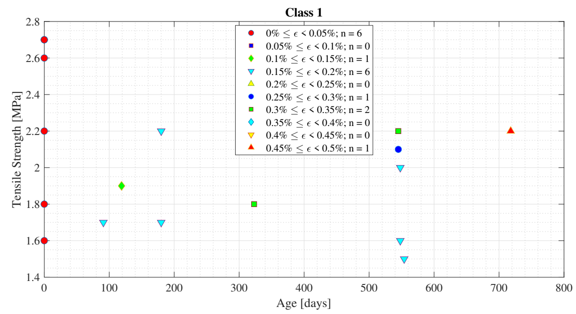

(h) f_t vs. age

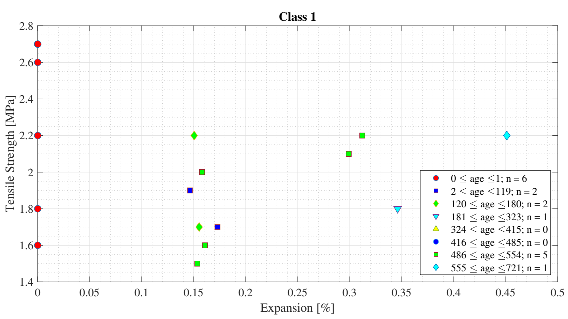

(i) f_t vs. expansion

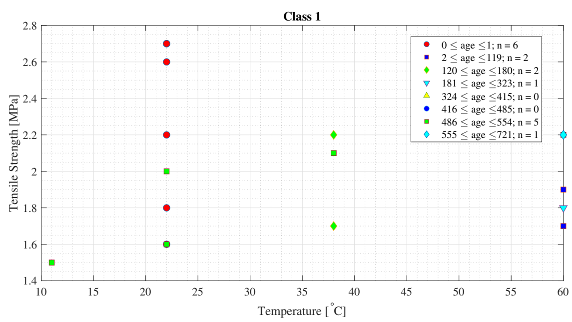

(j) f_t vs. storage temperature

Figure B.1: Class 1: Mechanical property deterioration

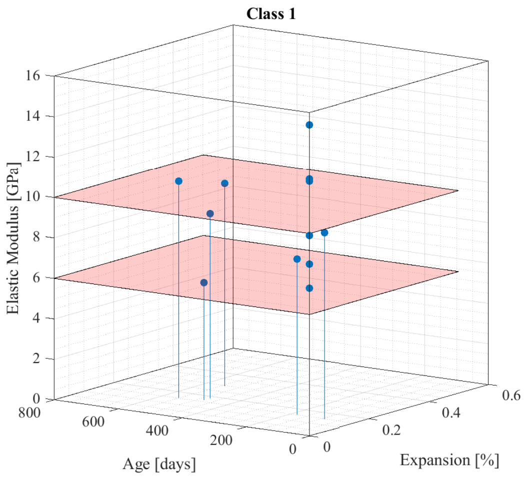

(a) E vs. age and expansion

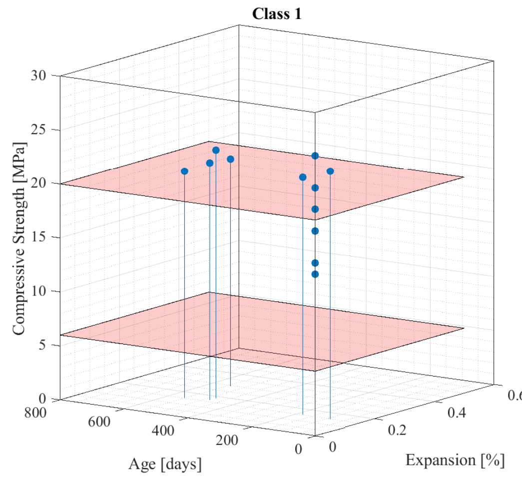

(b) f_c vs. age and expansion

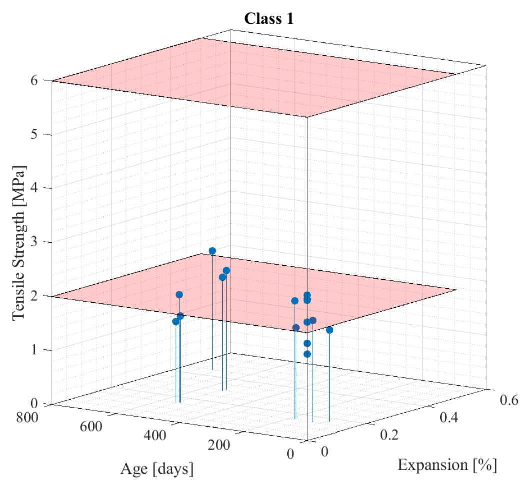

(c) f_t vs. age and expansion

Figure B.2: Class 1: E, f_c and f_t vs. age and expansion

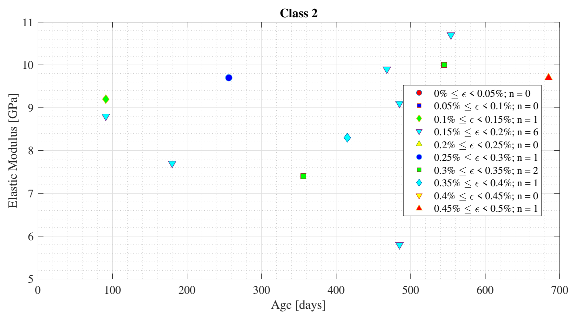

(a) E vs. age

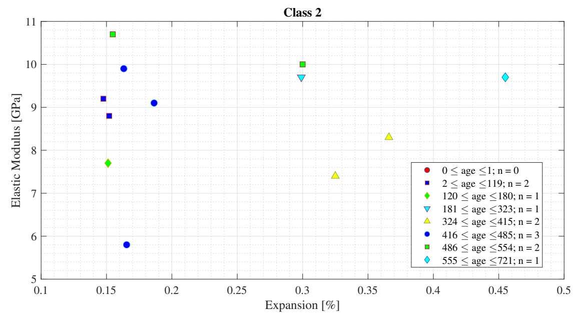

(b) E vs. expansion (age)

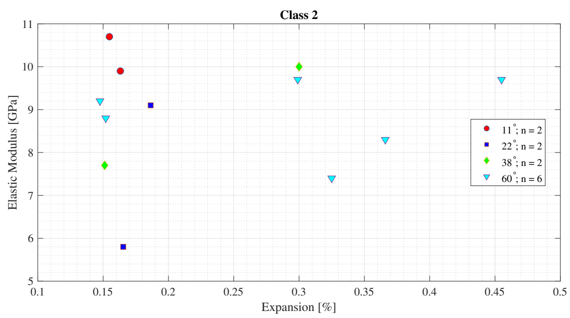

(c) E vs. expansion (Temperature)

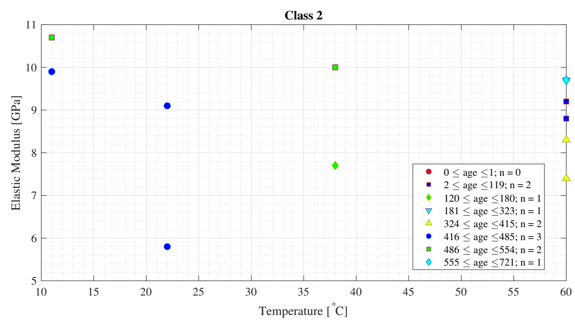

(d) E vs. storage temperature

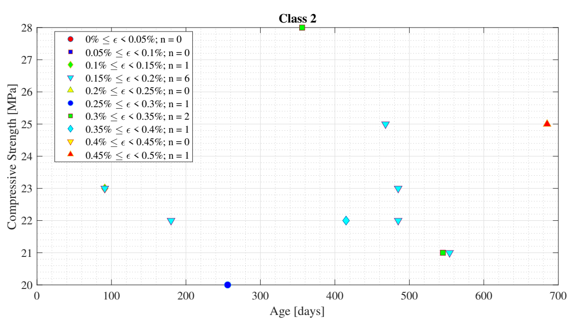

(e) f_c vs. age

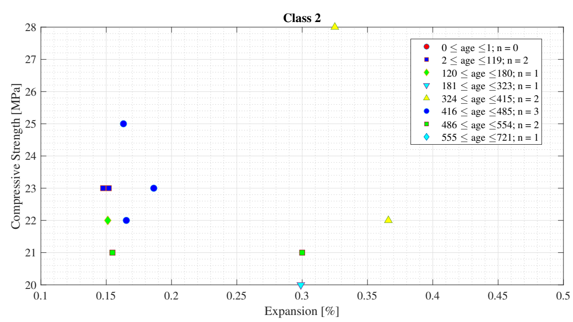

(f) f_c vs. expansion

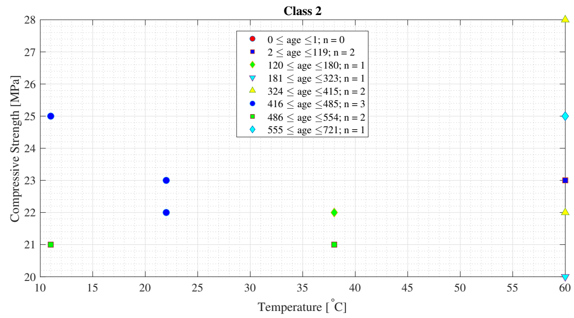

(g) f_c vs. storage temperature

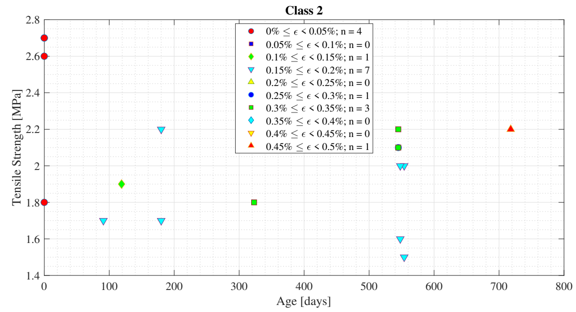

(h) f_t vs. age

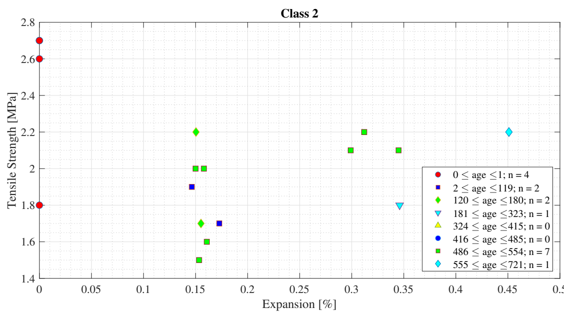

(i) f_t vs. expansion

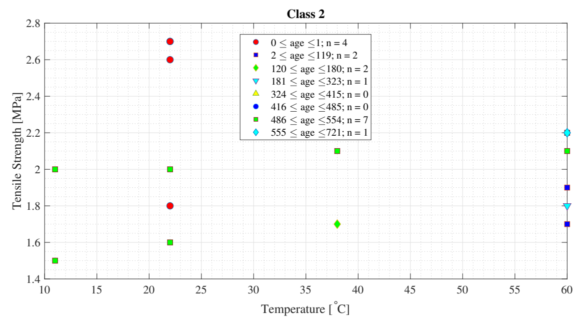

(j) f_t vs. storage temperature

Figure B.3: Class 2: Mechanical property deterioration

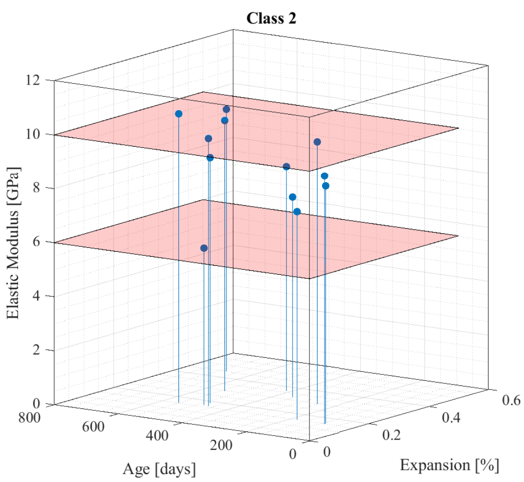

(a) E vs. age and expansion

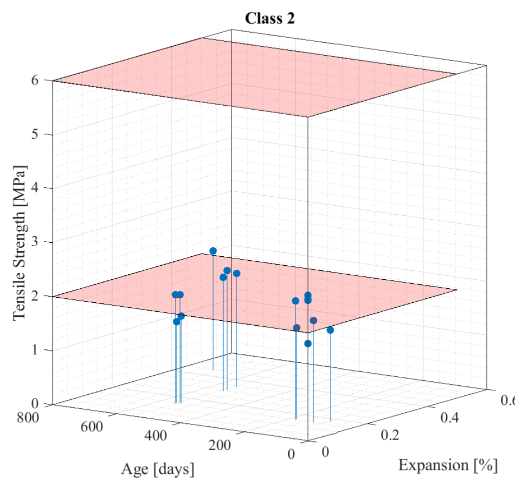

(b) f_t vs. age and expansion

Figure B.4: Class 2: E, f_c and f_t vs. age and expansion

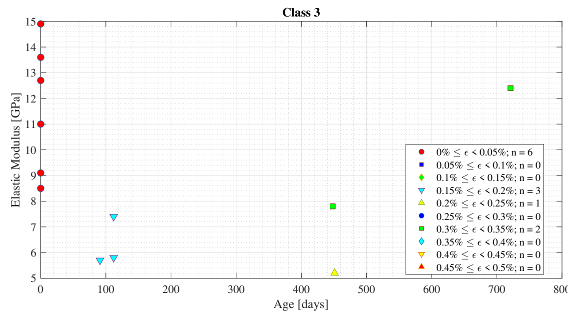

(a) E vs. age

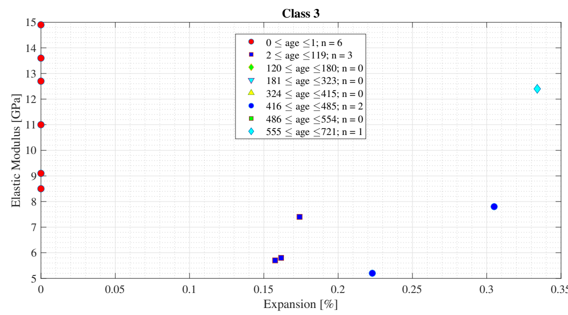

(b) E vs. expansion (age)

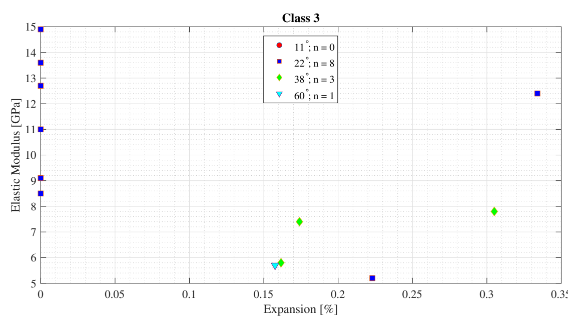

(c) E vs. expansion (Temperature) temperature

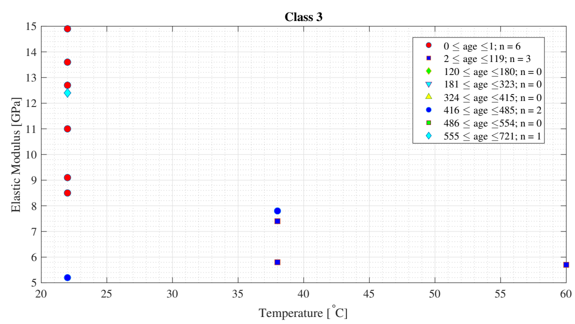

(d) E vs. storage temperature

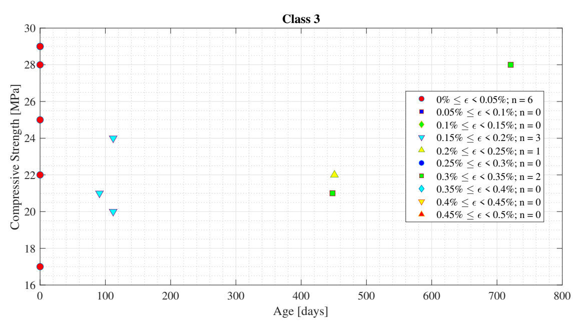

(e) f_c vs. age

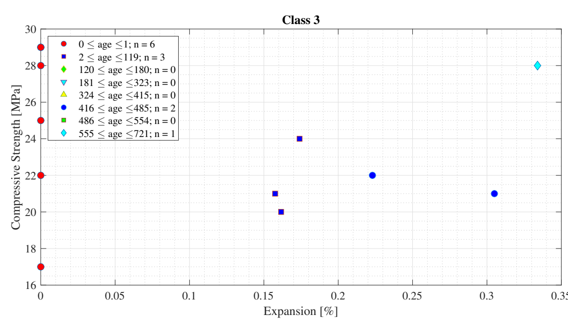

(f) f_c vs. expansion

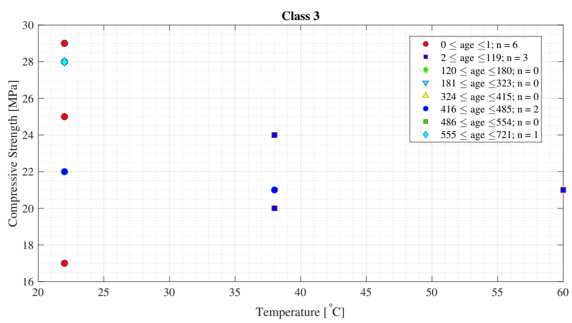

(g) f_c vs. storage temperature

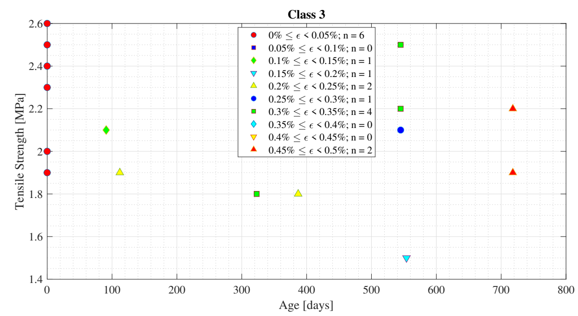

(h) f_t vs. age

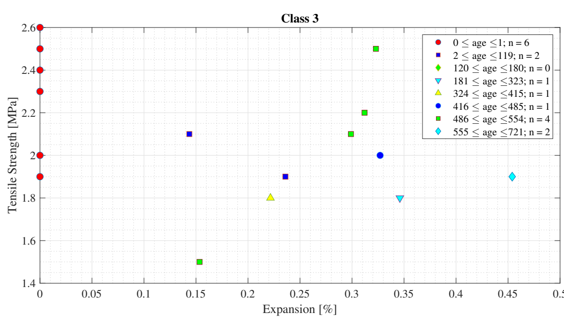

(i) f_t vs. expansion

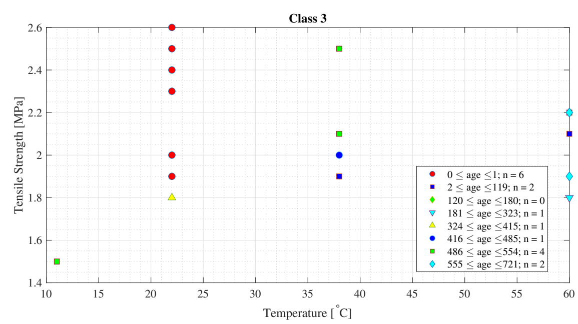

(j) f_t vs. storage temperature

Figure B.5: Class 3: Mechanical property deterioration

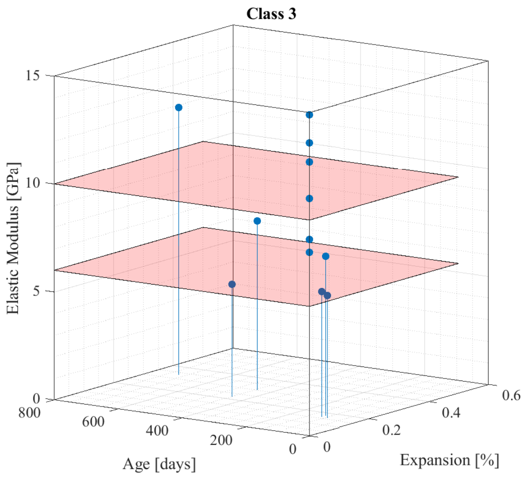

(a) E vs. age and expansion

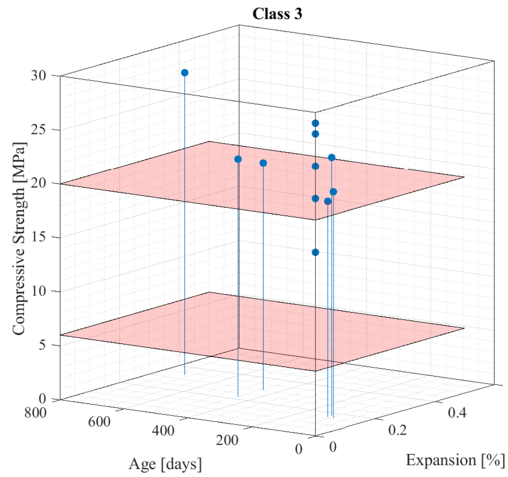

(b) f_c vs. age and expansion

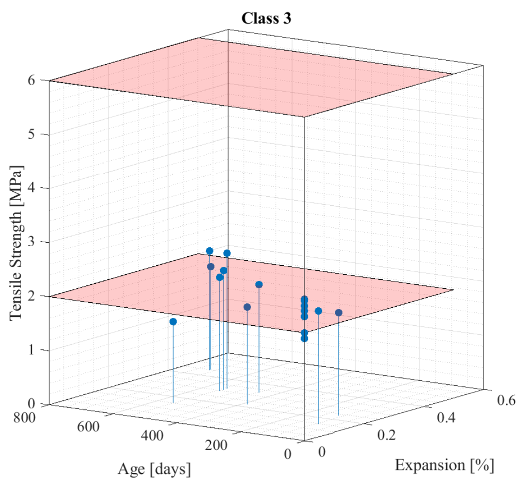

(c) f_t vs. age and expansion

Figure B.6: Class 3: E, f_c and f_t vs. age and expansion

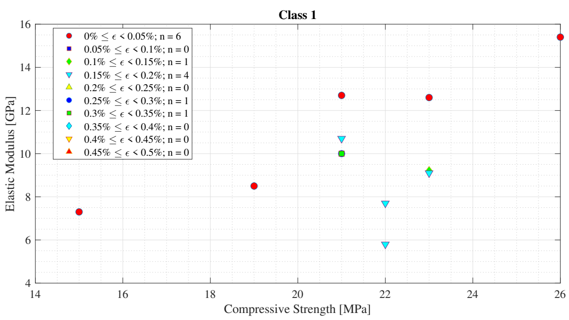

(a) Class 1

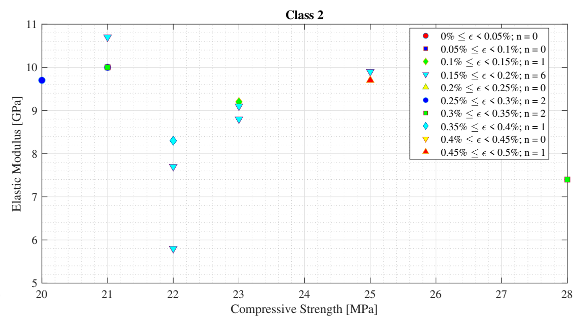

(b) Class 2

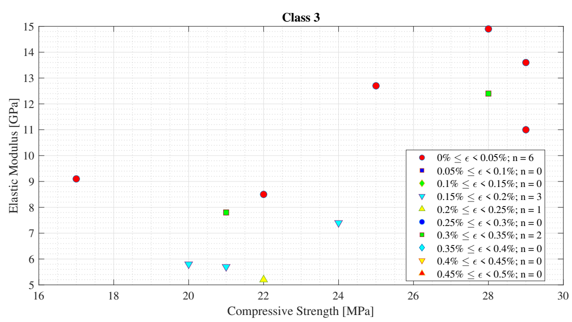

(c) Class 3

Figure B.7: E *vs.* f_c

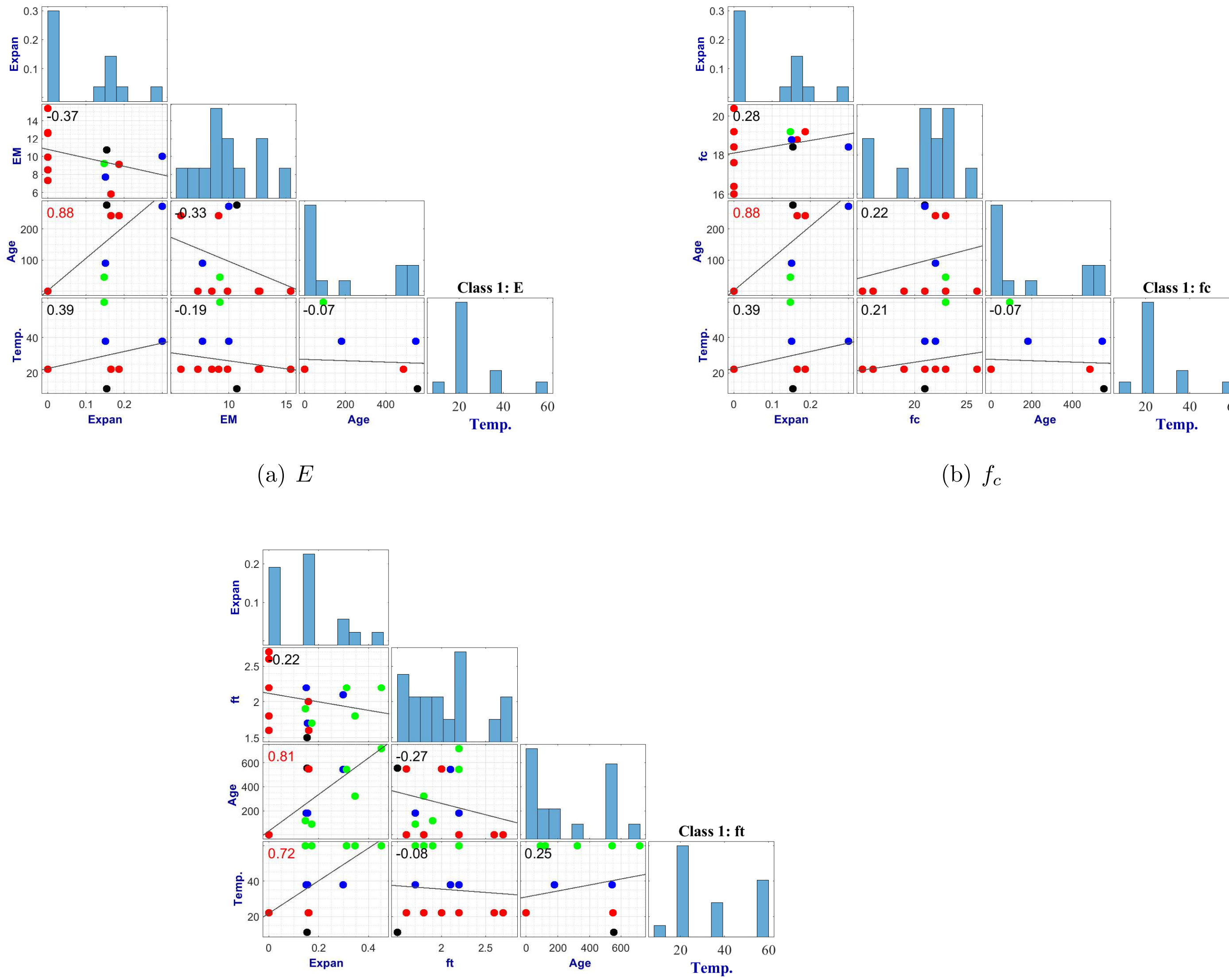

(a) E

(b) f_c

(c) f_t

Figure B.8: Class 1: Correlation matrices

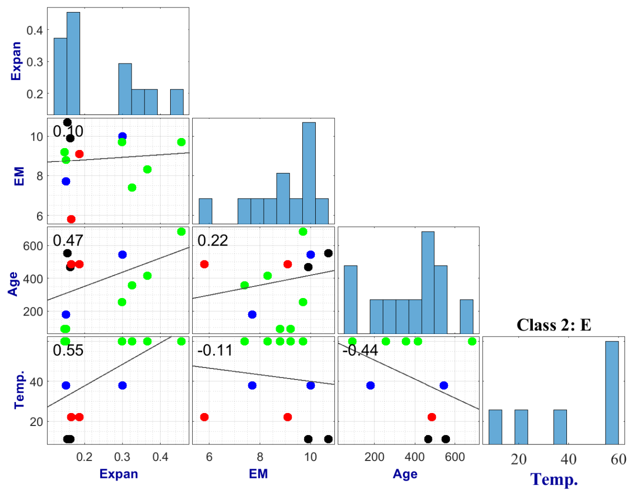

(a) E

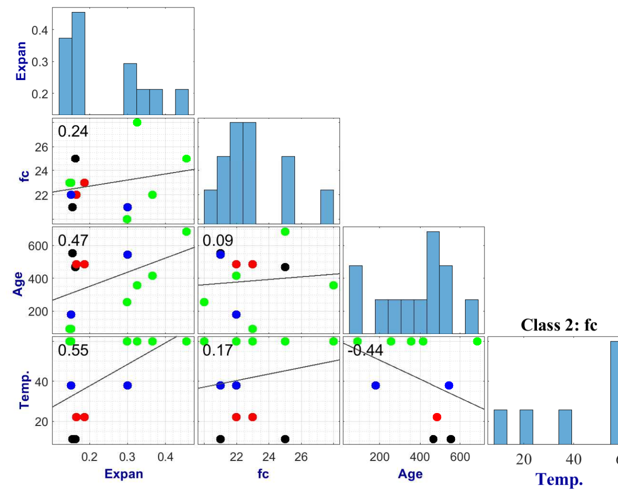

(b) f_c

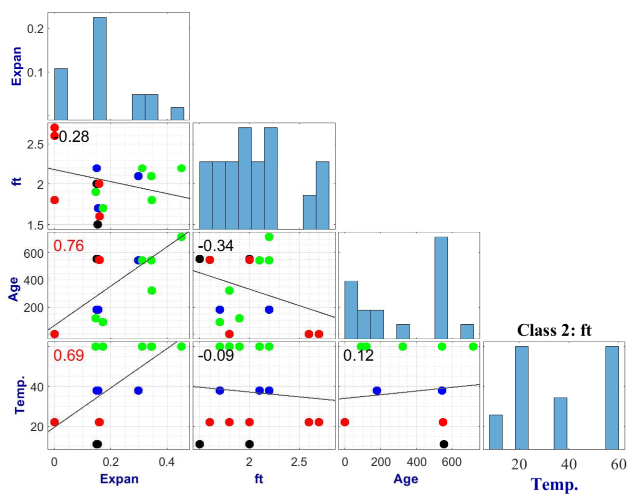

(c) f_t

Figure B.9: Class 2: Correlation matrices

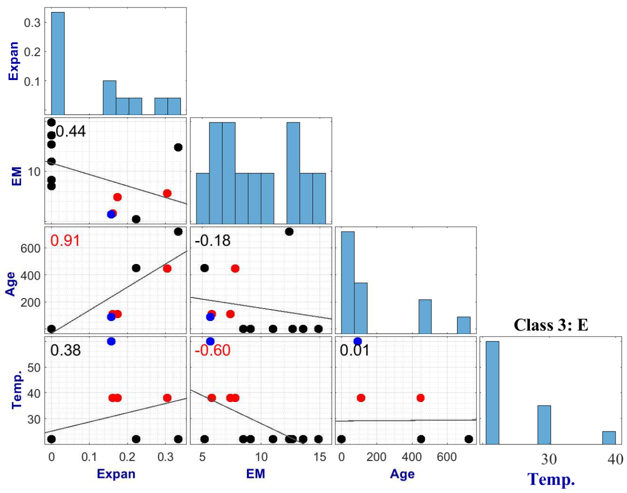

(a) E

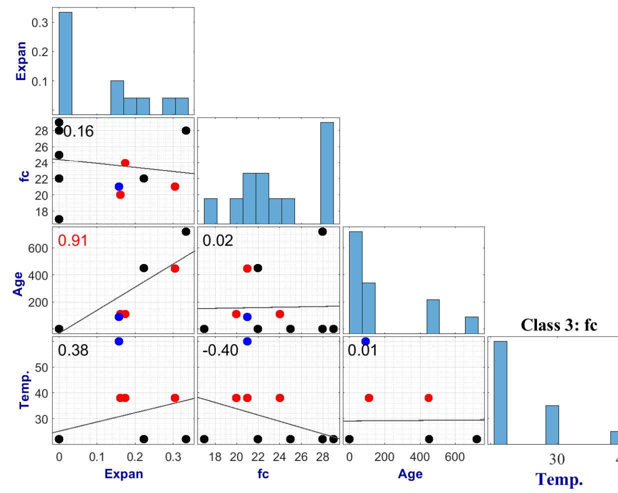

(b) f_c

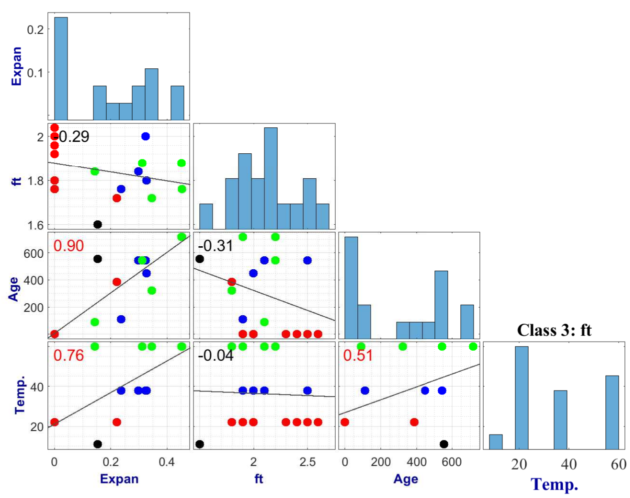

(c) f_t

Figure B.10: Class 3: Correlation matrices

C Finite Element Modeling of AAR

There are essentially two possible approaches to model AAR, Fig. C.1 in massive concrete tructures. The first is representative of the State of the Practice, while the second captures the State of the Art in AAR,

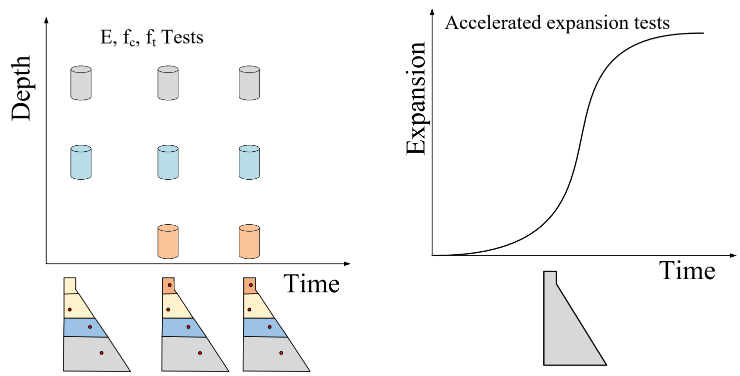

Figure C.1: AAR FEA models

A brief summary of the two methods is shown below.

Methods	State of the Practice (e.g. Hatch)	State of the Art (e.g. Merlin)
# of Analyses	Multiple, one for each year we are interested in	Single analysis that starts at time 0 (dam construction) up till desired year
	What do we need for input data	
Parameters	Topological distribution of damaged concrete properties over the dam at the time of analysis	Characteristics of the concrete expansion to capture its kinetics (3 parameters)

How do we obtain them	Subdivide the dam in multiple regions; Extract sufficient representative cores from each one of them; perform tests (E and f_c primarily)	1. Perform expansion and appropriate petrographic tests (Katayama), determine the 3 parameters that characterize the concrete since time of construction 2. Same as above, without petrographic tests, characterization since date of core extraction 3. Perform a parameter identification based on the historical record of crest deflections
	Analysis	
Advantage	Easier to perform the analysis if one does not have a finite element code that can track the expansion with time.	Single analysis that capture the entire response (displacements and internal deterioration of concrete); Requires only three parameters that capture the cause of the expansion (as opposed to multiple tests that reflect the consequences of the reaction); Truly captures the complex response of a structure subjected to AAR (listed as disadvantage for Method 1 below).
Disadvantage	Approximate as we have to assign material properties over large zones, many input data coming from tests. May not be representative enough as it does not capture: 1) interaction of temperature with expansion; 2) effect of confinement on the anisotropic expansion;	Some numerical instability may occur in a nonlinear time history analysis
	Analysis Output	
Displacements stresses	Yes, a snapshot at time t (of analysis), i.e. one single scalar quantity at time t	Yes, a "movie" that captures the evolution of the dam response, i.e. a vector for each response in terms of time)

Concrete deterioration	No, that was part of the input	Yes as computed by the AAR model
	Future Prediction	
Possible	Will have to be based on the time dependent concrete deterioration	By just letting the analysis go beyond present date.
Reliability	Low would rely on the extrapolation of concrete damage measured in the laboratory and inputted in the mesh	High, embedded in the analysis are the expansion characteristics measured in the lab (or extracted from a parameter identification based on historical record of crest displacement)

C.1 State of the Practice

The simplest approach, and one which does not require any specialized finite element code, is based on a mapping of the field determined concrete deterioration on the ensuing finite element mesh. The analysis, is then calibrated with some of the field measurements. Thus, a separate analysis will be conducted for each year of recorded mechanical properties.

One would start with testing cores (E, f_c and f_t, but not necessarily all three of them all the times) recovered from the dam at time t_i. Then, one would, semi-arbitrarily but certainly approximately, assign a representative region to each one of the cores. Within that region, elements of the mesh will be assigned the same mechanical properties.

Separately, at time t_i one would estimate the AAR expansion $\varepsilon^{\infty}(t_i)$, and its spatial distribution $\varepsilon^{AAR}(t_i, x, y)$.

Finally, combining those two, a finite element analysis is performed. However, this is very likely to yield good correlation with recorded field displacements. Hence, correction are made with *some* of the recorded data, and verification is made with the others. This is repeated until adequate comparison at time t_i is achieved. Adjustments are for a given time t_i and are very unlikely to be the same for time t_j.

The outcome of such a calibration (for $E|f_t|f_c$) is a spatial and temporal partitioning shown below, Fig. C.2

$$
\begin{aligned}
[E|f_t|f_c](h,t) &= \begin{cases} a_1 f_1(h) \times f_2(t) & yr_1 \leq t \leq yr_2 \quad \& \quad h \geq h_1 \quad ① \\ a_2 f_2(t) & yr_1 \leq t \leq yr_2 \quad \& \quad h < h_1 \quad ② \\ a_3 f_1(h) & t < yr_1 \quad \& \quad h \geq h_1 \quad ③ \\ a_4 f_1(h) & t > yr_2 \quad \& \quad h \geq h_1 \quad ④ \\ a_5 & t < yr_1 \quad \& \quad h < h_1 \quad ⑤ \\ a_6 & t > yr_2 \quad \& \quad h < h_1 \quad ⑥ \end{cases} \\
f_1(h) &= b_1 + b_2 h + b_3 h^2 \\
f_2(t) &= c_1 + c_2 t + c_3 t^2
\end{aligned}
\tag{C.1}
$$

The major (but not only) concern with this method, is that typically one would have not

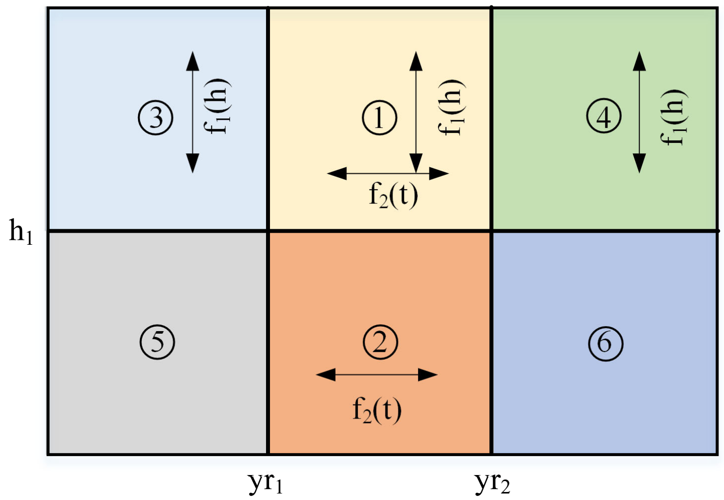

Figure C.2: Spatial and temporal partitioning

only very limited measurements but those are also widely spaced in times. This is further exacerbated by the seldom performance of tensile strength. This handicap is best illustrated by Fig. C.3. One can readily note the very gross approximation one has to resort to in such an analysis[1].

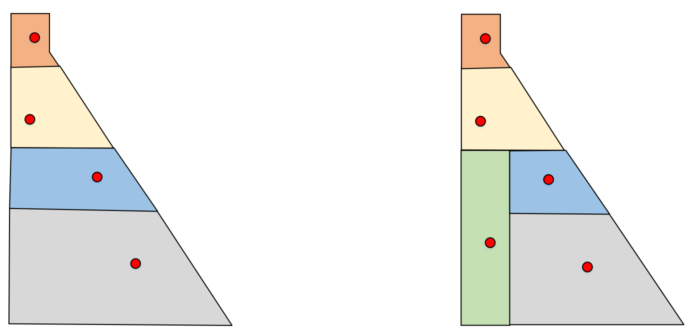

(a) Time t_1 (b) Time t_2

Figure C.3: Mapping of recovered core test results (E, f_c, f_t) measurement into finite element mesh

Typically, only few cores are drilled and tested during the life of the dam. Hence, mapping deterioration over the dam is at best approximate. Furthermore, the idiosyncrasies of the AAR (Saouma, V.E., 2014) are not captured.

This approach has been primarily used by consulting engineers.

Typically, the failure criterion is a post-processing of an otherwise linear elastic analysis (with possible exception for the contact elements). Those would include:

[1]Though an idealization, these curves are based on an actual study espousing this method.

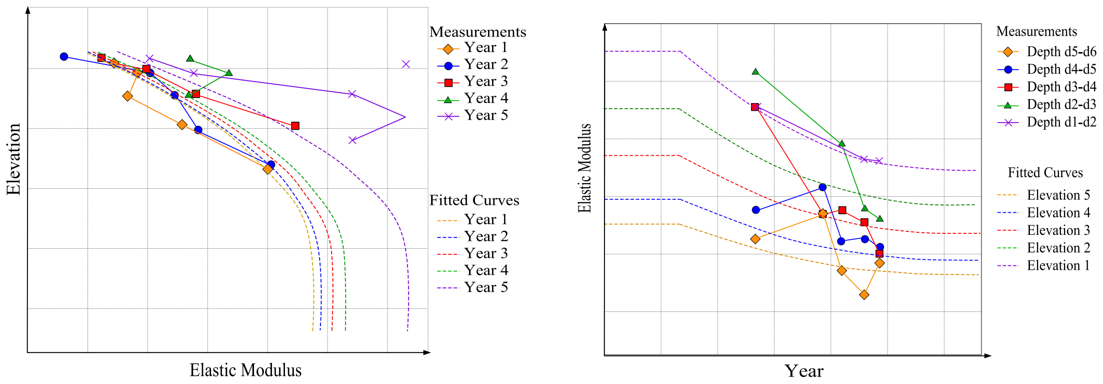

(a) Elastic modulus

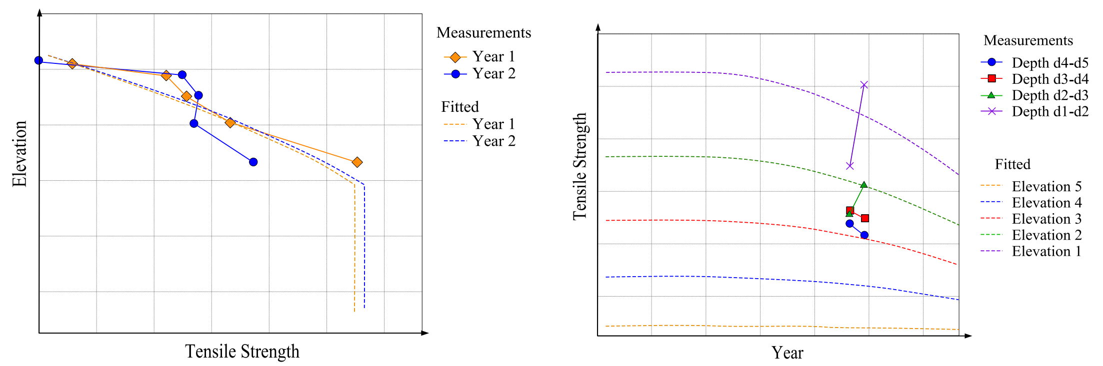

(b) Tensile strength

Figure C.4: Spatial and temporal fitting for concrete mechanical properties based on limited cores and observations (courtesy Y. Gakuhari)

1. Uniaxial compression failure criterion
2. Uniaxial tension failure criterion
3. Triaxial failure criterion

Also, a final '*concrete cracking analysis* may be performed using the so-called *smeared crack model*. This will inherently allow for internal stress redistribution and a corresponding increase in compressive stresses.

C.2 State of the Art

In this second approach, one that is rooted in the State of the Art, one would take into account apparent (or not so apparent) synergy between investigative tools, Fig. C.5.

It should be noted that the approach about to be presented has been used by some researchers already, (Saouma, Perotti, and Shimpo, 2007) (Comi, Fedele, and Perego, 2009) (Sellier, Bourdarot, Multon, Cyr, and Grimal, 2009) (Huang and Spencer, 2016) to name a

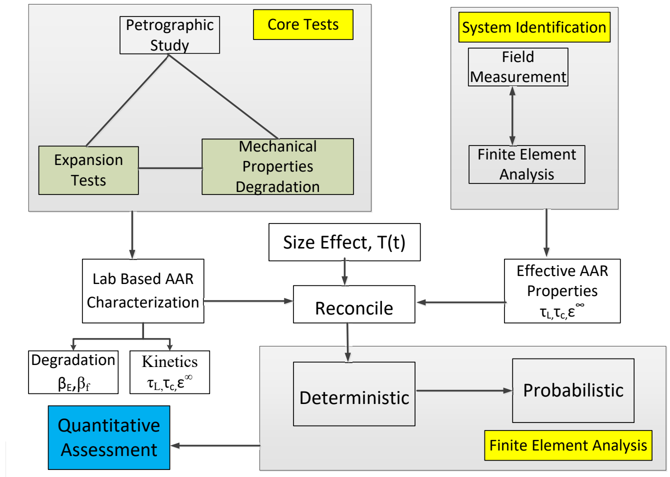

Figure C.5: Assessment paradigms for AAR affected structures

few. The most recent, and comprehensive, study was recently presented by Joshi, Sriprasong, Asamoto, and Sancharoen (2021).

C.2.1 Requirements

A finite element code seeking to perform AAR simulation, using this proposed State of the Art approach, should have the following features:

- Role of temperature, relative humidity in the expansion.
- Volumetric nature of the expansion.
- Induced anisotropy whereas high confinement would inhibit AAR expansion in that direction.
- Time dependent degradation of mechanical properties.
- Joint elements to properly model: a) vertical joints in a dam; b) concrete rock interfaces; and c) closure of cut slot.

Ideally a finite element code should be validated to the extent possible. Saouma (2020) has published a battery of problems for validation, and a number of analysts have submitted results of their analysis.

The finite element code Merlin (Saouma, Červenka, and Reich, 2010) seems to have addressed the largest number of problems. It is indeed the code that my group has developed over the years.

Further details for the finite element analysis can be found in Saouma and Hariri-Ardebili (2021).

C.2.2 Procedure

By now, the analyst has available key AAR characteristics to perform a detailed finite element simulation, more specifically the three key parameters $\varepsilon^{\infty}, \tau_c$ and τ_l. The following steps should be undertaken:

- The seasonal pool elevation variation (for both the thermal and stress analyses) must first be identified, Figure C.6(b).
- The stress-free temperature, T_{ref} (typically either the grouting temperature or the average annual temperature) needs to be identified, along with the external temperature, Figs. C.6(d).
- The pool elevation will affect the internal state of stress, which in turn will alter AAR expansion. This situation is more relevant for high Alpine dams (where the annual pool variation is greater than for low-head, low-altitude dams).
- This variation will then be replicated over n years for the duration of the analysis, Fig. C.6(c).
- External air and water temperatures will be considered next, Fig. C.6(d). In the absence of precise field data, the air temperature may be obtained from NOAA (2013).

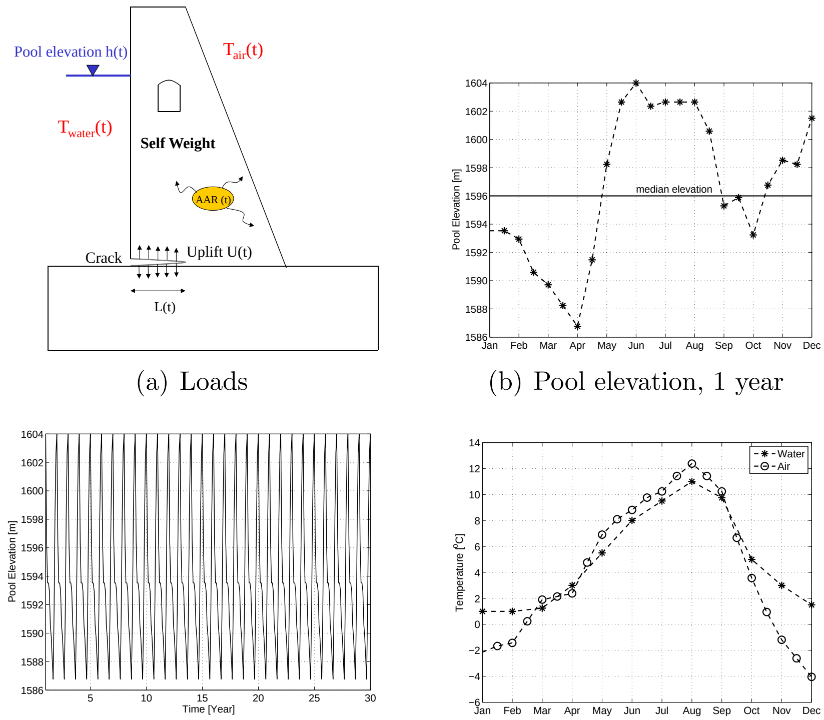

(a) Loads (b) Pool elevation, 1 year

(c) Pool elevation, 30 years (d) Water and air temperatures

Figure C.6: Preliminary load data to be collected for the AAR analysis of a dam

- For time, the ATU (Analysis Time Unit) has been adopted, which can be in the order of week or a month.
- The next step calls for conducting a transient thermal analysis since the reaction is thermodynamically activated. Consequently, the total temperature is included as part of the constitutive model. Heat transfer by both conduction and convection are taken into account, whereas radiation is implicitly incorporated, Fig. C.7(a).
- Radiation is implicitly included by means of a simplified procedure, whereby ambient air temperature is modified (Malla and Wieland, 1999):

$$\begin{array}{ll} T_{us} = 0.905 T_{air} - 0.4^o\text{C} & \text{Upstream} \\ T_{us} = 0.937 T_{air} + 7.2^o\text{C} & \text{Downstream} \end{array} \tag{C.2}$$

  resulting in the temperature distribution shown in Fig. C.7(c).
- Even though the external boundary conditions can be readily determined, the condition associated with the gallery is of primary importance for potential internal cracking (Fig. C.7(b)). More specifically, it is important to know whether during construction the gallery is closed or open to the outside air. The precise thermal analysis should be performed in accordance with Figure C.7(a).
- Next, the transient thermal analysis is to be performed for at least 3-5 years, until the

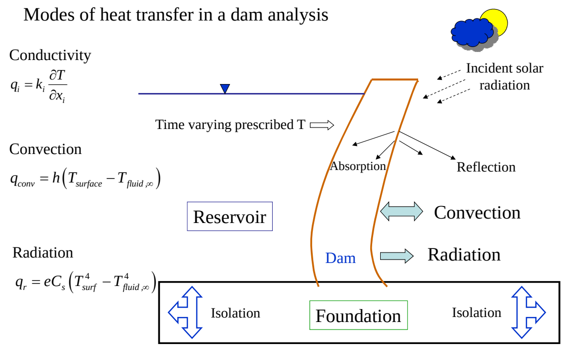

(a) Governing equations for the thermal analysis

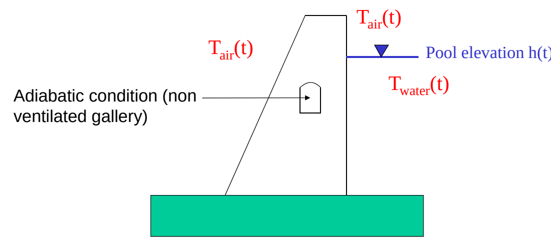

(b) Thermal boundary conditions

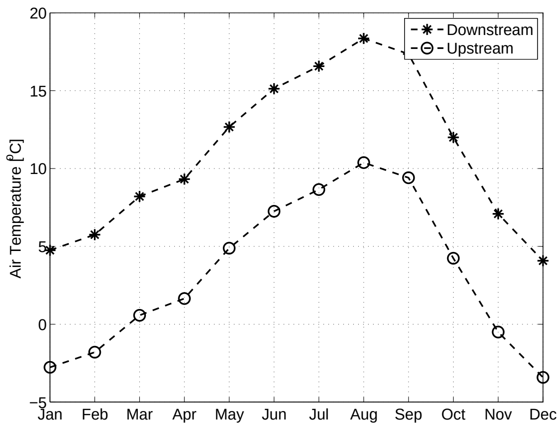

(c) Upstream and downstream air temperatures with inclusion of radiation

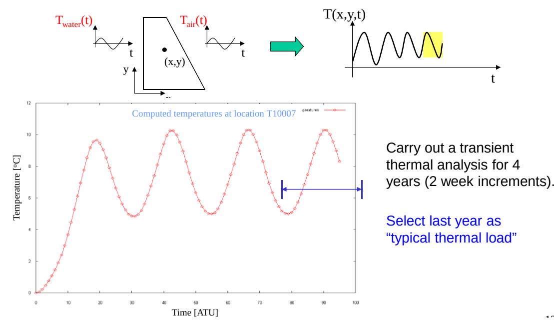

(d) Preliminary transient analysis

Figure C.7: Data preparation for thermal analysis of a dam subjected to AAR

annual variation appears to converge (Fig. C.7(d)). These analyses enable deriving, among other things, the spatial and temporal variations of temperature ($T(x, y, z, t)$).

- The dam however must first be discretized. As is the case with most dams, a set of analytical parametric curves defining the arches (in general, circular segments in the US, while parabolic or elliptical segments elsewhere) is (typically) given.
- Joint elements are placed at both the joints and the rock-concrete interface.
- Let's point out that a different mesh is (usually) required for the thermal analysis, since the interface elements needed to be removed.
- After N years of thermal analysis, the temperature field will be harmonic with a one-year frequency. At this point, the analysis is interrupted and $T_{thermal}(x, y, z, t)$ recorded. A sample computed temperature distribution is shown in Figure C.8. Note that these temperatures are to be used to evaluate the thermal strains, given that for the AAR analysis the total (i.e. absolute) temperature is needed.
- Subsequent to the thermal analysis, $T_{thermal}(x, y, t)$ must be transferred to $T_{stress}x, y, t$

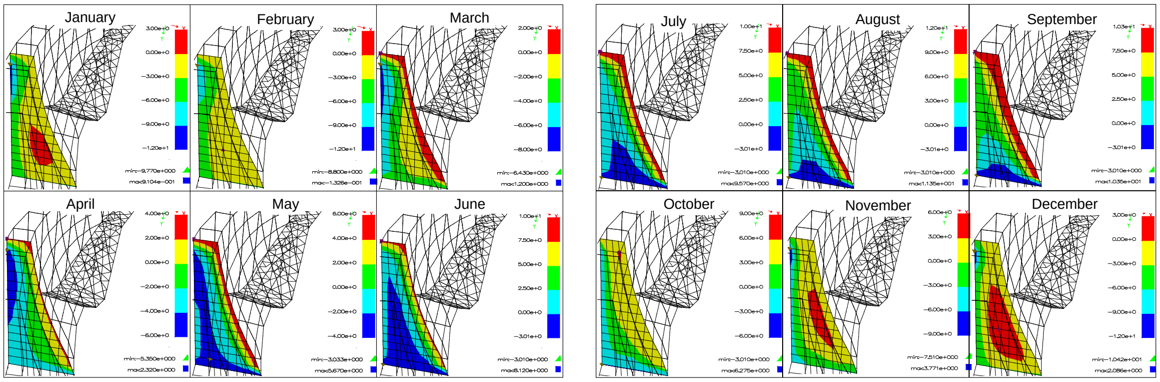

(a) January-June (b) July-December

Figure C.8: Computed internal temperature distribution variation

since, in general, the same finite element mesh is not available (the foundations, joints and cracks are not typically modeled as part of the thermal analysis).

- Lastly, a comprehensive input data file must be prepared for the stress analysis; this file includes:

  1. Gravity load (first increment only).
  2. $\Delta\dot{T}(x,y,t) = \dot{T}_{stress}(x,y,t) - T_{ref}$ in an incremental format. This is a subtle step that must not be overlooked. The stress analysis is in fact based on the difference between the actual and stress-free temperatures. In addition, an incremental analysis requires this set of data to be provided in an incremental format.
  3. Stress-free referenced temperature, which is to be added to the temperature data in order to determine the total absolute temperature needed for AAR.
  4. Cantilever and dam/foundation joint characteristics. The former must be included in any arch dam, since expansion may lead to an upstream joint opening, while the latter must be taken into account given that AAR-induced swelling may result in a separation of the dam from the foundation in the central portion of the foundation.
  5. Uplift load characteristics (typically matching the upstream hydrostatic load).
  6. AAR data, which has been described above.

- Moreover, the compiled set of data must be looped over at least 50 years in order to provide a complete and correct set of natural and essential boundary conditions, Fig. C.9.

- The dead load is applied during the first increment. Following this step, displacements are reset to zero, while maintaining the internal strains/stresses. During increments two through five, the hydrostatic (and uplift) load is applied, and the AAR expansion only initiates at increment six.

		January		February		March		April		May		June	
Incr.		**6.00**	**7.00**	**7.00**	**8.00**	**9.00**	**10.00**	**11.00**	**12.00**	**13.00**	**14.00**	**15.00**	**16.00**
Body force		dam											
Hydrostatic	**Pool Elevation**	1596.47	1593.53	1593.53	1592.94	1590.59	1589.71	1588.24	1586.76	1591.47	1598.24	1602.65	1604.00
	Incremental Elevation	-5.03	-2.94	0.00	-0.59	-2.35	-0.88	-1.47	-1.47	4.71	6.76	4.41	1.35
Uplift	**Pool Elevation**	1596.47	1593.53	1593.53	1592.94	1590.59	1589.71	1588.24	1586.76	1591.47	1598.24	1602.65	1604.00
	Incremental Elevation	-5.03	-2.94	0.00	-0.59	-2.35	-0.88	-1.47	-1.47	4.71	6.76	4.41	1.35
Temperature [^{o}C]	**Air**	-3.10	-2.14	-1.67	-1.43	0.24	1.90	2.14	2.38	4.76	6.90	8.10	8.81
	Water	1.00	1.00	1.00	1.00	1.00	1.50	3.00	3.00	5.00	6.00	8.00	8.00

		July		August		September		October		November		December	
Incr.		**17.00**	**18.00**	**19.00**	**20.00**	**21.00**	**22.00**	**23.00**	**24.00**	**25.00**	**26.00**	**27.00**	**28.00**
Body force		dam											
Hydrostatic	**Pool Elevation**	1602.35	1602.65	1602.65	1602.65	1600.59	1595.29	1595.88	1593.24	1596.76	1598.53	1598.24	1601.50
	Incremental Elevation	-1.65	0.29	0.00	0.00	-2.06	-5.29	0.59	-2.65	3.53	1.76	-0.29	3.26
Uplift	**Pool Elevation**	1602.35	1602.65	1602.65	1602.65	1600.59	1595.29	1595.88	1593.24	1596.76	1598.53	1598.24	1601.50
	Incremental Elevation	-1.65	0.29	0.00	0.00	-2.06	-5.29	0.59	-2.65	3.53	1.76	-0.29	3.26
Temperature [oC]	**Air**	9.76	10.24	11.43	12.38	11.43	10.24	6.67	3.57	0.95	-1.19	-2.62	-4.05
	Water	9.00	10.00	11.00	11.00	11.00	8.50	6.00	4.00	3.00	3.00	2.00	1.00
AAR	**AAR**	**Activated**											

Figure C.9: Data preparation, cyclic load

- Following completion of the transient thermal analysis, the stress analysis may be performed. It should be noted however that the finite element mesh for the stress analysis of a dam affected by AAR must differ from the mesh used for the thermal analysis and moreover includes joints, the interface between dam and rock foundation, and the rock foundation. These components are not required in the thermal analysis but are very important to capturing the real behavior of a dam affected by AAR (and thus capturing the real crest displacements on which parameter identification is based, as will be explained in the following section).

- AAR expansion can indeed result in: 1) opening of the downstream vertical joints and closure of the upstream vertical joints in an arch dam; 2) possible movement of the various buttresses on a gravity dam along the joints; and 3) sliding of the dam when subjected to a compressive state of stress on the foundation joint.

- With regard to the temporal and spatial variations of temperature, it should be kept in mind that the stress analysis requires a temperature difference with respect to the stress-free temperature (namely the grouting temperature $T(x, y, z) - T_{grout}$), whereas AAR evolution depends on the total absolute temperature inside the dam $T(x, y, z)$.

D Dr. Katayama Study

Methods of Estimating Past and Overall Expansion of Mactaquac Dam Concrete With Emphasis on the Importance of Petrography

April, 2021

Tetsuya Katayama
Katayama Petrographic Consulting Office
Sakura, Japan

SUMMARY

1. To estimate residual and overall expansion curves of the Mactaquac dam concrete undergoing late-expansive ASR, expansion parameters of two kinetic equations that characterize S-shaped curves after Larive and Brunetaud were determined, based on the expansion data of cores extracted horizontally (X direction) from the inspection gallery walls in 2015.
2. Two sets of expansion data tested at 11°C-60°C in 0.225 N-1N NaOH solutions were used: one was from Prof. Saouma's report with GEMTEC spreadsheet data provided through the Professor's contract, and the other was in the report by Moffatt and Thomas (2018).
3. Two sets of data were fitted mainly with Larive equation. As a result, two new equations to calculate apparent activation energy of expansion and coefficient of expansion were obtained as a function of alkali concentration and temperature.
4. With the case 1, final expansion data (ε_∞) calculated by Prof. Saouma (GEMTEC spreadsheet) for 0.225 N and 1N NaOH, and alkali level (0.5N NaOH) and average temperature (11°C) postulated here for the dam site concrete, gave residual expansion ($\Delta\varepsilon$) of 0.19%. This corresponds to 0.74% of overall expansion of the dam, i.e. the sum of the past and residual expansion, which possibly continues expansion for 30 years.
5. With the case 2, data combination with Moffatt and Thomas for 0.225 N NaOH and GEMTEC spreadsheet for 1N NaOH, residual expansion was 0.10% (Larive) with overall expansion of the dam was expected to be 0.65%, continuing about 20 years.
6. According to Whitehead (2006), bedrock from the dam site used as coarse aggregate was greywacke and slate, with fine-grained quartz (< 0.1mm) occupying 30% in these rocks is alkali-reactive. Analysis on his EDS data of clay minerals suggests that they occur as illite in slate and phengite in greywacke, and chlorite of the ripidolite variety in both rocks, all of which are typical of weakly metamorphosed sedimentary rocks. Terminology of the rock name differs by authors: slate corresponds to argillite.
7. Rodrigues (2020) identified ASR in greywacke and argillite in concrete core samples from the dam, along with abundant ettringite which he suspected of the occurrence of DEF in about 60% of the core samples.
8. Water intake of the dam reportedly increased height of 23cm, corresponding to 0.6% expansion (Moffatt et al.2016) in the vertical (Z) direction. However, its exact position has not been documented. It is therefore essential to examine whether the past vertical expansion of the dam varied locally by the structural type, position, orientation, depth, etc.
9. According to a preliminary study of the dam concrete parallelly done (Katayama et al. *in preparation*), expansion of boring cores in the vertical (Z) direction (taken mainly in 2017), as evaluated by the crack indices, was more than twice that of the horizontal (X) direction. This was due to the strong anisotropy of large bedded aggregate particles settled horizontally in concrete. Because of this, horizontally extracted cores from the gallery walls may underestimate the residual expansion, compared with the vertical expansion.
10. It is recommended to quantify past expansion of concrete in three directions (Z,X,Y) using core samples from different portions of the dam, as well as to estimate overall expansion curves according to the simulation method presented here.
11. Petrographic measurements of the crack indices in three directions of cores, extracted recording orientations (Z,X,Y) from different structures, levels, concrete mixes, etc., should be done in parallel with on-site determination of three-dimensional crack indices of concrete. Influence of the preferred orientation of coarse aggregate on concrete expansion should also be examined.
12. It is also recommended that petrographic examination be performed to compare the progress of ASR in concrete from many structures, by means of identifying the stage of ASR in thin section by rock types, and EDS analysis of gel composition.
13. It was believed that with a good petrographic and expansion study, we can obtain reliable kinetics parameters, and then one could use them in a reliably proven finite element analysis to perform a final structural safety assessment.

Table 1: Published field monitoring data of Mactaquac dam structures used to interpret past expansion of concrete

Approximate year	Event				Reference	Vertical past expansion as interpreted here
	Diversion sluisway	Main spillway	Intake	Powerhouse (except for throat ring)		
1968			Construction Units 1,2 & 3		Thompson and Steele (1992) Curtis (2000)	0.00%
1972			Unit 4			
1979			Unit 5			
1980			Unit 6			
Mid 70s (1975?)			Opening of vertical contraction joints			0.04%*
Early 80s (1983?)	Leakage through horizontal construction joints			Spalling on the generator floor beams		
1985		End pier internal crack		Draft turbine pier Growth rate 120με/yr		
		Gate 10 Displacement 25mm				
1989 (?)						
2007			Height increase 175mm		Thomas et al. (2008)	(175/41430) x100= 0.422%**
2015			Height increase 230mm Expansion 120-150 με/y, 6000 με		Moffatt et al. (2016)	(230/41430) x100= 0.556%** 6000με = 0.6%

*Assumption: cracking of concrete occurs at 0.04% expansion; **mean dam height over the lower and upper galleries 41.43m

PART ONE: data analysis of expansion tests

- **Parameters of averaged expansion of cores**

These were determined based on averaged expansion of core samples from the intake and main spillway of the dam, including lower gallery and upper gallery (section 2.1.1, core locations, Prof. Saouma report). Two cases are supplemented here.

Case 1

1N NaOH and 0.225 NaOH: final expansion (ε_∞) of core samples, calculated by Prof. Saouma with Larive equation (Table 3.2, Prof Saouma report) using all data in GEMTEC spreadsheet, was plotted in Fig.1 (a) and Fig.1 (b).

It should be noted that, with 1N NaOH, final expansion increases at higher temperature (Fig.1(a)), whereas it decreases at 0.225 N NaOH (Fig.1(b)). This is apparently in violation of thermodynamics (section 3.3.1, item 2, Prof. Saouma report). However, this could happen when the rate of dissolution of ASR sol/gel into surrounding NaOH solution becomes slower at lower temperature, possibly related to an increased viscosity of ASR gel, larger size of aggregate, higher alkali content of concrete than surrounding alkali solution, increased amount of alkali released from aggregate, etc. These aspects need clarification by a detailed study.

Fig. 1(c) shows that, where NaOH > 0.6N, apparent activation energy of final expansion (U_∞) is positive, expansion increases at higher temperature. Where NaOH > 0.7N (Fig.1(d), expansion coefficient (A) is positive.

Residual expansion was estimated, at which average temperature (T) is 11°C and postulated alkali concentration (N) in concrete is 0.5N NaOH.

From Fig.1(c), $U_\infty = 2922 \ln(N) + 1627$, $N = 0.5 \rightarrow U_\infty = 2922 \ln 0.5 + 1627 = -398.4$ (K)

From Fig.1(d), $\ln(A) = 9.891 \ln(N) + 3.772$, $N = 0.5 \rightarrow \ln(A) = 9.891 \ln 0.5 + 3.772 = -0.6931 + 3.772 = -3.084$

$A = e(-3.084) = 0.0458$

In general, $\varepsilon_\infty (\%) = A \times e(-U_\infty/K)$ $K=273+T(°C)$, $T= 11°C \rightarrow \varepsilon_\infty = 0.0458 \times e(398.4/(273+11)) = 0.0458 \times 4.0666 = 0.186\%$

Residual expansion is about 0.19%

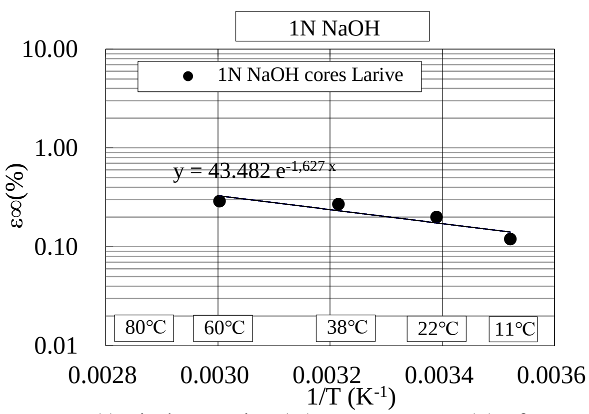

(a) Final expansion (ε_∞) vs temperature (T) of cores: Calculated by Prof. Saouma (Table 3.2, his report) using GEMTEC spreadsheet data provided through Prof. Saouma's contract

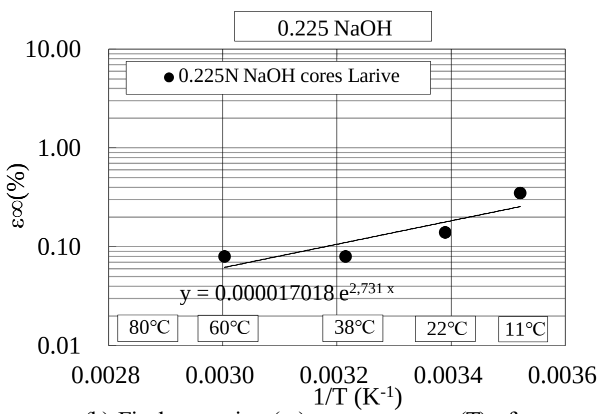

(b) Final expansion (ε_∞) vs temperature (T) of cores: Calculated by Prof. Saouma (Table 3.2, his report) using GEMTEC spreadsheet data provided through Prof. Saouma's contract

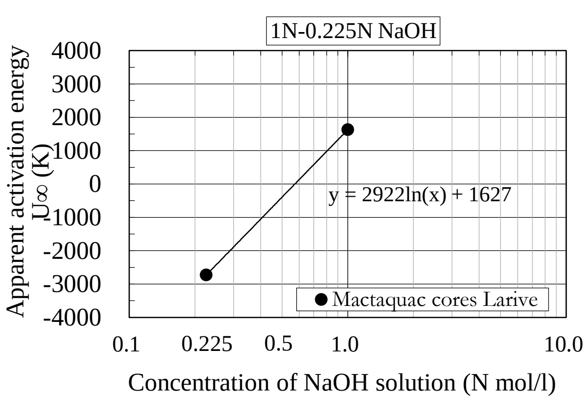

(c) Apparent activation energy (U_∞) of final expansion (ε_∞) vs concentration of enveloping NaOH solution of cores: Drawn using Fig.1(a) and Fig.1(b) originated from Prof. Saouma's data (Table 3.2, his report)

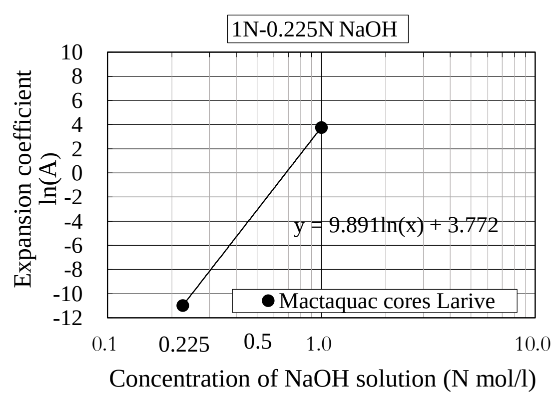

(d) Expansion coefficient (A) vs concentration of enveloping NaOH solution of cores: Drawn using Fig.1(a) and Fig.1(b) originated from Prof. Saouma's data (Table 3.2, his report)

Figure 1: Expansion parameters of Mactaquac dam concretes, calculated using data from Prof. Saouma (Table 3.2, his report) using GEMTEC spreadsheet data provided through Prof. Saouma's contract.

Case 2

For comparison, another combination of expansion data was used to calculate averaged expansion at temperatures 60°C, 38°C, 23-22°C and 11°C: (1) 0.225 N NaOH from Fig.12, Moffatt & Thomas 2018, and (2) 1N NaOH from GEMTEC spreadsheet data provided through Prof. Saouma's contract. For 0.225 N (Fig.2 left), expansion data were read from averaged expansion curves in the figure by Moffatt & Thomas, whereas for 1N (Fig.2 right) all the data in the spreadsheet were used, excepting a few data that presented minus expansion or a steady contraction after reaching a maximum expansion (hollow circles). Then, averaged expansion curves were fitted to Larive and Brunetaud equations. In contrast with the case 1, expansion at 0.225N from Maffatt data was larger at higher temperatures, but sample details were not given. Expansion by the Brunetaud equation at higher temperature was extremely larger than that of the Larive equation, which may not be realistic, as Prof. Saouma pointed out (section 3.5.2, Prof Saouma report).

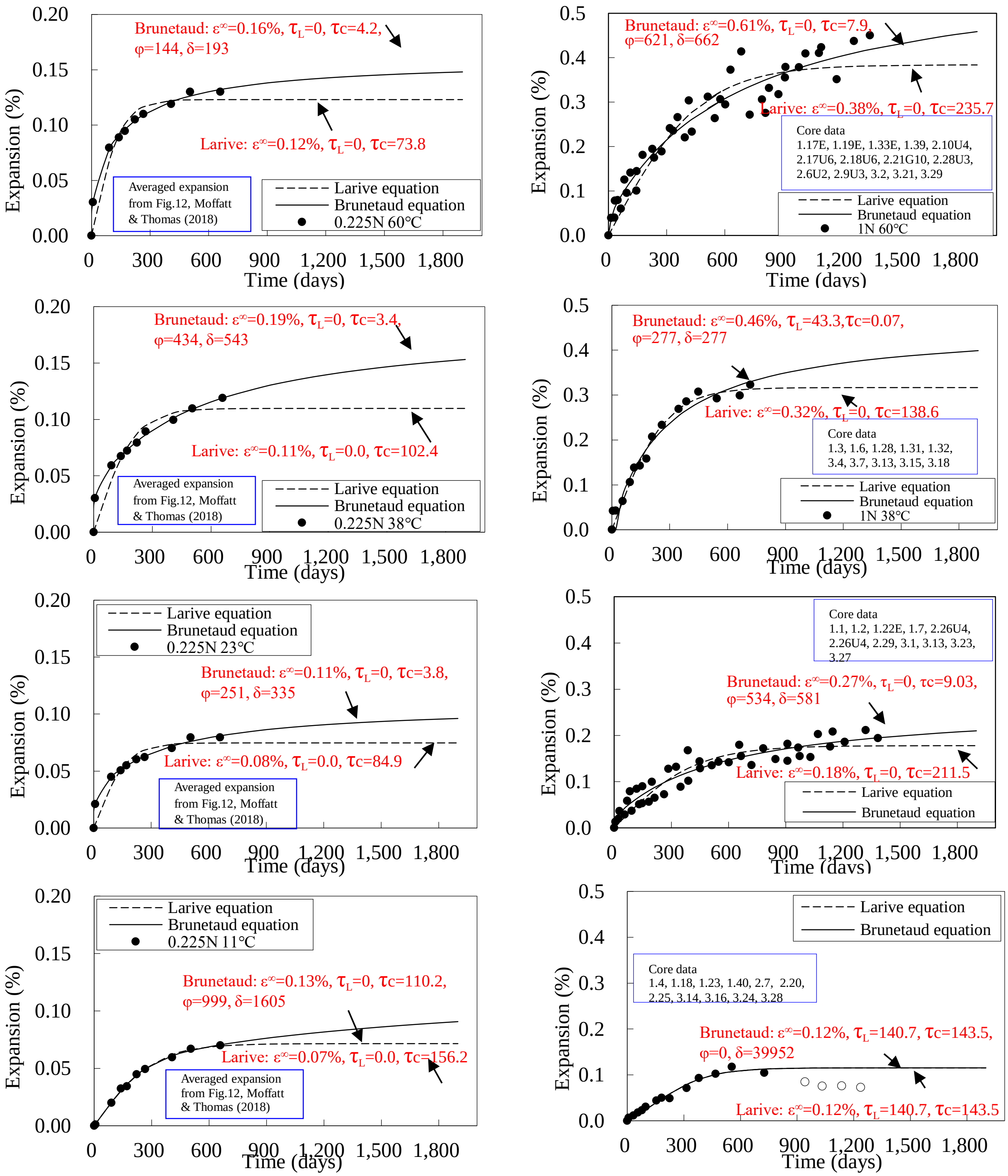

Left: 0.225N NaOH, drawn using data in Fig.12 by Moffatt and Thomas (2018)

Right: 1N NaOH, calculated using GEMTEC spreadsheet data provided through Prof. Saouma's contract

Figure 2: Averaged expansion of Mactaquac dam concrete cores.

Residual expansion of core samples was estimated, at which average temperature (T) is 11°C and postulated alkali concentration (N) in concrete is 0.5N NaOH. Fig.3(a) and Fig.3(b) indicate that expansion increases at higher temperatures, irrespective of whether NaOH concentration is 1N or 0.225N. This is evident from Fig.3(c) and Fig.3(d) that apparent activation energy (U_∞) and expansion coefficient (A) are always positive.

Larive equation

From Fig.3(c), $U_\infty = 829.3\ \ln(N) + 2388$, $N = 0.5 \rightarrow U_\infty = 829.3\ \ln 0.5 + 2388 = 1813.2$ (K)

From Fig.3(d), $\ln(A) = 3.311\ \ln(N) + 6.332$, $N = 0.5 \rightarrow \ln(A) = 3.331\ \ln 0.5 + 6.332 = -0.2.295 + 6.332 = 4.037$

$A = e(4.037) = 56.66$

ε_∞ (%) $= A \times e(-U_\infty/K)$ $K = 273 + T(°C)$, $T = 11°C \rightarrow \varepsilon_\infty = 56.66 \times e(-1813.2/(273+11)) = 56.66 \times 0.001688 = 0.096\%$

Residual expansion is about 0.10%.

Brunetaud equation

Likewise, from Fig.3(c), $U_\infty = 1629.5\ \ln(N) + 3121$, $N = 0.5 \rightarrow U_\infty = 1629.5\ \ln 0.5 + 3121 = 1991.5$ (K)

From Fig.3(d), $\ln(A) = 5.853\ \ln(N) + 9.042$, $N = 0.5 \rightarrow \ln(A) = 5.853\ \ln 0.5 + 9.042 = 4.985$

$A = e(4.985) = 146.20$

ε_∞ (%) $= A \times e(-U_\infty/K)$ $K = 273 + T(°C)$, $T = 11°C \rightarrow \varepsilon_\infty = 146.20 \times e(-1991.5/(273+11)) = 146.20 \times 0.000901 = 0.132\%$

Residual expansion was found to be around 0.13%.

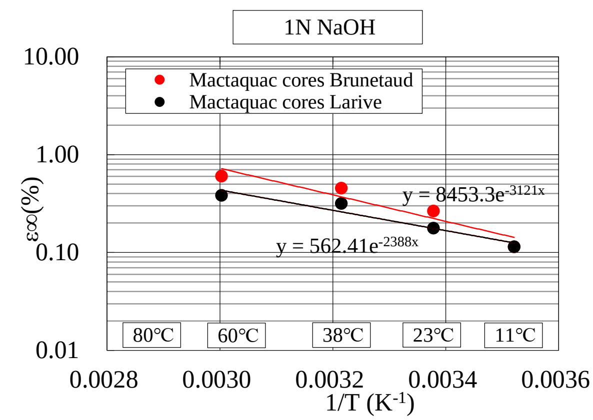

(a) Final expansion (ε_∞) vs temperature (T) of cores calculated using GEMTEC spreadsheet data provided through Prof. Saouma's contract

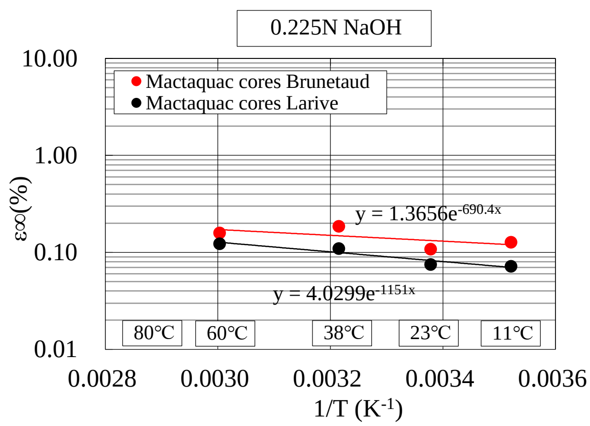

(b) Final expansion (ε_∞) of cores calculated using averaged expansion in Fig.12 of Moffatt and Thomas (2018)

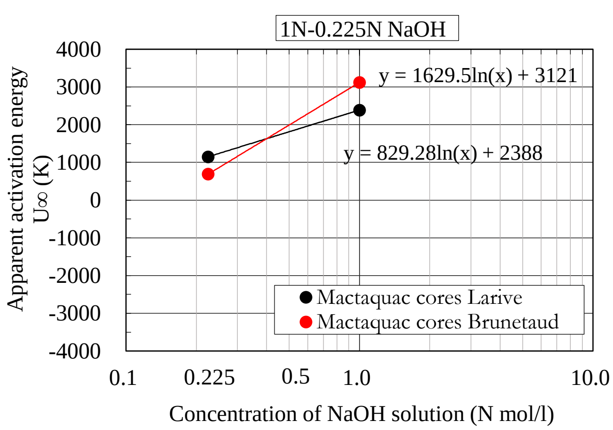

(c) Apparent activation energy (U_∞) of final expansion (ε_∞) vs concentration of enveloping NaOH solution of cores: Drawn using Fig.3(a) (from GEMTEC spreadsheet data provided through Prof. Saouma's contract) and Fig.3(b) (Fig.12, Moffatt and Thomas 2018)

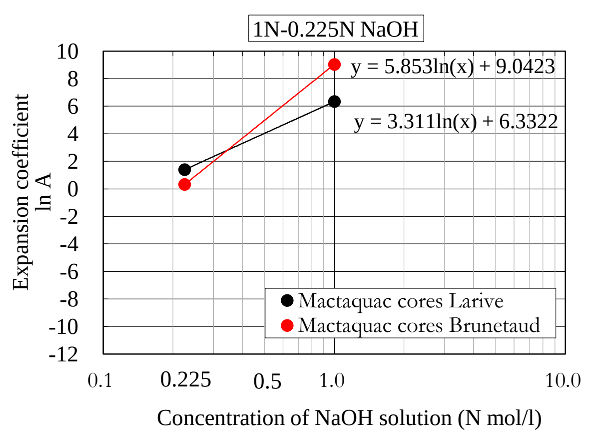

(d) Expansion coefficient (A) vs concentration of enveloping NaOH solution of cores: Drawn using Fig.3(a) (from GEMTEC spreadsheet data provided through Prof. Saouma's contract) and Fig.3(b) (Fig.12, Moffatt and Thomas 2018)

Figure 3: Expansion parameters of Mactaquac dam concretes, calculated using data from Prof. Saouma's report (Table 3.2) and GEMTEC spreadsheet data provided through Prof. Saouma's contract

- **Overall expansion of dam concrete**

Overall expansion of dam concrete was estimated using on-site past expansion (at least two time points) and residual expansion from accelerated expansion tests, as follows (Katayama 2020):

$$\text{Overall expansion } (\varepsilon_\infty) = \text{Past expansion } (\varepsilon_1) + \text{Residual expansion } (\Delta\varepsilon)$$

In the above equation, residual expansion ($\Delta\varepsilon$) is calculated as final expansion (ε_∞) from accelerated concrete core expansion tests by means of the Larive equation or Brunetaud equation. In this method, latency time (τl) and characteristic time (τc) of concrete in the Larive or Brunetaud equation are not used. Although the residual expansion thus determined by this test is a free expansion of concrete core samples, this can be a good measure of potential expansion of concrete. Results for the case 1 and case 2 were shown in Table 2.

The expansion curve thus determined has a larger slope than the average slope (120μ/year) estimated in the 1980s, suggesting that the expansion rate has been increasing until the coring. However, Fig. 4(a) (case 1) and Fig.4(b) (case 2) shows that the future expansion will be decreasing within 30 years.

The sigmoidal expansion curves thus determined have a larger slope than the average slope (see the triangle: 120μ/year) estimated in the 1980s, implying that the expansion rate has been increasing. However, Figure 3A and B show that the future expansion will be decreasing within 20 years (case 2) to 30 years (case 1).

Table 2: Input data to estimate the sigmoidal expansion curves of intake, fitted with Larive equation

Estimated year: oldest units 1-3	1968	1975	2007	2015	11°C, 0.5N NaOH	
Case					1	2
Time after construction (year): t	0	7	40	47	∞	∞
Interpreted vertical expansion (%): ε	0	0.04	0.42	0.56 = ε_1		
Event at intake	construction	first opening horizontal joint	height increase 175mm	height increase 230mm		
Residual expansion from expansion test (%): Δε					0.19	0.10
Overall expansion (%): $\varepsilon_\infty = \varepsilon_1 + \Delta\varepsilon$					0.74	0.65

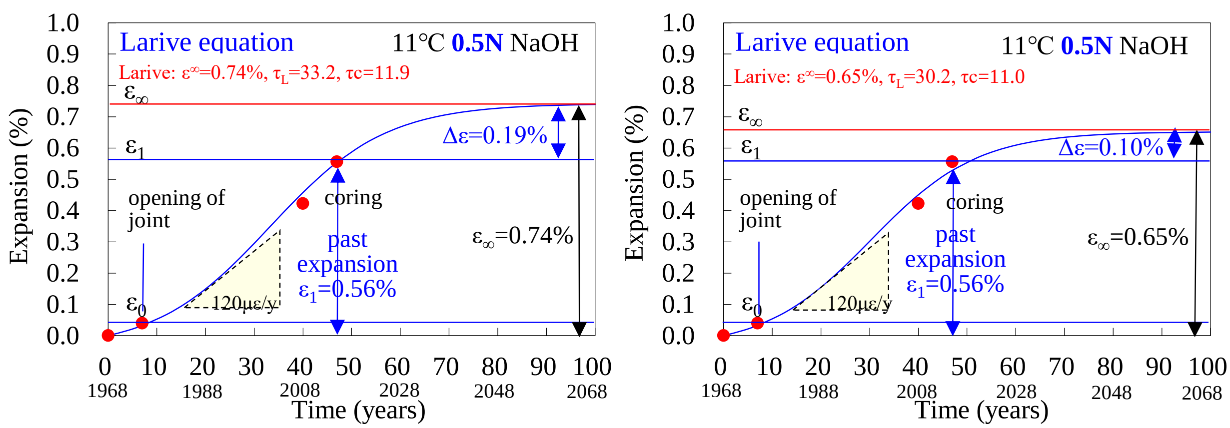

(a) Case 1: Overall expansion (ε_∞) of dam calculated based on final expansion of cores (Table 3.2, Prof. Saouma's report)

(b) Case 2: Overall expansion (ε_∞) of dam calculated using averaged expansion of cores (Fig.12, Moffatt and Thomas 2018)

Figure 4: Estimated curves of overall expansion of Mactaquac dam concrete, based on residual expansion from Larive equation and field data of past expansion

- Differences in two prediction methods

Prof. Saouma's method for predicting future expansion of concrete (section 5.1, Professor's report) does not use final expansion (ε_∞) of cores, obtainable as a residual expansion of concrete in the accelerated expansion test. It is based on characteristic time (τ_c) of cores and its activation energy (U_c) to project a normalized sigmoidal curve by using Larive equation and Arrhenius law (section 3.4). A great merit of this method is that it can predict future expansion of concrete, based on laboratory testing of core samples without knowing past expansion or field monitoring record of concrete structure. According to prediction by this method, expansion of cores simulated for field conditions of Mactaquac dam (11-18°C) will soon reach a maximum around 2024, about 9 years after the beginning of testing (Fig.5.1, Prof. Saouma's report). It will be useful to compare the predicted free expansion of cores with actual expansion of strained concrete in the dam.

In the Katayama's method, Larive equation and Arrhenius law are also employed (Fig.1(a),(b)). However, instead of characteristic time, it uses activation energy (U_∞) of final expansion (ε_∞) of cores. In addition, measurements of crack index of concrete from either field survey or petrographic examination of cores, as well as records of field inspection are used to estimate past expansion of concrete. In this method, overall expansion of concrete can be estimated as the sum of past expansion and residual expansion from accelerated expansion test of cores. One merit of this method is that it can reflect actual state of expansion of a structure in a scale from macroscopic to microscopic about what is going on in field concrete. This method suggested that expansion of the dam concrete will continue at least 20-30 years (Fig.4(a)(b)), which is longer than that of the prediction by the Prof. Saouma's method. Thus, the above two prediction methods can be chosen according to the purpose of investigation by the engineer.

- Larive equation vs Brunetaud equation

Larive equation has universally been accepted kinetic analysis of ASR (section 1.3, Prof. Saouma's report), whereas Brunetaud equation has been limited for sloped expansion curves with large expansion (section 3.5, Prof. Saouma's report). These two equations produce the same result of latency time (τ_l) and characteristic time (τc), only when expansion curve is flat (Fig.2, Right, bottom: data points of hollow circles omitted).
However, unlike the Larive equation and its graphical explanation (Fig.1.2(b), Prof. Saouma's report), parameters φ and δ used in the correction term of the Brunetaud equation (section 3.5, Prof. Saouma's report) do not have a physical meaning. It should be noted that Brunetaud equation, when used for steep curves created by the late-expansive aggregate in Mactaquac dam concrete, can produce unrealistically large final expansion (ε_∞), such as 106.20% (Fig.A9(g), Prof. Saouma's report) and 59.69% (Fig.A10(g), Prof. Saouma's report). From these observations, Brunetaud equation should not be used for kinetic analysis of ASR in the Mactaquac concretes.

PART TWO: Data analysis of petrographic examination

- **Petrography of bedrock and aggregate**

Rocks from the dam site used as coarse aggregate were, according to Whitehead (2020), greywacke and slate (Table 3). They contained fine-grained quartz (< 0.1mm), which he thought alkali-reactive, nearly occupying 30% in these rocks. The ledge rock has a similarity of lithology to that of the quarried aggregate in Springhill, New Brunswick.

Table 3: Mineral assemblage of bedrock at Mactaquac dam summarized from data by Whitehead (2006)

		Quartz	Feldspar (albite)	Amphi-bole	Muscovite		Chlorite		Carbonate		Rock clasts	Opaque*	Matrix
					clasts	secondary	clasts	secondary	calcite	dolomite			
Mactaquac bed rock	Greywacke	45 (28**)	15		0-15		5	2	+	+	2	1	15-30
	Slate	30	+		+		15		30		25		
Springhill quarried rock	Greywacke	40 (19**)	20	2	2		2		+	+	5	1	
	Slate	25	+		+		+			+			

*including pyrite and titanite ** fine-grained quartz (<0.1mm), likely alkali-reactive + supplemented by XRD

Compositional formulae of the clay minerals in these rocks were calculated here using the EDS data by Whitehead (Table 4). It can be seen that a mineral originally termed as mica in slate was generally poor in potassium (K<0.8), suggestive of illite, whereas mica in the greywacke (Psam 1) contained small amounts of Mg and Fe indicative of phengite, a variety of muscovite. In addition, chlorite in both slate and carbonate vein in the Mactaquac bedrock contained appreciable amounts of Fe and Al, corresponding to ripidolite (Fe richer than clinochlore). All these varieties of the clay minerals are typical of weakly metamorphosed sedimentary rocks.

Table 4: Compositions of clay minerals in the Mactaquac bedrock calculated using EDS data from Whitehead (2006)

	Original description	Host rock	Compositional formula	Suggested variety
Mactaquac bedrock	Chlorite	Slate 2	$(Mg_{2.52}, Fe_{2.02}, Al_{1.36}, Mn_{0.01}, Na_{0.04}, K_{0.03})_{5.98}[Al_{1.28},Si_{2.72}]_{4.00}\,O_{14}\,nH_2O$	Ripidolite
		Slate 4	$(Mg_{2.19}, Fe_{2.18}, Al_{1.49}, Mn_{0.01}, Na_{0.04}, K_{0.03})_{5.94}[Al_{1.37},Si_{2.63}]_{4.00}\,O_{14}\,nH_2O$	Ripidolite
		Carb 1	$(Mg_{2.40}, Fe_{2.25}, Al_{1.28}, Ti_{0.01}, Na_{0.04}, K_{0.01})_{5.99}[Al_{1.30},Si_{2.70}]_{4.00}\,O_{14}\,nH_2O$	Ripidolite
	Mica	Slate 1	$\{K_{0.55}, Na_{0.05}\}_{0.60}(Al_{1.18}, Mg_{0.75}, Fe_{0.63}, Ti_{0.01})_{2.57}[Al_{1.02},Si_{2.98}]_{4.00}\,O_{11}\,nH_2O$	Illite
		Slate 3	$\{K_{0.70}, Na_{0.09}\}_{0.79}(Al_{1.62}, Mg_{0.31}, Fe_{0.34}, Ti_{0.02})_{2.29}[Al_{1.07},Si_{2.93}]_{4.00}\,O_{11}\,nH_2O$	Illite
		Psam 4	$\{K_{0.94}, Na_{0.04}\}_{0.98}(Al_{1.38}, Mg_{028}, Fe_{0.40}, Ti_{0.06})_{2.12}[Al_{0.77},Si_{3.23}]_{4.00}\,O_{11}\,nH_2O$	Phengite (muscovite)
Springhill aggregate	Mica	Slate 2	$\{K_{0.86}, Na_{0.02}, Ca_{0.01}\}_{0.88}(Al_{1.55}, Mg_{0.29}, Fe_{0.25}, Ti_{0.01})_{2.10}[Al_{0.69},Si_{3.31}]_{4.00}\,O_{11}\,nH_2O$	Illite
		Slate 3	$\{K_{0.77}, Na_{0.04}\}_{0.81}(Al_{1.56}, Mg_{0.36}, Fe_{0.15}, Ti_{0.04})_{2.11}[Al_{0.74},Si_{3.26}]_{4.00}\,O_{11}\,nH_2O$	Illite

From Table 3 and Table 4, the mineral assemblage of greywacke and slate can roughly be regarded as follows:
Quartz – Feldspar (albite) – Mica (illite or phengite) – Chlorite (ripidolite) – Calcite – Pyrite – Titanite.

Knowing this, then, potential contents of each mineral (normative mineral compositions) could be calculated from the chemical composition of the rock or aggregate, if the whole rock chemical analysis is available and the amounts of Mg and Fe in the solid solutions of chlorite and mica are taken into consideration. This kind of calculation of quartz could be a rough measure of the potential alkali-reactivity of fine-grained rocks, such as slate and argillite.

- **Petrography of Mactaquac dam concrete**

Petrographic examinations of concrete core samples from the dam, performed in accordance with ASTM C856 (Rodrigues 2020) using thin sections, revealed that coarse aggregates of greywacke and argillite were producing ASR, and that ettringite was abundant in about 60% of the core samples and some of which occurred as crack-filling within cement paste, casting a possibility of DEF (delayed ettringite formation). However, to confirm DEF, detailed SEM observation coupled with EDS analysis will be necessary.

The original report did not contain any table to compare the progress of ASR by each rock type of the aggregate among the core samples examined. Hence, Table 5 has been prepared here by reading information from the microphotographs attached in the report. It should be noted that the terminology of the rock types differs by geologist and petrographer, e.g. “argillite” by Rodrigues corresponds to “slate” by Whitehead.

Table 5: Summary of petrographic examination ASTM C856 of Mactaquac dam concrete adapted from Rodrigues (2020)

Barrel	Core No.	Depth (m)	Aggregate				Cement paste (%)	Voids (%)	Cracks in aggregate		Cracks in Cement paste			Voids	
			Coarse (%)		pyrite	Fine (%)			ASR gel	Crystalline ASR products	ASR gel	Crystalline ASR products	Ettrin-gite	ASR gel	Ettrin-gite
1	2	0-0.36	35	Greywacke	x	30	32	3	x	x	x		+	x	+
1	4	0-0.30	35	Greywacke, argillite	x	30	29	6	x	x	x	x	+	x	+
1	6	0-0.44	38	Greywacke, argillite	x	30	28	4	x	x	x	x	+		+
2	11	0.25-0.63	40	Greywacke, argillite	x	28	27	5	x	x	x				x
1	12	0.25-0.44	40	Greywacke, argillite	x	30	25	5	x	interface			+		+
2	14		38	Greywacke, argillite	x	30	27	5	x			x		x	+
3	19		38	Greywacke, argillite	x	30	26	6	x	x	x			x	x
1	22	0-0.40	35	Grwk, argil, QC vein	x	30	30	5	x	x	x			x	x
full	23	0-0.45	40	Grwk, argil, QC vein	x	30	27	3	x					x	x
1	24	0.05-0.20	40	Greywacke, argillite	x	30	28	2	x		x				x
1	27	0-0.48	35	Grwk, argil, QC vein	x	32	28	5	x	x			+		+
1	30	0-0.44	38	Grwk, argl, granite	x	22	37	3	x	x	x	x	+	x	+
3	36	0.7-1.0	35	Grwk, argil, QC vein	x	30	29	6	x						x
2	38	0.38-0.59	42	Grwk, argl, andesite	x	30	23	5	x				+		+

\+ abundance of ettringite cannot exclude DEF x present

PART THREE: Suggestions

According to Moffatt et al. (2018), water intake of the dam increased height of 23cm, i.e. 0.6% expansion in the Z direction. It is important to confirm whether the expansion occurs uniformly 1) in all directions (Z, X, Y) of the dam, 2) at entire levels of the intake (upper, middle, lower, etc.), or 3) in the structural units with different construction age (older units 1-3, younger units 5-6).

In view of the scarcity of the data of past expansion, which is essential in drawing overall expansion curves of the dam, following examinations are suggested.

- Past expansion of concrete: this can be determined in two ways, i.e. external expansion and internal expansion.
- The external expansion can be obtained on the concrete surface as crack indices (Z,X,Y) by visual inspection of the lower and upper inspection galleries, as well as on the concrete surface of dam body.
- The internal expansion of concrete can be determined as crack indices (Z.X,Y) on the sections of core samples, either by the stereomicroscopy or polarizing microscopy. Cores should be extracted recording three directions (Z,X,Y).

A preliminary study of the dam concrete parallelly done (Katayama et al. *in preparation*) indicated that expansion of boring cores in the vertical (Z) direction (taken mainly in 2017), as evaluated petrographically by the crack indices before and after the accelerated expansion test, was more than twice that of the horizontal (X) direction. This was due possibly to preferred orientation of relatively flat and bedded coarse aggregate in concrete.

- In view of the anisotropy of large particles of coarse aggregate, horizontally extracted cores from the gallery walls may underestimate the residual expansion, compared with the vertical expansion of the dam concrete. In this case, it is recommended to measure expansion or crack index in the vertical direction as well.
- Petrographic examination should be linked with field observations of cracking and deterioration of concrete structures, ranging from the megascopic dimension through the macroscopic to the microscopic dimension.
- To facilitate compare the progress of ASR in core samples from different structures, members and levels with various concrete mix and exposure conditions, it is recommended to tabulate results of petrographic examination under the microscope.
- With a good petrographic and expansion study, we can obtain reliable kinetics parameters, and then one could use them in a reliably proven finite element analysis to perform a final structural safety assessment.

- **Past expansion of concrete**

Field work: External expansion

Petrographic examination should be linked with field observation of cracks in concrete. When result of accelerated expansion test is unavailable, past expansion is determined on-site (Fig.5) to extrapolate future expansion by fitting with Larive's S-shaped expansion curve (Fig.6).

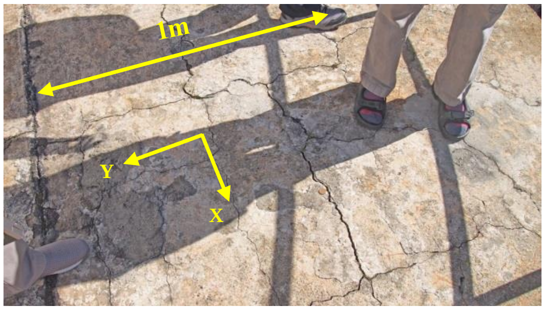

(a) Rectangular cracking affected by steel reinforcement

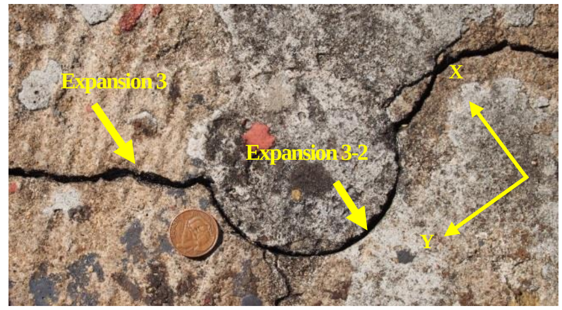

(b) Continued expansion around previous borehole. Adapted from Katayama (2017).

Figure 5: Example for estimation of three-dimensional on-site past expansion of a Brazilian dam.

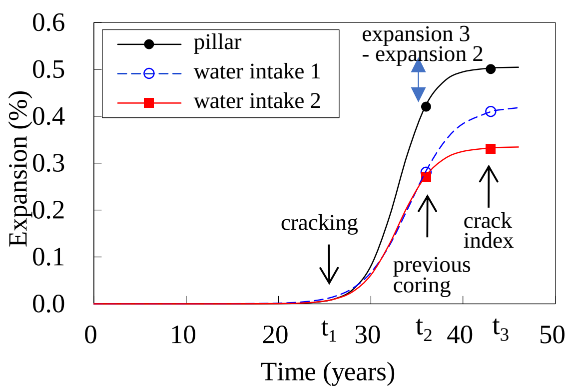

Past expansion: at times t_1, t_2, and t_3

t_1: first cracking, expansion 1 (= 0.04%)

t_2: previous coring, expansion 2

t_3-t_2: expansion after coring (new gap)

t_3: current inspection, expansion 3

Figure 6: Example of Larive's sigmoidal expansion curves of a Brazilian dam, based on field inspection in 2016. Adapted from Katayama (2017)

- Overall expansion of concrete

When result of accelerated expansion test of core is available, this expansion should be corrected for temperature, alkali content, relative humidity, etc., then combined with the past expansion estimated from the field inspection, an overall expansion curve is synthesized (Fig.7). Overall expansion of concrete (ε^{∞}) = Past expansion (ε_1) + Residual expansion ($\Delta\varepsilon$)

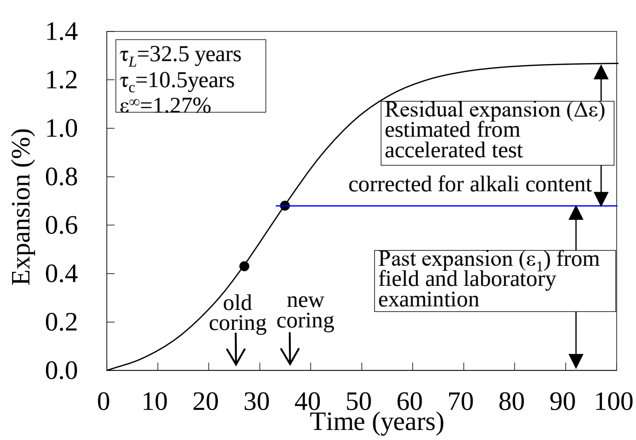

Figure 7: Example of overall expansion of concrete (ε^{∞}) = Past expansion (ε_1) + Residual expansion ($\Delta\varepsilon$), corrected for alkali content, temperature, relative humidity, etc. Adapted from Katayama (2020)

- **Laboratory work: Internal expansion**

Macroscopic: Polished core section

It has been pointed out that expansion of concrete structures differs between the concrete surface and interior. Because of this, it is necessary to examine internal expansion based on boring cores of concrete. For this purpose, core samples should be extracted recording the orientation (Z.X,Y), then past expansion in three directions is determined in terms of crack indices on the polished concrete section (Fig.8). In general, expansion cracks formed in the reactive coarse aggregate are wide and important, affecting concrete expansion.

For macroscopic examination, half-cut core (length 13-20cm) is impregnated with fluorescent dye, then the width of cracks is measured (Fig.8). Preliminary petrographic study (Katayama et al. *in preparation*) indicated that coarse aggregate from Mactaquac dam generally had a flat shape tending to settle horizontally during concrete casting, and that major expansion of the dam concrete as evaluated in terms of crack indices occurred normal to the bedding plane of the coarse aggregate (i.e. Z direction (Fig.9A). Where the coarse aggregate is embedded obliquely, expansion in Z and X (or Y) directions should be corrected as shown in Fig.9B.

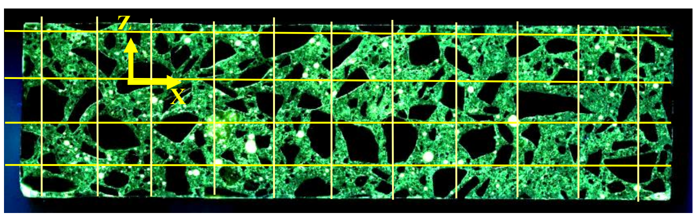

(a) Horizontal core with reacted sand and cracked paste. Adapted from Katayama, Mukai and Sato (2020)

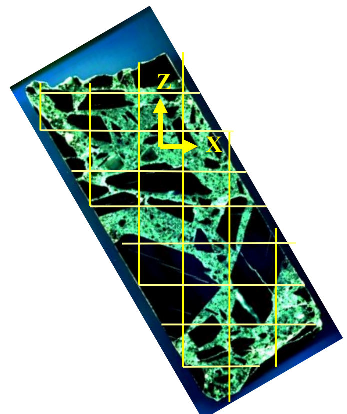

(b) Obliquely extracted core with reacted coarse aggregate.

Figure 8: Example of half-cut core, impregnated with fluorescent dye and superimposed grids for measuring crack indices in three directions (Z,X,Y)

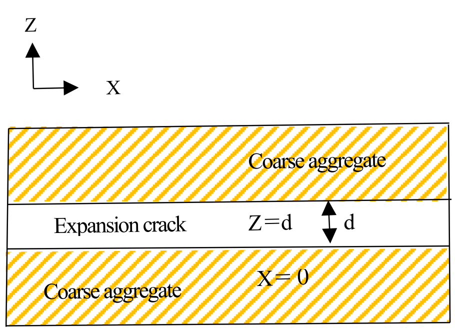

(a) Horizontal settling of coarse aggregate particle. Adapted from Katayama et al. *(in preparation)*

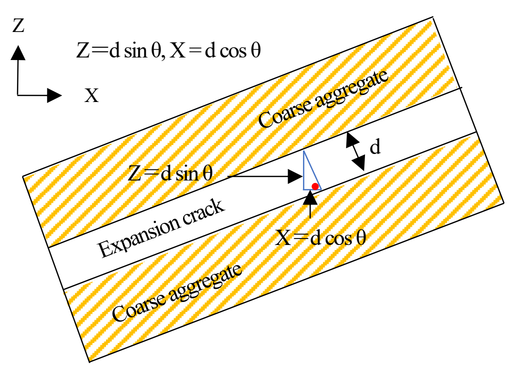

(b) Inclined setting of aggregate need for angle correction. Adapted from Katayama et al. *(in preparation)*

Figure 9: Example of vertical (Z) and horizontal (Y, X) expansion of cracked coarse aggregate observed in concrete section.

Microscopic: Thin section

Crack indices can be measured with thin sections when sufficient number of thin sections is prepared. For this purpose, thin sections should be cut at a right angle representing three directions Z,X,Y (Fig.10). In this figure, half cylinder for macroscopic fluorescence observation is cut at an angle of 45° from the plane of thin sectioning. However, it is desirable to minimize this angle or coincide the direction with that of the thin sections.

Table 6 is an example of measurement of the crack indices of concrete containing reactive sand aggregate. In this case, expansion in the Z direction was 27% larger than that of the horizontal directions. Three-dimensional determination of the crack indices like this would contribute to clarify anisotropic expansion in the dam concrete as well.

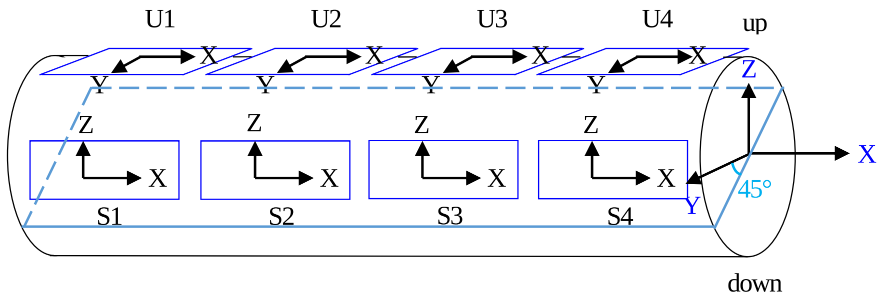

Figure 10: Example of thin sectioning of horizontal core to measure crack indices in three directions (Z,X,Y). Adapted from Katayama, Mukai and Sato (2020)

Table 6: Example of crack indices (%) of concrete with reactive sand as measured in thin sections. Adapted from Katayama, Mukai and Sato (2020).

	Horizontal section					Vertical section					Crack index (%)
Direction	U1	U2	U3	U4	av	S1	S2	S3	S4	av	av
Z						0.49	0.35	0.14	0.14	0.28	0.28
X	0.27	0.19	0.26	0.25	0.24	0.19	0.20	0.22	0.14	0.19	0.22
Y	0.17	0.12	0.24	0.33	0.22						0.22

- **Mapping of elements in concrete**

It is important to clarify whether crack-filling ettringite is a result of DEF or other internal or external causes. In view of the presence of pyrite in all coarse aggregate in the Mactaquac dam concretes (Table 7), it should be worthwhile to examine whether pyrite in concretes had decomposed to supply sulfate ions, and whether compositions of CSH gel is rich in sulfate ions and aluminate ions suggestive of DEF. It should also be important to check whether ettringite fills a preexistent crack formed by ASR within cement paste. Fig.11 is an example of mapping elements of such a case in a hydraulic structure in Japan.

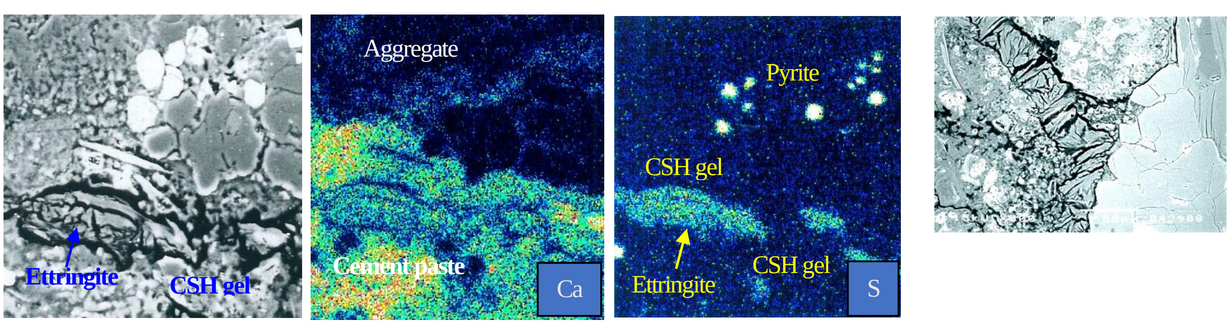

Figure 11: Example of mapping elements at the contact zone between framboidal pyrite grains (sandstone aggregate) and cement paste, hydraulic structure in Japan. Adapted from Katayama et al. (2004)

- Petrographic examination for progress of ASR

The progress of ASR in concrete can be rated in 5 or 6 stages, based on the texture of rimmed or cracked aggregate and the occurrence of AAR gel in cement paste (Table 7, Fig.12). This can apply to both the early- and the late-expansive ASR.

In a case study of Japanese highway structures, it has been recognized that the grade of ASR proceeded one stage within 10 years, at ages exceeding about 30 years old, and that even late-expansive granite and gneiss took part in the reaction (Table 8). The illustrated format to describe the rock types and stage of ASR for each aggregate type is suitable in understanding what stage of ASR is happening in concrete.

Table 7: Petrographic stage of ASR by polarizing microscopy. Adapted from Katayama (2017)

Stage	Site	Development of microscopic textures
i	Aggregate	Formation of reaction rim. no cracks
ii	Cement paste	Halo of ASR sol/gel in cement paste around the reacted aggregate. no cracks. Air voids adjacent to the reacted aggregate may be filled with ASR gel migrated through permeation
iii	Aggregate	Formation of gel-filled cracks within reacted aggregate
iv	Cement paste	Propagation of gel-filled cracks from reacted aggregate into cement paste
v		Widening of gel-filled cracks. Air voids distant from the reacted aggregate are lined with ASR gel migrated along cracks in cement paste
vi		Formation of network of gel-filled cracks connecting the reacted aggregate. Lamination of cracks

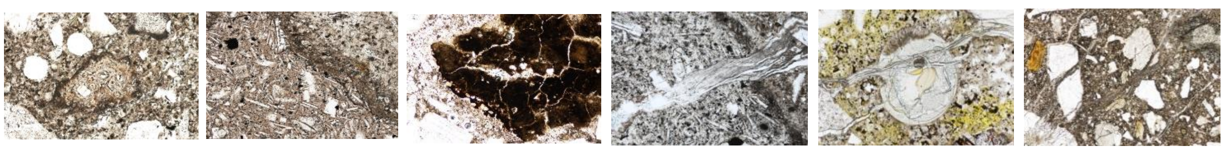

Figure 12. Example of the representative stages of ASR in concrete as observed by thin section petrography. Mainly early-expansive andesite. Adapted from Katayama (2017)

Table 8: Example of the progress of ASR in highway structures in Japan. Manifestation of late-expansive ASR by granite and gneiss aggregate in additional 10 years to 19-24years old structures. Adapted from Katayama (2017)

struc-ture	aggre-gate	rock type	1999 progress of ASR →						2008 (2010) progress of ASR →							*
			i	ii	iii	iv	v		i	ii	iii	iv	v	vi		
To bc 1975	gravel	andesite	x					i	x	x	xx	x	x	(x)	v	3
		gneiss									x	(x)				
	sand	andesite	x		x	x	x	v	x		xx	x	x	x	vi	
		rhyolite	x		x	x			x							
Ku br 1975	gravel	andesite			x	x	x	v	x	x	x	x	x		v	3
		rhyolite							x							
		rhyolitic tuff	xx													
		gneiss									x	x				
	sand	andesite			xx	x		iv	x	x	x	x	x	x	vi	
		glassy rhyolite			x											
		rhyolitic tuff							x							
Ji br 1975	gravel	andesite	x		x	x	x	v			x	x	x		v	3
		rhy.welded tuff							x							
		granite (quartz)			x											
	sand	andesite	x		x	x		iv	x	x	x	x			iv	
		rhyolite	x		x	x			x							
		rhy.welded tuff	x						x							
Sh br 1973	gravel	andesite	x		x			iii							v	2
		rhyolite			x	(x)										
		gneiss									x	x	x			
		rhy.welded tuff	x		x											
	sand	andesite	x		x			iii	x						iv	
		dacite	x						x							
		rhyolitic tuff	x													
		chert									x	x				
Te vd 1980	gravel	andesite	x		x	x	(x)	iv	x	x	xx	x	x	x	vi	3
		granite									x	x				
	sand	andesite			xx	x		iv	x		x	x	x		v	
		rhy.welded tuff							x							
		rhy.welded tuff	x						x							

xx abundant; x common; (x) rare; * Field severity of ASR: 3 conspicuous; 2 moderate; 1 weak; 1 none

- **EDS analysis of ASR gel in concrete**

This analytical technique, performed on polished thin section, reveals the evolutionary stage of ASR in concrete, whether it is at the early stage, the middle stage or the late stage of ASR. In concrete, cement minerals alite and belite hydrate to CSH gel liberating calcium and converge to a certain point on the Ca/Si-Ca/(Na+K) diagram (Fig.13). On the other hand, during migration of ASR gel from reacted aggregate into cement paste, its composition evolves to that of CSH gel by absorbing calcium from cement paste and losing alkalis, and finally approaches the composition identical with CSH gel, which is called convergent point. Calcium rich ASR gel having a composition of CSH gel is no longer expansive. It should be informative if this analysis is performed with several concretes from Mactaquac dam.

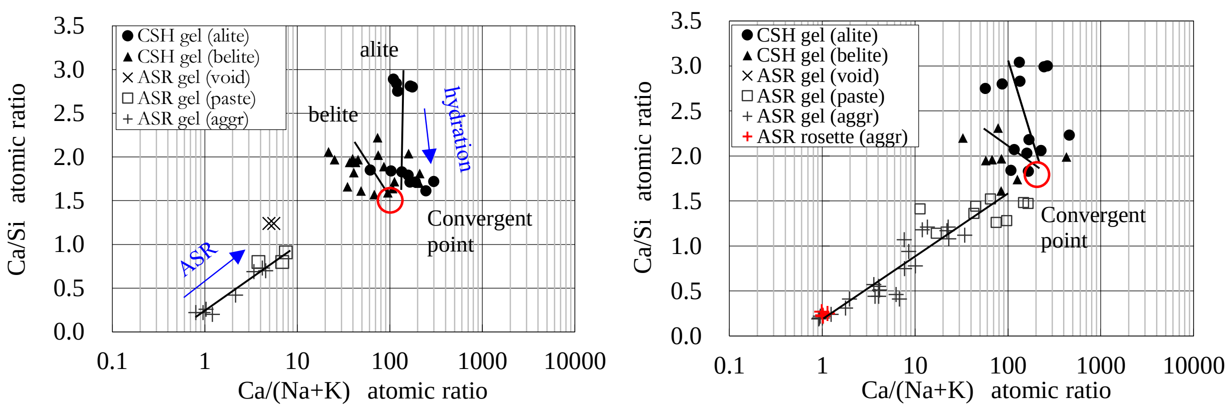

(a) Early stage of ASR in the sound dry area of concrete pavement, Japan. Adapted from Katayama et al. (2016).

(b) Advanced stage of ASR in old dam concrete (c.a. 70 years) undergoing late-expansive ASR of greywacke aggregate, Newfoundland. Adapted from Katayama (2008)

Figure 13: Example of compositional trends of ASR gel in ASR-affected concrete.

References (in chronological order)

Thompson GA and Steele RR (1992): Alkali aggregate reaction at Mactaquac generating station remedial measures progress report. *International Conference on Concrete Alkali-Aggregate Reaction in Hydroelectric Plants and Dams*. 16p. Fredericton, New Brunswick, Canada

Larive, C. (1998). Apports combinés de l'expérimentation et de la modélisation à la comprehension de l'alcali-reaction et de ses effets mécaniques. Monograph LPC, *Laboratoires des Ponts et Chaussées, Paris* (in French).

Curtis DD (2000): Analysis and structure response to recent slot cutting at Mactaquac generating station. *Proc.11th ICAAR*, pp.1283-1291, Quebec City, Canada

Katayama T, Sarai Y, Higashi Y, Honma A (2004): Late-expansive alkali-silica reaction in the Ohnyu and Furikusa headwork structures, central Japan. *Proc. 12th ICAAR*, Beijing, China. pp. 1086-1094.

Brunetaud, X. (2005): Etude de l'influence de différents paramètres et de leurs interactions sur la cinétique et l'amplitude de la reaction sulfatique interne au beton. *Chautenay-Malabry, Ecole Centrale, de Paris* (in French).

Whitehead J (2006): A comparative study of Silverwood quarry aggregate and Mactaquac dam-site bedrock. August 19th, 2006. 25p. submitted to Prof. Thomas M, University of New Brunswick, Department of Civil Engineering.

Thomas M, Beaman N, Hayman S and Gilks P (2008): Evaluating ASR preventions strategies for the reconstruction of concrete structures at Mactaquac generating station. *Proc. 13th ICAAR*, pp.1271-1280, Trondheim, Norway

Katayama T. (2008): ASR gel in concrete subject to freeze-thaw cycles – comparison between laboratory and field concretes from Newfoundland, Canada. *Proc.13th ICAAR*, Trondheim, Norway. pp. 174-183.

Moffatt EG, Thomas MDA, Hayman S, Fournier B, Ideker J and Fletcher J (2016): Remediation strategies intended for the reconstruction of the ASR-induced Mactaquac dam. *Proc. 15th ICAAR*, paper 069, Sao Paulo, Brazil

Katayama T, Sarai Y, Sawaguchi H (2016): Diagnosis of ASR in airport pavement in Japan – early-expansive sand aggregate missed by conventional test. *Proc. 15th ICAAR*, Sao Paulo, Brazil. 10p.

Katayama T (2017): An attempt to estimate past expansion of concrete based on petrographic stage of alkali-silica reaction. *Proc.39th International Conference on Cement Microscopy (ICMA)*. pp.217-236, Toronto, Canada

Moffatt T and Thomas M (2018): Predicting residual expansion and changes in mechanical properties of the concrete at Mactaquac generating station. *Progress Report*. April 23, 2018

Rodrigues A (2020): Petrographic examination ASTM C856. Submitted to GEMTEC

Katayama T (2020): Accelerated expansion test. *In: Saouma VE (ed.) Diagnosis & Prognosis of AAR Affected Structures; State-of-the-Art Report of the RILEM Technical Committee 259-ISR*. pp.141-173. Springer Nature

Katayama T, Mukai K and Sato T (2020): Accelerated expansion test sample report: Japan. *In: Saouma VE (ed.) Diagnosis & Prognosis of AAR Affected Structures; State-of-the-Art Report of the RILEM Technical Committee 259-ISR*. pp.259-311. Springer Nature

Katayama T, Mukai K, Sato T, Campbell I, McLean BD, Brad Manderville, B, Curtis DD: Characteristics of ASR expansion and pyrite oxidation at Mactaquac generating station ***(In preparation).***